MODELING $1/f$ NOISE IN HEMTS WITH SPICE-BASED MICRO-CAP

BY

DONNA KUBIK

BS, Binghamton University, 1995

THESIS

Submitted in partial fulfillment of the requirements for
the degree of Master of Electrical Engineering
in the Graduate School of
Binghamton University
State University of New York
1998

Accepted in partial fulfillment of the requirements for
the degree of Master of Electrical Engineering
in the Graduate School of
Binghamton University
State University of New York
1998

James Constable _____ July 30, 1998
Electrical Engineering Department

William Blose _____ July 30, 1998
Electrical Engineering Department

James Morris _____ July 30, 1998
Electrical Engineering Department

Abstract

Micro-Cap was used to model HEMTs, with special attention paid to $1/f$ noise. The development of HEMTs as driven by noise reduction was investigated. The mechanisms of $1/f$ noise generation and survey of CAD for noise analysis is presented.

The motivation for this study was twofold. A HEMT model was developed that includes $1/f$ noise that would be useful in circuit design. This model, referred to as the discrete $1/f$ noise model, places all of the observed $1/f$ noise in one noise source at the input of the device. Low frequency noise spectra published for an AlGaAs/GaAs HEMT were successfully simulated by the discrete $1/f$ noise model.

The second motivation was to develop a noise model that would be helpful in understanding the $1/f$ noise sources within a HEMT by defining noise sources that reflect the physical processes actually taking place in the device. Three sources of noise that become dominant at low frequencies (0.01Hz to 100MHz) in HEMTs are quantum $1/f$ noise, generation-recombination noise (g-r noise), and thermal noise. A model for thermal noise is integral to the circuit analysis program used. A noise source capable of simulating $1/f$ noise and another capable of simulating g-r bulge noise were developed. Any number

of these sources could be distributed at various locations in the equivalent network model of a HEMT. For this reason, this model is referred to as the distributed $1/f$ noise model. Insight into the physical source of $1/f$ noise in HEMTs may be gained by examining the effect of varying the location, number, and properties of these noise sources. Simulation of published low frequency noise spectra for a GaInP/GaInAs/GaAs HEMT was used to demonstrate the application of the distributed $1/f$ noise model.

Dedicated to my Mom and Dad

Contents

Abstract iii

Dedication v

1 Introduction 1

2 HEMT development, operation and fabrication 9

2.1 HEMT development 9

2.2 Conventional AlGaAs/GaAs HEMT 17

2.3 Pseudomorphic InGaAs/AlGaAs HEMT 27

2.4 InP-based HEMT 31

2.5 GaInP/GaInAs/GaAs graded barrier HEMT 34

3 $1/f$ noise 37

3.1 Introduction 37

3.2 Algebra of self-similarity 38

3.3 Ubiquity of power laws 38

3.4 Noise 41

3.5 Electrical noise 47

3.6 Low-frequency noise in materials 50

3.6.1 Quantum $1/f$ noise 53

3.6.2 g-r noise 58

4 CAD for noise analysis 60

4.1 Noise modeling 60

4.1.1 Analytical models 61

4.1.2 Empirical models 62

4.1.3 Noise simulation with CAD 63

4.2 Noise analysis with Micro-Cap 64

4.2.1 Micro-Cap circuit analysis 66

4.2.2 Micro-Cap noise analysis 66

4.2.3 Micro-Cap AC analysis 68

4.2.4 Micro-Cap macros 69

4.2.5 Micro-Cap noiseless resistors 69

4.3 Micro-Cap applications 72

5 Discrete $1/f$ noise model 73

5.1 Presentation of problem 73

5.2 Two things Micro-Cap can do 75

5.2.1 Model $1/f$ noise using Micro-Cap device models 75

5.2.2 Micro-Cap can be used to model 1/*f* noise externally 79

5.3 What Micro-Cap cannot do 82

5.4 The discrete 1/*f* noise model 84

5.5 Results 85

6 Distributed 1/*f* noise model 91

6.1 Introduction 91

6.2 Resistances 97

6.2.1 Source and drain resistance 97

6.2.2 Gate resistance 100

6.2.3 Gate-to-source leakage conductance 101

6.2.4 Output conductance 101

6.2.5 Summary of resistances 102

6.3 Capacitances 103

6.3.1 Gate-to-drain capacitance 103

6.3.2 Drain-to-source capacitance 104

6.3.3 Gate-to-source capacitance 104

6.3.4 Summary of capacitances 105

6.4 DC characteristics 106

6.5 Small signal characteristics 113

6.6 Noise sources 120

6.6.1 1/*f* noise macro 121

6.6.2 g-r bulge noise macro 123

6.6.3 Thermal noise 125

6.6.4 Noise transfer functions 126

6.6.5 Noise simulation 128

7 Conclusion 141

References 143

Chapter 1

Introduction

> The known is finite, the unknown infinite; intellectually we stand on an islet in the midst of an illimitable ocean of inexplicability. Our business in every generation is to reclaim a little more land.
>
> T. H. Huxley

High electron mobility transistors, HEMTs, have been shown to be high performance millimeter wave devices. Due to their high power gain and low noise figures at frequencies above 60GHz, HEMTs are often used in high frequency applications. The key microwave analog circuit application of HEMT devices is in receiver front ends. Modest cooling requirements, large instantaneous bandwidth, and very low noise of HEMT millimeter-wave amplifiers have spurred interest in their use as broadband continuum radiation detectors, especially for cosmic microwave background radiation measurements. The radiometric sensitivity of such receivers may be limited by random gain fluctuations of the receivers (Pospieszalski & Wollack 1997). Often, the desired signal is much weaker than the background noise arising from the telescope structure and the atmosphere. A commonly used method to extract the signal from the noise is to switch observations between the source and the nearby sky (Kitchin 1991). The rate of switching is a function of the random gain fluctuations due to the $1/f$ noise of the receiver.

Lower corner frequencies for $1/f$ noise are desirable to avoid the difficulty of implementing very fast switching rates. HEMTs are also used in microwave and millimeter wave power amplifiers, mixers, oscillators, frequency converters, frequency doublers, attenuators, and phase shifters. Their low frequency noise could be the limiting factor to applications involving signal mixing and local signal generation (Ali & Gupta 1991). It has thus become common to examine the low frequency noise of any HEMT once it has been shown to have promising high frequency behavior.

The motivation for this study was twofold. The first was to develop a HEMT model that includes $1/f$ noise that would be useful in circuit design. This model, referred to as the discrete $1/f$ noise model, places all of the observed $1/f$ noise in one noise source at the input of the device. Application of the discrete $1/f$ noise model requires noise data measured for several values of drain voltage. Such low frequency noise spectra were published for an AlGaAs/GaAs HEMT (Tacano & Sugiyama 1991) and were chosen as the example for the discrete $1/f$ noise model.

The second motivation was to develop a noise model that would be helpful in understanding the $1/f$ noise sources within a HEMT by defining noise sources that reflect the physical processes actually taking place in the device. Three sources of noise that become dominant at low frequencies (0.01Hz to 100MHz) in HEMTs are quantum $1/f$ noise, generation-recombination noise (g-r noise), and thermal noise. Thermal noise is generated by the resistors representing the intrinsic and parasitic resistances of the HEMT

in the equivalent network. A model for thermal noise is integral to the circuit analysis program used. A noise source capable of simulating $1/f$ noise and another capable of simulating g-r bulge noise were developed. Any number of these sources could be distributed at various locations in the equivalent network model of a HEMT. For this reason, this model is referred to as the distributed $1/f$ noise model. Insight into the physical source of $1/f$ noise in HEMTs may be gained by examining the effect of varying the location, number, and properties of these noise sources. To accurately simulate the transfer of the noise to the output nodes of the device, the distributed $1/f$ noise model requires an accurate equivalent network for the HEMT being modeled. Since the device parameters, material properties, and layer structure necessary to determine the equivalent network as well as low frequency noise spectra were published for a GaInP/GaInAs/GaAs HEMT (Pereiaslavets 1997), this device was chosen to demonstrate the application of the distributed $1/f$ noise model.

HEMTs are based on the principle reported in 1969 that the mobility of electrons would be enhanced near a heterojunction, an interface between two semiconductors of different bandgaps (Esaki & Tsu 1969). The first working HEMT was demonstrated in 1978 (Dingle *et al.* 1978). The HEMT evolved from the GaAsFET. In both devices, electrons are provided by donor impurity atoms intentionally added to certain semiconductor layers. The flow of these electrons from source to drain is modulated by a voltage applied to the gate electrode. The devices act as voltage controlled current sources, in which small changes in gate voltage produce large changes in drain current.

The devices differ in where the source to drain current flows. In the FET, the electrons flow in a doped channel layer, thus experiencing scattering. In the HEMT, the electrons flow in a channel that is created in an undoped semiconductor that is on one side of a heterojunction. Since the electrons are physically separated from the donor ions, ionized impurity scattering is greatly reduced and mobility and velocity are enhanced. This makes the rf performance of HEMTs superior. HEMT development and operation are discussed in the following chapter.

In general, the term $1/f$ noise is applied to any fluctuating quantity whose spectral density, $S_v(f)$, varies as $1/f^{\beta}$ over many decades with $0.5 < \beta < 1.5$. There are many other common names for $1/f$ noise. When first observed in vacuum tubes, this noise was called flicker noise, possibly because of the flickering observed in the plate current. Other names are pink noise, semiconductor noise, current noise, and contact noise. Some researchers believed that the $1/f$ noise in resistors is due to the way the resistor's leads are connected, hence the term contact noise. The term pink noise is derived from the exponent of the power law, β, which is between the exponent corresponding to white noise, 0, and the exponent corresponding to red noise, 2.

$1/f$ noise gets its name from the characteristic of its spectrum. A $1/f$ spectrum means that the noise power varies inversely with frequency. Thus the noise voltage increases as the square root of the decreasing frequency. By decreasing the frequency by a factor of 10, the noise voltage increases by a factor of approximately 3. Since $1/f$ noise

has a $1/f$ power spectrum, most of the noise appears at low frequencies. This is why $1/f$ noise if often called low-frequency noise. Low-frequency noise has been measured as low as $6 \times 10^{-5}\,Hz$, which corresponds to just a few cycles per day (Motchenbacher & Connelly 1993).

Inverse power laws describe many natural phenomena. No electronic amplifier has been found to be free of $1/f$ fluctuations. The ubiquity of $1/f$ noise is discussed in the chapter on $1/f$ noise. $1/f$ noise is greater in HEMTs than in Si-based devices, a consequence of the smaller effective mass of GaAs than Si (Yngvesson 1991). Possible $1/f$ noise generation mechanisms in HEMTs include fluctuations in mobility and fluctuations in the number of carriers.

There are other motivations to understand $1/f$ noise. As circuits run on lower power, there is interest in decreasing the $1/f$ noise to maintain the signal-to-noise ratio. Since the intensity of $1/f$ noise rises before device failure, $1/f$ noise has been used as a device reliability indicator (Mladentsev & Yakimov 1993). Bandwidth narrowing techniques are often applied to improve signal/noise ratios. However, if the noise signal has a large $1/f$ noise component, simple low pass filtering does little good. The signal should be modulated, thus centering the bandwidth far enough from the $1/f$ noise present near dc (Horowitz & Hill 1994).

There are several methods to model devices and device noise. Among these are small signal analysis, analytical models based on device physics, numerical models, and CAD analysis. The section on HEMT noise modeling reviews the capabilities of several methods available, with emphasis on the circuit simulator, Micro-Cap, from Spectrum Software. Micro-Cap V was used to create both the discrete $1/f$ noise model and the distributed $1/f$ noise model. Micro-Cap is a member of the SPICE family of circuit simulators, all of which derive from the SPICE2 circuit simulator developed at the University of California, Berkeley, during the mid-1970's. SPICE is an acronym for Simulations Program with Integrated Circuit Emphasis. The development of SPICE was supported using US public funds, so the software is in the public domain. SPICE2 is not supported by U.C. Berkeley. This led to commercial versions of SPICE2 that have technical support. Micro-Cap is a commercial version for use on PCs.

Meyer, Nagel, and Lui (1973) show that with the specification of two additional parameters per transistor, AF and KF, $1/f$ noise in complex circuits can be efficiently analyzed by SPICE to give valuable circuit design information for BJTs and FETs. AF and KF are the $1/f$ noise exponent and coefficient in the expressions SPICE uses in its noise calculations. Since SPICE does not provide a HEMT model, SPICE's provision to simulate $1/f$ noise in a diode was used to create a $1/f$ noise model for a HEMT. The method used by Meyer *et al.* to extract the values of the two noise parameters for transistors was applied, with some modification, to extract the values of AF and KF from low frequency noise data to apply to SPICE's $1/f$ noise calculations for the diode. A

detailed description of this method is described in the chapter on the discrete $1/f$ noise model.

Data demonstrates how the superposition of g-r noise and $1/f$ noise occurs and where the thermal noise floor lies (Liu *et al.* 1985; Ali & Gupta 1991). The $1/f$ noise source and the g-r bulge noise source created for the distributed $1/f$ noise model can be used to simulate this superposition of noise sources. The corner frequency is strongly dependent on the magnitude of the transconductance and the series gate and source resistances (Ali & Gupta 1991). The resistances and transconductance in the equivalent network of the distributed $1/f$ noise model can be varied to simulate their effect on the total noise output. The implementation of such simulations is described in the chapter on the distributed $1/f$ noise model.

A potential enhancement to the distributed $1/f$ noise model would be to include a temperature dependence on the g-r noise bulge. For example, unlike quantum $1/f$ noise, g-r bulge noise is temperature sensitive. If there is a sufficiently wide range of time constants associated with the g-r centers, the spectral response of these noises becomes $1/f$-like for extended frequencies, and often they overshadow the quantum $1/f$ noise. When there is a discrete trap present, however, its contribution to the low frequency noise spectra becomes apparent in the form of a bulge. In the low-frequency spectra of HEMTs, these g-r noise bulges are common occurrences (Ali & Gupta 1991). When the temperature is lowered, g-r bulges move toward lower frequencies and their magnitudes

increase. When the temperature is raised, the bulge moves toward higher frequencies and the magnitude decreases. This temperature dependence can be used to characterize the related deep level trap energy and its capture cross-section (Ali & Gupta 1991). It would therefore be interesting to include a temperature dependence on the g-r noise source.

Another potential enhancement is to make provision for total and partial correlation of noise sources. Throughout this study, all noise sources were assumed to be uncorrelated. Models such as the Pucel-Haus-Statz noise model for MESFETs (Yngvesson 1991) considers partial correlation between the noise induced in the gate due to electrons in the channel and the noise current at the drain output node.

Chapter 2

HEMT development, fabrication, and operation

2.1 HEMT development

HEMTs are high-speed, high-frequency, low-noise devices. HEMTs evolved from GaAs MESFETs, which had been the transistor of choice for microwave systems. GaAs MESFETs combine the advantages of the high electron mobility and velocity of GaAs with the technology to make short gate lengths (<1um).

The speed of a device is a function of the time for electrons to travel from source to drain. To increase the speed further, electron transit time must be decreased via increasing electron velocity or by decreasing gate length. As the gate length is decreased, all transistor parameters must be scaled to avoid short channel effects. For GaAs MESFETs, this means increasing channel doping in order to decrease channel thickness while maintaining high conductivity in the channel. Increased doping results in increased impurity scattering which decreases mobility and peak velocity. The result is that GaAs MESFET improvements are limited to 50GHz for 0.25um gate lengths (Morgan &

Williams 1991). To achieve shorter transit times over these short distances, the donor impurity atoms must be removed from the electron's path to eliminate impurity scattering. HEMTs achieve this via a high quality, abrupt heterojunction between two compound semiconductors.

Heterojunctions are junctions formed between two compound semiconductors possessing different band gaps, such as AlGaAs and GaAs. This is in contrast to conventional Si-based and GaAs-based devices which utilize junctions between like materials, as *n*-type and *p*-type Si or *n*-type and *p*-type GaAs. A heterojunction permits the band structure as well as the doping level and type in the layers of the device to be varied, providing an additional degree of freedom in design. Significant improvements in charge transport properties have been developed using this additional degree of freedom.

The relative positions of the energy bands of an *undoped* AlGaAs/GaAs heterojunction are shown in FIG. 2.1. The Fermi levels are aligned. There is no band bending, because there are no, or few, free carriers since the AlGaAs is not doped. When only the AlGaAs is doped, the Fermi level of the *n*AlGaAs moves closer to the conduction band. This configuration, called modulation doping, results in conductive GaAs when electrons from the doped AlGaAs fall into the well and become trapped there. Mobile electrons generated by the donors in the *n*AlGaAs diffuse into the small band gap GaAs layer, moving the Fermi level above the conduction band in the GaAs near the interface, where they are prevented from returning to the *n*AlGaAs layer by the potential

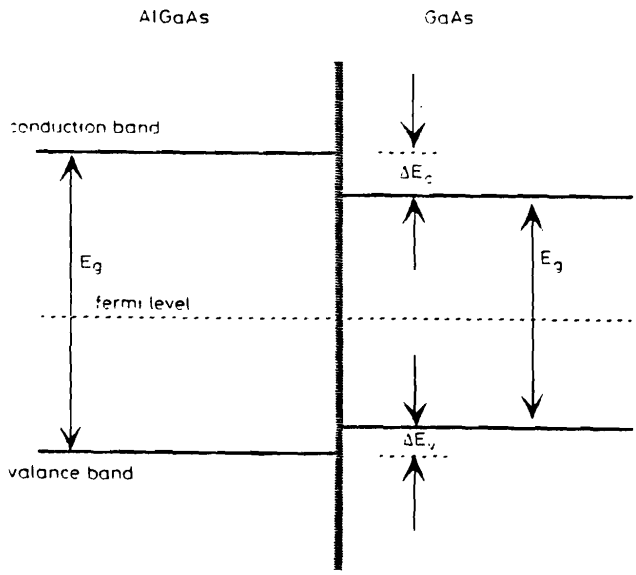

FIG. 2.1 Relative positions of the energy bands of an undoped AlGaAs/GaAs heterojunction (Streetman 1990)

barrier at the AlGaAs/GaAs interface. These electrons move to the GaAs conduction band, because it is at a lower energy. This electron movement causes the bands to bend as shown in FIG. 2.2. The electrons in the well form a two-dimensional electron gas, 2-DEG. Sheet carrier densities as high as 10^{12} electrons / cm^2 can be formed at a single interface.

The electrons are trapped in a thin layer very close to the gate (FIG. 2.3). This makes the region a very good conductor. The *n*AlGaAs above the 2-DEG, now depleted of free carriers, acts like an insulator. The 2-DEG constitutes the channel whose conductivity can be modulated by the gate potential. HEMTs are usually operated as depletion mode devices. This means that the HEMT is "on" when the gate voltage is zero (FIG. 2.4). If a positive voltage is applied to the drain while the source and gate are grounded, electron current will flow from source to drain. A voltage put on the gate will control the amount of current flow by changing the density of electrons in the 2-DEG channel. The degree of depletion in *n*AlGaAs is independent of the gate voltage. The *n*AlGaAs can be viewed as the dielectric of a capacitor with the gate and GaAs as the plates. A negative gate voltage will cause the 2-DEG density to decrease, thus modulating the source-to-drain current.

The electrons in the 2-DEG are spatially separated from the ionized donor centers, therefore there is no direct ion-electron interaction that would reduce electron mobility. This effect is especially important at low temperatures where lattice (phonon) scattering is no longer a significant noise source. Even though the electrons and donors are separated

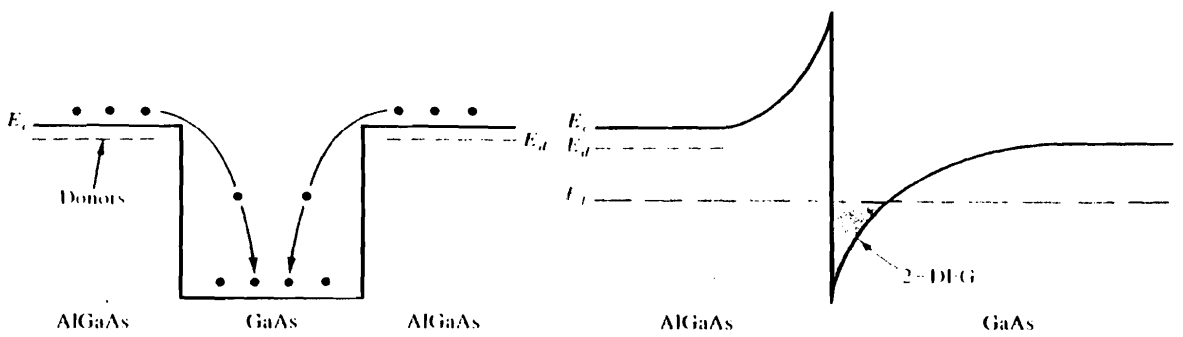

FIG. 2.2 Band bending and 2-DEG formation as a result of modulation doping of AlGaAs in an AlGaAs heterojunction (Streetman 1990)

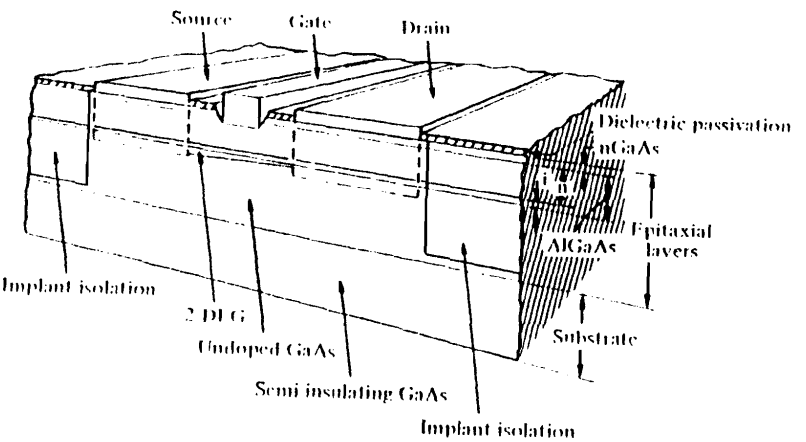

FIG. 2.3 Perspective view of a HEMT structure.
Electrons are trapped in a thin layer close to the gate (Pierret 1990).

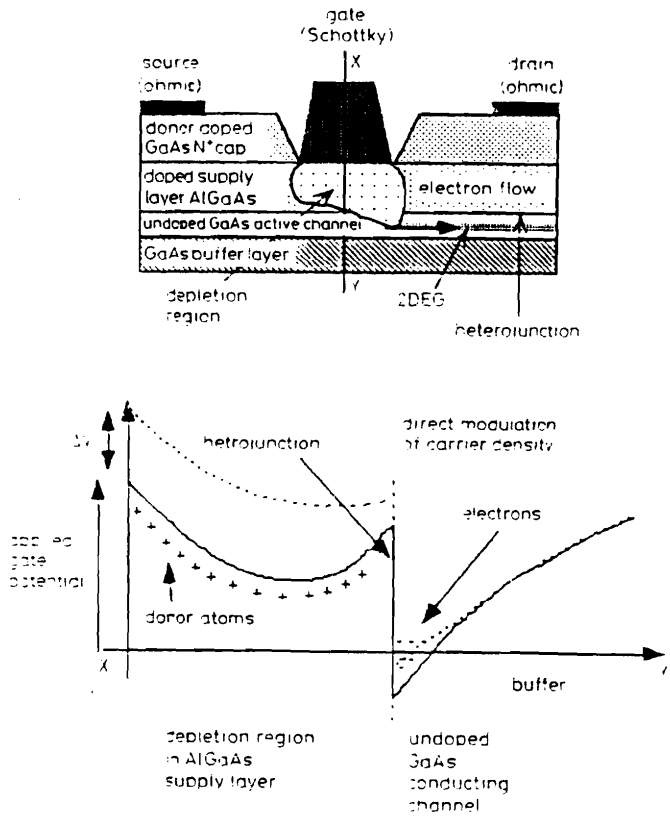

FIG. 2.4 HEMT operation as a depletion mode device (Morgan & Williams 1991)

spatially, their close proximity permits an electrostatic interaction resulting in Coulomb scattering. This scattering can be attenuated by placing a thin spacer layer of undoped AlGaAs between the *n*AlGaAs and GaAs to separate the negatively charged 2-DEG from the ionized dopant atoms. The electrons then interact only with the lattice defects present in the GaAs layer, mainly with the optical phonons at room temperature and with the acoustic phonons at temperatures below 100K. Because the electron-ion interactions are made so weak; the electrons in the channel can move very fast. Electron mobilities of $9000\ \mathrm{cm}^2 / \mathrm{V} \cdot \mathrm{s}$ at room temperature, $250{,}000\ \mathrm{cm}^2 / \mathrm{V} \cdot \mathrm{s}$ at 77K, and $2{,}000{,}000 \frac{cm^2}{V \cdot s}$ at 4K, with typical densities of 10^{12} electrons / cm^2 have been observed (Conti *et al.* 1992; Streetman 1991). In addition to enhanced mobility, the molecular beam epitaxy technology used to construct HEMTs permits structures with submicron gate lengths, resulting in reduced stray impedance in series and parallel with the channel and gate. This results in extremely high transconductance.

Several other names given to the HEMT by different research groups, each emphasizing one of the device's aspects, are shown in TABLE 2.1.

Acronym	Name	Device Aspect	Origin
HEMT	High Electron Mobility Transistor	Electron mobility	Fujitsu
MODFET	Modulation Doped FET	Epitaxial layer doping	Cornell University Univ.of Illinois, Rockwell
TEGFET	Two-Dimensional Electron Gas FET	Electron distribution	Thomson CSF
SDHT	Selectively Doped Heterojunctions Transistor	Epitaxial layer doping	AT&T Bell Labs

TABLE 2.1 Heterojunction field-effect transistor names and their origins

One of the unique attributes of compound semiconductors is the rich selection of semiconductors of the same lattice constant yet differing in band gap available for heterojunction fabrication, providing a broad selection and tuning range of desired characteristics. The HEMT was discussed above in terms of the AlGaAs/GaAs heterojunction. There are three types of commercially available HEMTs: the conventional HEMT (based on the AlGaAs/GaAs heterojunction), the pseudomorphic HEMT (based on the InGaAs/AlGaAs heterojunction), and the InP-based HEMT (based on an AlInAs/GaInAs heterojunction). The basic structures of these three HEMT types, shown in FIG. 2.5, are described below.

2.2 Conventional AlGaAs/GaAs HEMT

The conventional HEMT has unprecedented noise performance at cryogenic temperatures and good microwave and millimeter wave noise and power performance at

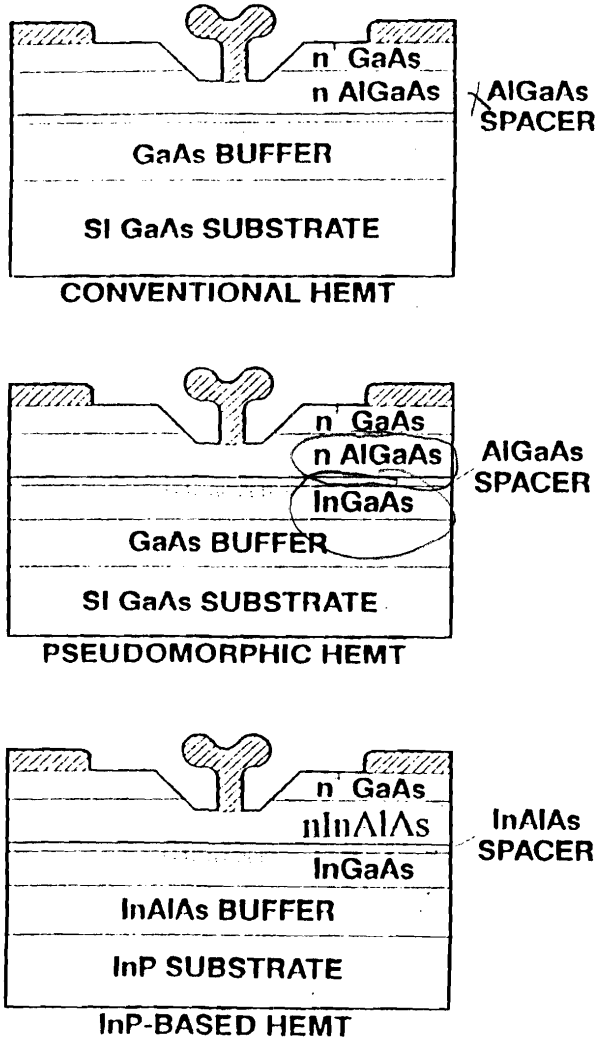

FIG. 2.5 Basic channel structure of the 3 types of commercially available HEMTs (Smith & Swanson 1989)

room temperature at frequencies from 1GHz to 60GHz. Cryogenic conventional HEMTs were used to receive and amplify signals from the Voyager 2 spacecraft during the Neptune encounter in August 1989 and are used in the 8GHz receivers installed on NASA's Very Large Array (Smith & Swanson 1989).

The main reasons HEMTs have surpassed GaAsFETs in noise performance have been their higher sheet charge density, electron mobility, and velocity in the undoped channel resulting in lower parasitic source resistance, higher transconductance, and their lower Fukui constant, as seen in the expression for the minimum noise figure of a HEMT (Fukui 1979),

$$F_{\min}(dB) = 10\log\left(1 + kfC_{gs}\sqrt{\frac{R_g + R_s}{g_m}}\right),$$

where k is the Fukui constant, which is an indication of material qualities as they relate to noise,

f is frequency,

C_{gs} is input gate capacitance,

R_g is the gate resistance,

R_s is the source resistance,

and g_m is the transconductance.

Another reason HEMTs are attractive for low noise applications is that $|S_{21}|$ is higher than for a GaAsFET of comparable size, giving increased gain. In addition, $|S_{22}|$ is

typically lower, facilitating wideband output matching, and hence increasing the transistor's gain-bandwidth product.

The HEMT also has a lower noise conductance, g_n, where

$$g_n = \frac{\langle |i_n|^2 \rangle}{4kT},$$

$\langle |i_n{}^2| \rangle$ is the equivalent input noise current,

k is Boltzman's constant,

and T is the absolute temperature.

The reduction of noise by lower noise conductance is indicated by the linear dependence of noise figure, F, on g_n (Rothe & Dahlke 1956),

$$F = F_{\min} + \frac{g_n}{R_{opt}} |Z_s - Z_{opt}|^2 .$$

In addition, a HEMT usually has a lower ratio of X_{opt} / R_{opt}, where $R_{opt} + jX_{opt}$ is the optimum source impedance, Z_{opt}. This makes it easier to provide a wideband noise match. To see this, consider the impedance transforming network at the input of an amplifier. The purpose of this network is to transform the source impedance, often $50 + j0\ \Omega$, into $R_{opt} + jX_{opt}$, the source impedance for which the transistor will exhibit its minimum noise figure. The network can therefore be designed as if it were an ordinary (power) matching network for a 50-ohm generator which must drive a load whose impedance is $R_{opt} - jX_{opt}$. Fano (1950) showed that, when the load is not purely resistive,

i.e. X is not zero, it is impossible to build a lossless network which will provide a perfect power match over a non-zero bandwidth. In particular, Fano showed that

$$\int_0^\infty \ln\left|\frac{1}{\Gamma}\right| d\omega \le \frac{\pi}{RC},$$

where Γ is the reflection coefficient between the generator and impedance-matching network,

R is the series load resistance,

and C is the series load capacitance.

The best utilization of the area under the curve $\ln|1/\Gamma|$ is obtained when $|\Gamma|$ is constant over the frequency range ω_a to ω_b and equal to 1 outside that range (Gonzalez 1984). It follows that

$$|\Gamma| = e^{-\pi/(\omega_b - \omega_a)RC},$$

$$|\Gamma| = e^{-\pi(Q_2/Q_1)},$$

where

$$Q_1 = \frac{X_C}{R},$$

and

$$Q_2 = \frac{\omega_o}{\omega_b - \omega_a},$$

where ω_o is the resonant frequency. Solving for the bandwidth,

$$\frac{\omega_b - \omega_a}{\omega_o} = \frac{R}{X_C}\left(-\pi \ln|\Gamma|\right).$$

Fano's integral relation applies to *power* matching, but it can be inferred that wideband noise matching is also made easier for lower values of the ratio X_{opt} / R_{opt}, since X_{opt} corresponds to the unavoidable reactance considered by Fano in power matching situations. (No one has yet derived an exact "Fano integral relation" for wideband noise matching).

The HEMT noise figure is also less sensitive to drain voltage or drain current variations than GaAsFETs. Unlike GaAsFETs, HEMTs can be designed to obtain the minimum noise figure close to I_{dss}, the device drain current with gate bias voltage of 0V, or maximum transconductance, g_m, for high associated gain, G_a, where

$$G_a = \frac{\text{power available from the "noise - matched amplifier"}}{\text{power available from the source}}.$$

Note that G_a involves the noise matched network while available power gain, G_A, refers to the power-matched network,

$$G_A = \frac{\text{power available from "power - matched network"}}{\text{power available from the source}}.$$

HEMTs possess some characteristics that are less desirable than GaAsFETs. They are not as linear and exhibit larger temperature dependence of g_m, noise figure, and gain.

Below 1GHz, $1/f$ noise causes the HEMT noise figure, F, to increase sharply. F is the ratio of the total output noise power density to the portion of that power density engendered by the resistive part of the source impedance. It is known that when donors are introduced into the AlGaAs, a significant fraction forms traps associated with the *n*-type doping known as DX centers (Ali & Gupta 1991). The origin of these centers is still subject to debate. They exhibit differing thermal emission and capture energies, large optical ionization energy, and multiple time constants of emission. The $1/f$ noise is strongly related to the DX center in the doped AlGaAs region. DX center problems are insignificant at room temperatures and do not affect device performance at high frequencies. At low temperatures, however, the DX center causes a collapse of the I-V characteristics, persistent conductivity effect, and threshold voltage shift.

The collapse of the I-V characteristic, shown in FIG. 2.6 (Tiwari 1992), occurs when accelerated electrons acquire sufficient energy to overcome the potential barrier and transfer back into the AlGaAs. This is termed the real space (as opposed to momentum space) transfer effect (Yngvesson 1991). These electrons will have a much lower velocity which results in a decrease of the transconductance as well as a lower speed for the device. When the carriers get trapped in the DX centers, the change in ionization state of the donors leads to a depletion of carriers at the drain end, the high-field region, and, hence a collapse of the I-V characteristics due to a larger resistance. The effect is time-dependent since the carriers can de-trap on time scales that can range from μs to times exceeding seconds depending on the temperature.

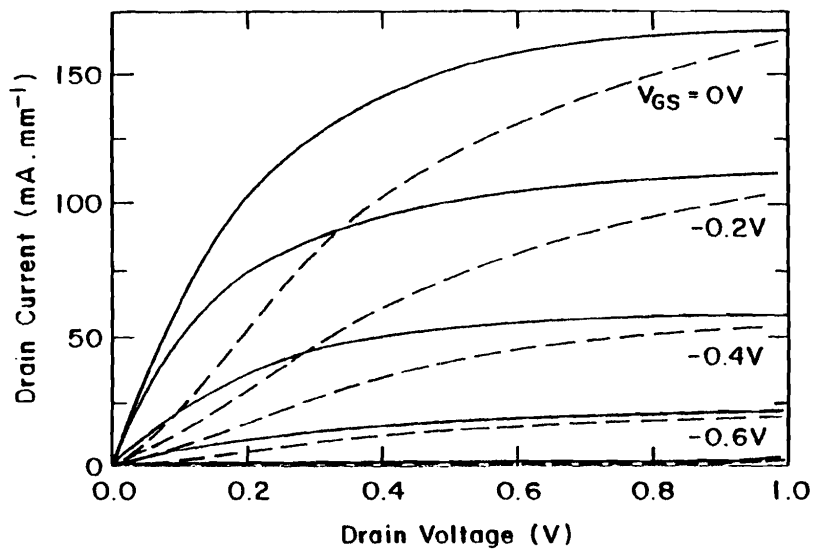

FIG. 2.6 Current-voltage behavior of HEMT at 77 K in the dark (dashed lines) and with light (solid lines). The dashed lines demostrate the collapsed I-V characteristic effect (Tiwari 1992).

The collapse of the I-V characteristic is also dependent on other excitation processes present and can be more pronounced at lower temperatures. In this case, electrons may be captured by traps in the AlGaAS and cause the I-V characteristics to collapse since the traps are deep enough that the electrons will not be released from them by thermal energy. In the dark, because the electrons have been captured by the DX centers, the density of the 2-DEG is lower, hence smaller currents and larger resistances exist in the channel. A remedy is to excite the electrons out of the trap by using visible light. FIG. 2.6 shows the I-V collapse effect in the dark and compares the same effect with illumination from a light source near the bandgap energy. Illumination recovers normal behavior. The trapping still takes place, but the DX centers emit electrons rapidly in the presence of light whose energy exceeds the optical ionization threshold energy (Tiwari 1992). A small LED is often used to provide this visible light (Yngvesson 1991). Additionally, these characteristics are a function of the AlAs mole-fraction and, secondarily, on the dopant species that gives rise to the DX center (Tiwari 1992).

HEMTs suffer from the persistent photoconductivity effect below 100K. The large time constants of capture and emission associated with the DX centers following shutting off optical illumination result in persistent photoconductivity. After photoemission of the captured electrons, there exists a larger electron population, both in the 2-DEG and in the AlGaAs, which will be recaptured with rather long time constants (Tiwari 1992).

It has been observed that the threshold voltage of HEMTs is a function of temperature. The shift in threshold voltage implies that DX centers trap electrons. The pseudomorphic HEMT, described below, shows negligible shift in threshold voltage, due to reduction in DX center concentration (Tiwari 1992).

Due to increased sensitivity to DX centers at low-temperatures, low doping levels or, since trap density increases with Al content, lower AlAs mole fraction are used for the AlGaAs donor layer. The resultant higher parasitic source resistance and lower g_m are insignificant and less important than the resultant increase in electron mobility and drift velocity.

Unfortunately, a higher Al fraction, x, in the $Al_xGa_{1-x}As$ is desirable because the bandgap discontinuity increases with Al content. The conduction band discontinuity, ΔE_c, at the $Al_xGa_{1-x}As$/GaAs heterojunction interface is related to x by

$$\Delta E_c = 0.806x$$

for $x<0.47$. A higher AlAs mole fraction results in an increase in total carrier density and reduces the real space transfer effect.

The associated gain decreases with increasing frequency. Since multistage noise figure is given by

$$F = F_1 + \frac{F_2 - 1}{G_1} + \frac{F_3 - 1}{G_1 G_2} + \ldots \qquad (2.1)$$

where F_i and G_i are the noise figure and gain of the ith stage, the second stage contribution to amplifier noise figure will increase with frequency. In order to operate above 60GHz, higher gain is required. One way to increase gain is to decrease the 0.5um-0.25um gate length of typical conventional HEMTs. However, proper scaling of the HEMT layer structure is also necessary to maintain sufficient gate-length/channel thickness ratio with good confinement of the channel electrons. This is difficult to accomplish in a conventional HEMT since hot carriers are injected into the GaAs buffer. As a result, it was found that 0.1um conventional HEMTs display high output conductance, poor pinchoff characteristics and poor rf performance. The pseudomorphic HEMT overcomes these problems, allowing extremely short gate lengths of 0.1um-0.15um.

2.3 Pseudomorphic InGaAs/AlGaAs HEMT

One way of improving HEMT performance is to use InGaAs as the 2-DEG channel material instead of GaAs. The benefits of using a thin InGaAs layer as the pseudomorphic channel include enhanced mobility, improved confinement of carriers in the quantum well channel, shorter gate length, and a larger conduction band discontinuity at the AlGaAs/InGaAs which allows even higher sheet charge density and higher current density and transconductance than possible with conventional AlGaAs/GaAs HEMTs. The thin (50-200 angstrom) layer of $In_xGa_{1-x}As$ (x=0.15-0.35) is inserted between the doped AlGaAs barrier layer and the GaAs buffer. There is a lattice constant mismatch between the InGaAs channel layer and the AlGaAs donor and GaAs buffer layers. The

strain from this lattice mismatch is taken up in the thin InGaAs quantum well. The InGaAs layer undergoes a distortion from its normal cubic crystalline structure such that this InGaAs layer is compressed to match the lattice of GaAs and AlGaAs. Because the thin InGaAs layer is unnaturally compressed to fit the structure of GaAs, it is termed "pseudomorphic".

Higher electron velocity and improved confinement results in higher g_m. Higher g_m results in a larger gain-bandwidth product, f_T, and higher forward transducer gain, G_T, which translates into higher power gain, G_P, where

$$G_T = \frac{\text{power delivered to the load}}{\text{power available from the source}}$$

and

$$G_P = \frac{\text{power delivered to the load}}{\text{power input to the network}}.$$

This permits pseudomorphic HEMTs to be used in higher frequency and broadband applications. They have a maximum frequency of oscillation, $f_{\max}$, of 350GHz and an f_T of 150GHz. This is the best performance reported for GaAs-based transistor devices (Ali & Gupta 1991).

Since its first millimeter wave demonstration in 1986 (Masselink *et al.* 1986) pseudomorphic HEMTs have been used in high frequency, low noise applications from 1GHz-100GHz. Their noise figures are comparable to conventional HEMTs as shown in TABLE 2.2 (Ali & Gupta 1991), but with an additional 1-2dB associated gain, G_a.

Higher gain is due to the enhanced mobility of electrons in InGaAs compared to GaAs, the larger conduction band discontinuity which allows higher 2-DEG density, and hence higher current, and improved confinement of carriers. The higher gain gives the pseudomorphic HEMT an advantage over conventional HEMTs at higher frequencies by reducing the second-stage contribution to amplifier noise figure. Noise measure, F_∞, is a special case of Equation (2.1). F_∞ is defined as the noise figure of an infinite chain of cascaded stages, each with the noise figure, F, and gain, G, of the HEMT,

$$F_\infty = F + \frac{F-1}{G} + \frac{F-1}{G^2} + \ldots = \frac{FG-1}{G-1}.$$

F_∞ is a useful device figure of merit, because a low-gain amplifier scores low even if its noise figure is good (Hagen 1996).

Device	Gate length (um)	F_{min} (db)	G_a (dB)	F_∞ (dB)
Pseudomorphic HEMT	0.25	1.8	7.2	2.13
Pseudomorphic HEMT	0.15	1.6	7.6	1.87
Pseudomorphic HEMT	0.08	1.9	9.2	2.11
Conventional HEMT	0.25	1.8	6.0	2.27

TABLE 2.2 60GHz Performance of GaAs-based Pseudomorphic and Conventional HEMTs

Simply reducing the gate length of a device does not guarantee better noise performance, because other parasitic elements can dominate. The data in TABLE 2.2 indicate that as gate length gets very small, F_{min} increases, which is a result of an increase

in gate resistance. At the same time, however, associated gain is improved by reducing the gate length. The increase in S_{21} and decrease in S_{12} obtained as a result of reducing the gate length increases the gain of the 0.08um gate length HEMT in spite of the increased gate resistance.

Pseudomorphic HEMTs have lower $1/f$ noise than conventional HEMTs. This is because of a lower AlAs mole fraction in the doped AlGaAs layer, The InGaAs channel has a lower band gap than GaAs, therefore a lower AlAs mole fraction can be used in the AlGaAs while maintaining the necessary conduction band discontinuity for a high sheet charge density. The lower AlAs mole fraction in the doped AlGaAs layer results in fewer traps which reduce I-V collapse and trap-related generation-recombination noise.

The conduction band offset, carrier concentration and carrier transport properties improve with higher InAs mole fraction in the pseudomorphic HEMT, so it is desirable to increase the InAs mole fraction. However, the lattice mismatch strain between the InGaAs and GaAs has limited how high the mole fraction can be made.

2.4 InP-based HEMT

The InP-based HEMT can be fabricated with GaInAs with a higher percentage of InAs than can be achieved in the pseudomorphic AlGaAs/InGaAs strained-layer growth on GaAs. These materials are grown on an InP substrate using $In_{0.53}Ga_{0.47}As$ to match the InP lattice. Pseudomorphic InP-based HEMTs are also possible if an InAs mole fraction other than 53% is used. Devices fabricated from GaInAs/AlInAs heterojunctions exhibit higher current gain cut-off frequency and lower noise figures than GaAs-based pseudomorphic HEMTs, as shown in TABLE 2.3 (Ali & Gupta 1991).

Device	Frequency (GHz)	F_{min} (dB)	G_a (dB)	F_∞ (dB)
GaAs Pseudomorphic	18	0.55	15.0	0.57
GaAs Pseudomorphic	60	1.6	7.6	1.87
GaAs Pseudomorphic	94	2.4	5.4	3.09
InP Lattice-Matched	18	0.3	17.1	0.31
InP Lattice-Matched	60	0.9	8.6	1.03
InP Lattice-Matched	94	1.4	6.5	1.73

TABLE 2.3 Noise Comparison of 0.15um GaAs-based pseudomorphic HEMT and InP-based HEMT

The most important advantage of the GaInAs/AlInAs heterojunction is the higher conduction band discontinuity, 0.5eV, compared to 0.25eV for the AlGaAs/GaAs heterojunction and 0.4eV for the GaInAs/AlGaAs pseudomorphic heterojunction. The higher conduction band discontinuity creates a higher 2-DEG concentration. A resultant

charge density of the order of $3.7 \times 10^{12} cm^{-2}$ coupled with a higher room temperature electron mobility in GaInAs leads to more than twice the conductivity in the channel. In the conventional AlGaAs/GaAs HEMT, the conductivity is limited by the relatively small conduction band discontinuity and by the difficulty in doping AlGaAs to very high concentrations due to problems with DX centers. AlInAs does not suffer from similar DX center problems.

The GaInAs/AlInAs HEMT has a large g_m even at low drain currents. Since devices are operated at the lowest current levels to minimize shot noise, the GaInAs/AlInAs HEMT allows operation at low drain currents without sacrificing gain.

The input circuit of the HEMT contributes the majority of the noise to the system because the noise appears amplified by g_m at the output. The AlInAs/GaInAs HEMT has a large advantage over GaAs-based HEMTs because its important noise sources are closer to the output. The extremely high conductivity of the 2-DEG caused by the large sheet charge density and mobility lowers the source resistance and the associated Johnson noise. The thermal noise from the gate metallization is reduced (as in most HEMTs) by using a T-gate structure which allows for a small gate footprint with a large feed section. This enables a low gate resistance and simultaneously a low gate capacitance. In the band structure, the large Γ - L valley separation reduces the intervalley transfer probability which leads to high channel velocities and high f_T. This results in reduced capacitive

coupling of input channel noise sources to the gate from where they can be amplified to the output.

The improved noise and frequency performance of the AlInAs/GaInAs HEMT indicates that it will be the preferred choice for low noise receiver applications in the millimeter-wave range (Ali & Gupta 1991). InP-based HEMTs do have some disadvantages, such as excessive gate leakage current and low gate-drain breakdown voltages.

2.5 GaInP/GaInAs/GaAs graded barrier HEMT

In addition to the three commercially available types of HEMTs described above, there is ongoing research fabricating HEMTs from other compound semiconductors. There is evidence that GaInP/GaInAs/GaAs pseudomorphic HEMTs can become the best devices for high power, high frequency, low noise applications (Pereiaslavets 1997). In an effort to avoid the limitations of AlGaAs, GaInP was substituted as the barrier material on GaAs substrates. This avoids the limitations of the Al mole fraction due to the DX centers and conduction band offset and eliminates certain processing complications caused by the presence of Al (Pereiaslavets 1997). GaInP is a promising barrier material for HEMT fabrication, because it can have a larger conduction band discontinuity than AlGaAs and the capability of increasing the energy separation between the bottom of the conduction band and the Fermi level by compositional grading the barriers.

The equivalent $1/f$ noise spectra shown in FIG. 2.7 is much lower for the GaInP/GaInAs/GaAs HEMT than that of the AlGaAs/GaInAs/GaAs HEMT, even though the Al concentration of the AlGaAs/GaInAs/GaAs HEMT is below 22% (Pereiaslavets 1997).

Two figures of merit for transistors are unity current gain, f_T, and maximum frequency of oscillation, f_{max}. f_T is the frequency for which the short-circuit current gain becomes 1 (also referred to as gain bandwidth product above). f_{max} is the maximum

frequency at which a device can amplify power. GaInP/GaInAs/GaAs HEMTs with 0.1um gate lengths achieved f_T over 100GHz and f_{max} over 250GHz (Pereiaslavets 1997).

The GaInP/GaInAs/GaAs pseudomorphic HEMT and its published $1/f$ noise spectra were chosen to demonstrate the application of the distributed $1/f$ noise model.

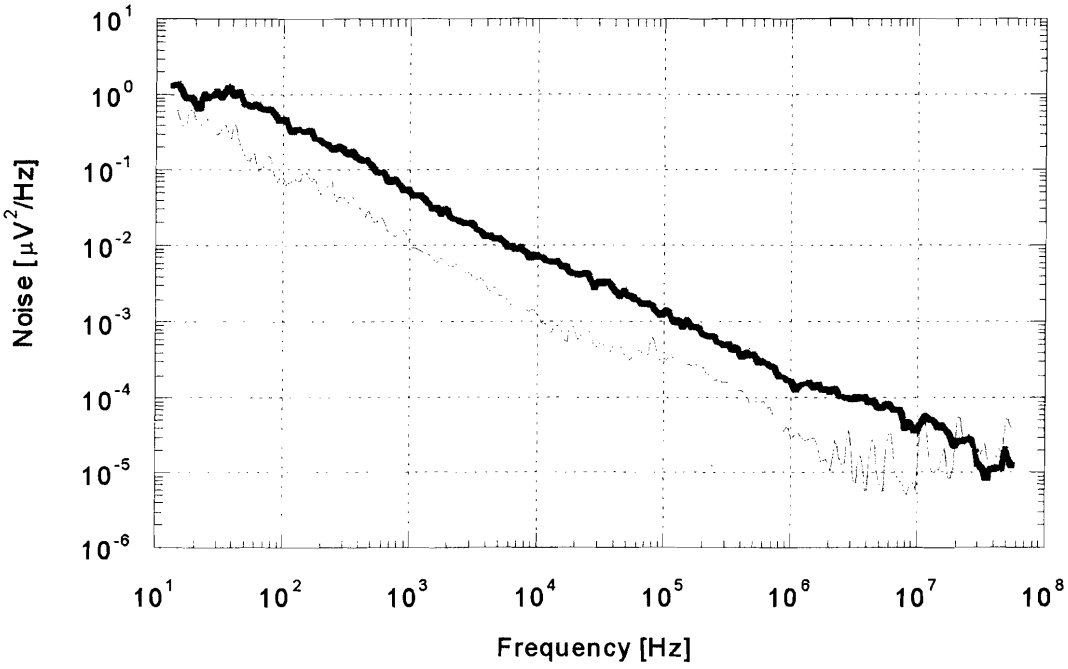

FIG. 2.7 Equivalent gate noise voltage spectra of GaInP/GaInAs/GaAS device (thin line) and for a AlGaAs/GaInAs/GaAs (thick line) device with the same gate length and width given for comparison (Pereiaslavets 1997).

Chapter 3

$1/f$ noise

> The universality of $1/f$ noise transcends the limits of electrophysics. Indeed, 1/f noise is present in the phase and frequency of all known frequency standards ... It has also been found in the flow rate of sand in an hourglass, the frequency of sunspots, the light output of quasars, the flow rate of the Nile over the last 2000 years, the central Pacific Ocean current velocities at a depth of 3100 meters, the flux of cars on an expressway, and in the loudness and pitch fluctuations of classical music.
>
> Peter H. Handel (1980)

3.1 Introduction

Self-similarity, or scaling, is a property of $1/f$ noise. Similarity underlies much of algebra. Homogeneous functions have a scaling property. These functions and their application to $1/f$ noise will be described. Many natural phenomena exhibit patterns that can be fit with homogeneous power functions. Examples of these will be given. Possible origins of low frequency noise in semiconductors are explored by examining low frequency noise in HEMTs.

3.2 Algebra of self-similarity

Homogeneous power functions are often used to describe nature. A homogeneous power function is described as a function where

$$f(x) = cx^{\alpha},$$

where c and α are constants (Schroeder 1991).

These functions are self-similar. Qualitatively, self-similarity can be described as appearing the same over all ranges of scale. Quantitatively, when something is self-similar, if x is rescaled (multiplied by a constant), then $f(x)$ is still proportional to x^{α}, with a different constant of proportionality. Homogeneous functions reproduce themselves upon rescaling. Scaling invariance results from the fact that homogeneous power laws lack natural scales (Schroeder 1991).

3.3 Ubiquity of power laws

Data from many natural phenomena follow homogeneous power laws with the form f^{-n} as functions of frequency. Some phenomena include plant genera populations, journal articles, cardiac pulse frequencies, word lengths, and annual income. FIG. 3.1 displays these sociobiological examples (West & Schlesinger1990). FIG. 3.2 displays spectral density measurements of pitch variations in various types of music and their correlations to $1/f$ noise (Voss & Clark 1978). Similar spectra are obtained for loudness fluctuations (Gardner 1978).

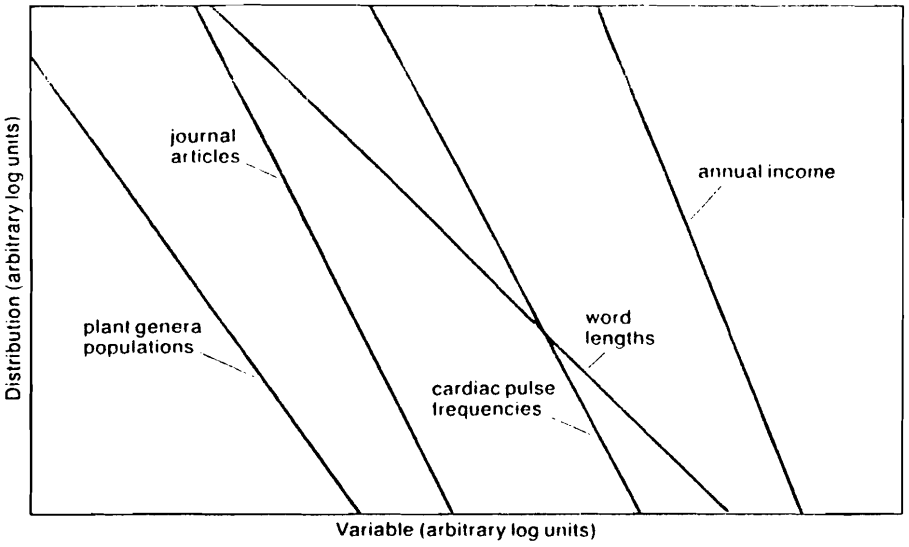

FIG. 3.1 Sociobiological examples of inverse power laws (West & Schlesinger 1990)

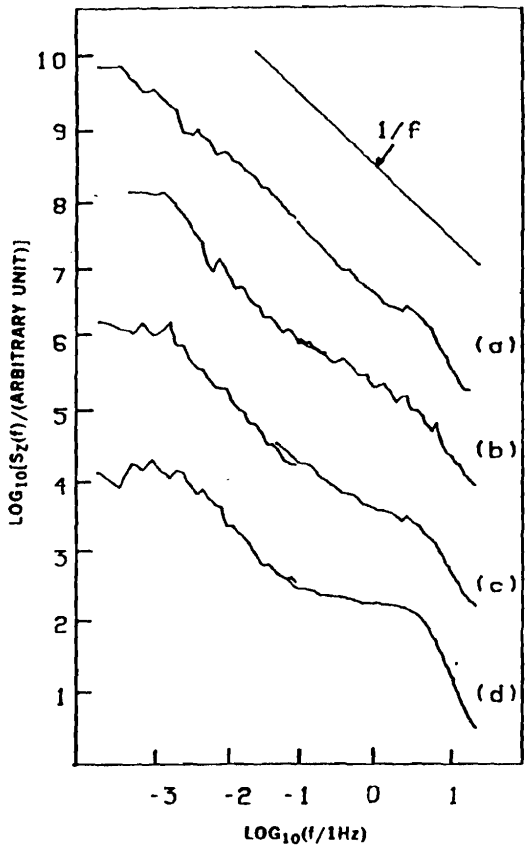

FIG. 3.2 Spectral density of pitch fluctuations for four radio stations (a) classical (b) jazz and blues (c) rock (d) news and talk (Voss & Clark 1978).

Many objects that occur in different sizes have a self-similar power law distribution of their relative abundance over large size ranges. The mean frequency with which different kinds of interplanetary objects enter the earth's atmosphere is inversely proportional to the squared diameter of the projectile as shown in FIG. 3.3 (Schroeder 1991).

Little is known about the physical origins of $1/f$ noise, but it is found in many physical systems including electrical noise in electronic components, in all time standards from atomic clocks and quartz oscillators to the hourglass, in ocean currents and the changes in yearly flood levels of the Nile, in traffic patterns, variations in sunspots, the wobbling of the earth's axis, and in music. Uncertainties in time measured by an atomic clock are $1/f$. The error is 10^{-12} regardless of whether one is measuring an error on a second, minute, or hour (Schroeder 1991).

3.4 Noise

The power spectrum of a statistical time series is often called noise. The power spectrum is the squared magnitude of the Fourier transform of the noise levels. Analysis of noise yields scaling properties. Noise can be defined as unpredictable changes in a quantity, V, varying in time, t. Noise can be analyzed in both the time and frequency domain. The space and time of homogeneous spectra exhibit scaling invariance. If the process is compressed by a constant factor, the corresponding Fourier spectrum is

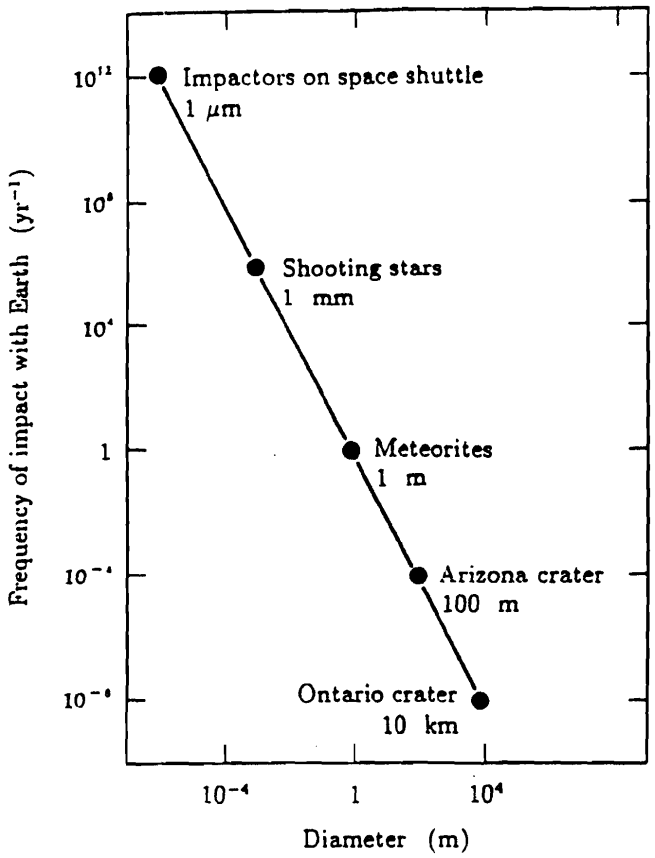

FIG. 3.3 Frequency of meteor collisions with earth in relation to particle diameter (Schroeder 1991)

expanded by the reciprocal factor. Changing the frequency scale by any constant factor does not change the frequency dependence of power law spectra. This scaling invariance can be seen in the distribution of heartbeat frequencies displayed in FIG. 3.4 (Schroeder 1991).

Plots of three types of noise, white, $1/f$ and Brownian (or $1/f^2$) displayed in the time domain can be viewed in FIG. 3.5. The traces made by each of these types of noise is a fractal curve. As will be described below, the dimension of a fractal is not an integer. A fractal curve, a nominally one-dimensional object in a plane which has two dimensions, has a fractal dimension that lies between one and two. The names 'white noise', '$1/f$ noise', and '$1/f^2$ noise' refer to the spectral distribution of the noise. Spectral density, $S_v(f)$, is used to estimate the mean square fluctuations at frequency f of variations over a time scale of order $1/f$. Noise can be studied in the frequency domain by plotting $S_v(f)$ vs f. The logarithmic slope is the fractal dimension. Frequency domain plots of the three time domain plots referred to above can be viewed beside their corresponding time domain plot in FIG. 3.5.

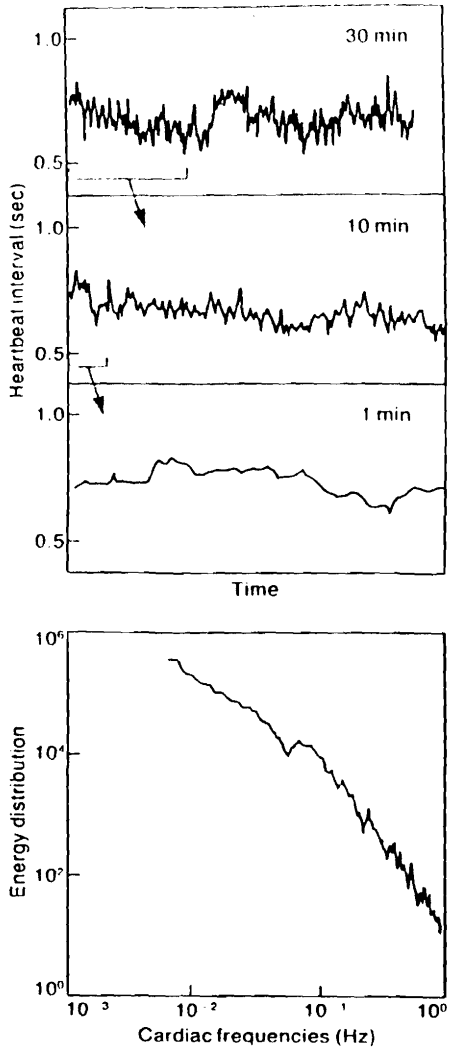

FIG. 3.4 Scaling invariance of heartbeat frequencies (Schroeder 1991)

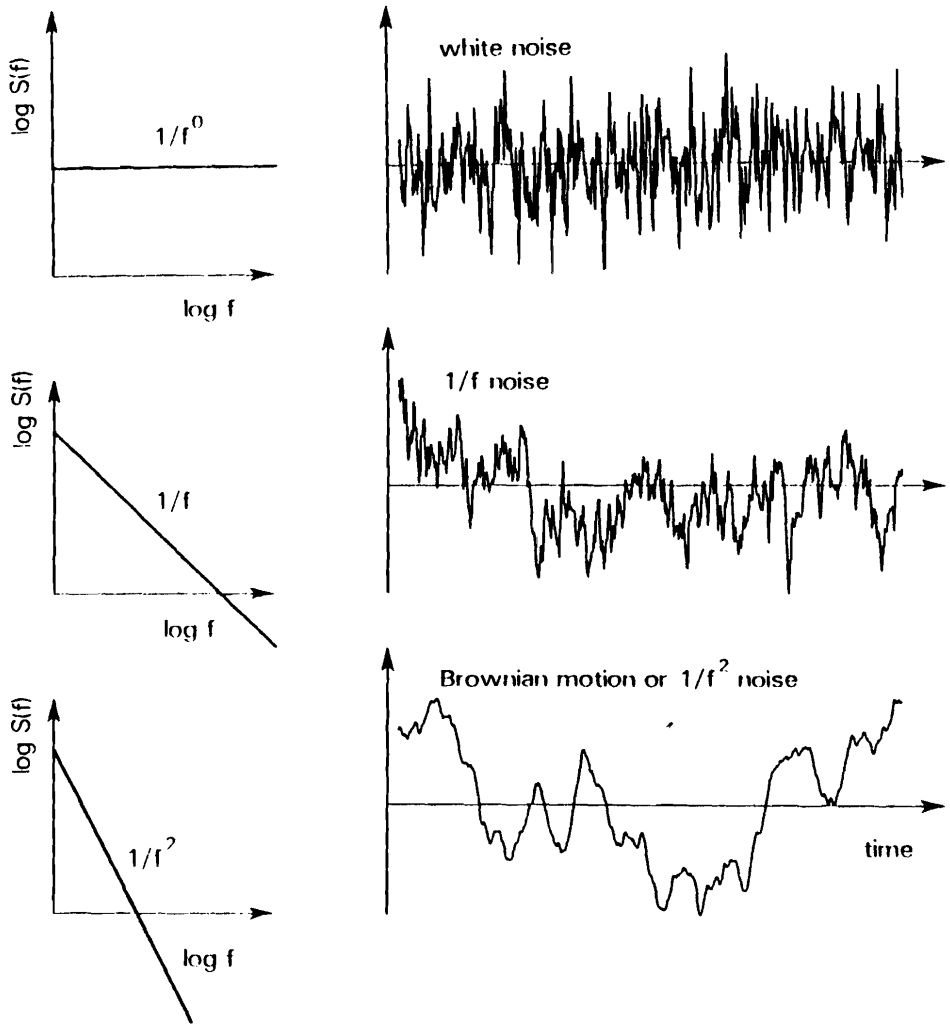

FIG. 3.5 Frequency domain plots and their corresponding time domain plots for white, $1/f$ and $1/f^2$ noise (Peitgen, *et al.* 1988)

The analogy between fractal dimension in space and time can be viewed as follows:

For spatial fractals (Schroeder 1991; Peitgen, *et al.*), the relationship

$$N(r) = \frac{1}{r^D}$$

is used, where *N(r)* is the number of identical parts, each of which was scaled down by a ratio r. The fractal dimension, D, is

$$D = \lim_{r \to 0} \frac{\log(N)}{\log \frac{1}{r}}.$$

For temporal fractals, the relationship

$$S_v(f) = \frac{1}{f^\beta},$$

is used, where $S_v(f)$ is the amount of noise at a particular frequency, and f is the particular frequency. The dimension, β, is

$$\beta = \lim_{f \to 0} \frac{\log S_v(f)}{\log \frac{1}{f}}.$$

Of the three types of noise mentioned above, white noise is the most random. Its spectral density is a straight line, and therefore $\beta = 0$, This indicates an equal amount of power at all frequencies. Brownian noise is derived from Brownian motion or a random walk. For this type of noise, $\beta = 2$. This is the most correlated of the three. $1/f$ noise was named after the functional form of its spectral density. In general, the term $1/f$ is applied to any fluctuating quantity, *V(t)*, with $S_v(f)$ varying as $1/f^\beta$ over many decades with $0.5 < \beta < 1.5$ (Schroeder 1991).

It has been proposed that $1/f$ spectra makes pleasing music because it is intermediate between randomness and predictability. In a white noise process, every value is completely independent of the previous one. In a Brownian distribution, only the increments are independent of the past, which may yield a boring tune. Voss (Gardner 1987) used measured $1/f$ noise from a transistor to generate a random tune, and it turned out to be more pleasing than tunes based on white and brown noise sources.

Both white and $1/f^2$ noise are well-understood in terms of mathematics and physics. The origin of $1/f$ noise is poorly understood, yet it represents the most common type of noise found in nature. There are no simple mathematical models that produce $1/f$ noise other than the assumption of a specific distribution of time constants (Schroeder 1991). Discussions of the occurrence of inverse power laws in electrical noise follow.

3.5 Electrical noise

There are electrical examples of each type of noise mentioned above (FIG. 3.6). Thermal noise (also known as Johnson noise or Nyquist noise) and shot noise are examples of white noise. These follow a $1/f^0$ power law. There is the same amount of power in all frequencies due to these types of noise. The cause of electrical white noise is well-understood. Thermal noise is found in any resistive material. The charge distribution over a device is not uniform, because charge carriers are in constant thermal motion. This causes fluctuations in the potential across the device. Shot noise arises because current is

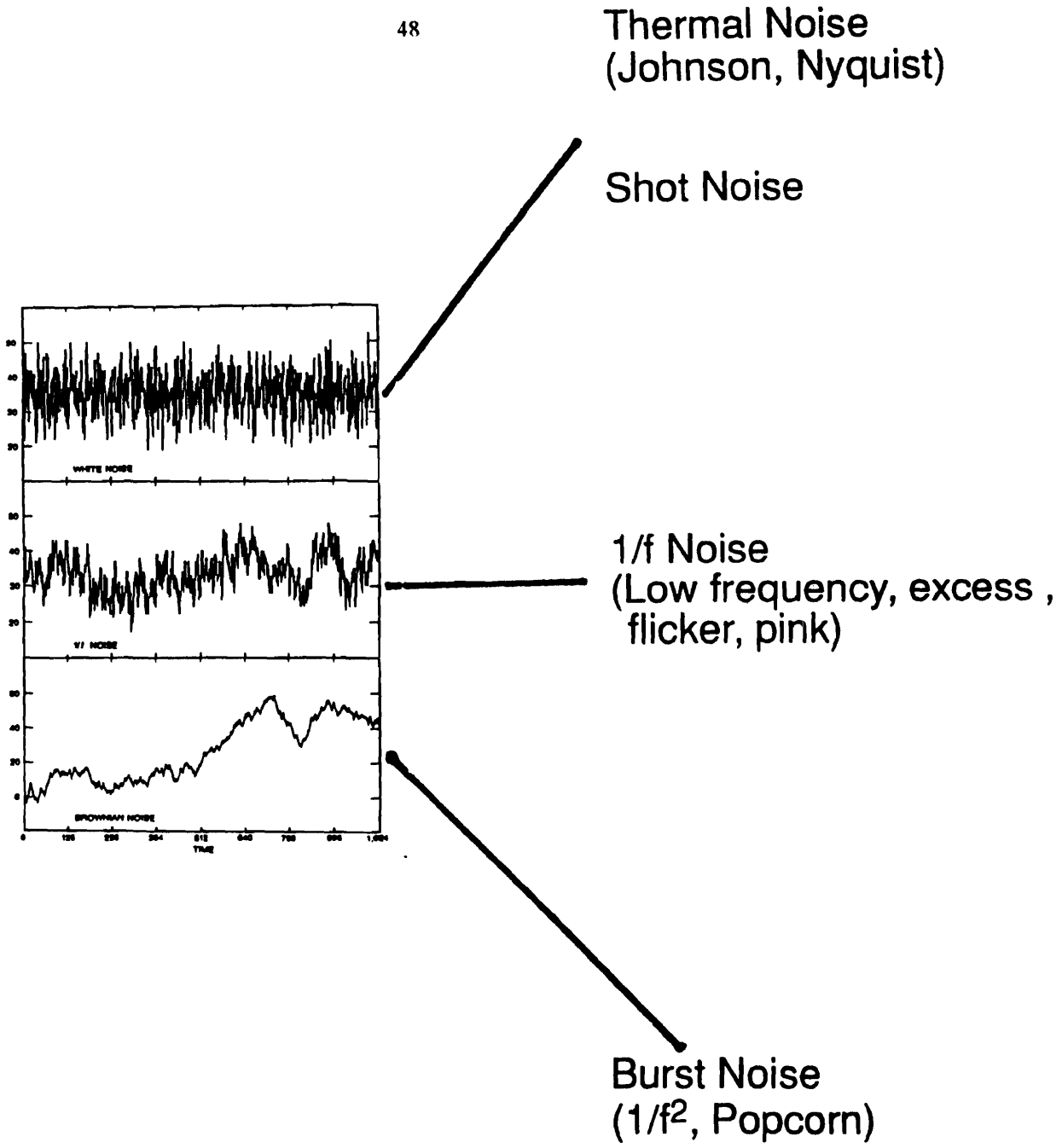

FIG. 3.6 Electrical examples of white, $1/f$, and $1/f^2$ noise (Peitgen, *et al.* 1988)

not a smooth continuous flow of charge. It is the sum of pulses of current caused by electrons and holes, each causing an impulse of current (Motchenbacher & Connelly 1993).

$1/f^2$ noise (also called burst noise or red noise) is evidenced by a burst of current on the order of 1uA and a few ms in duration. It may be explained by a modulation mechanism with a few carriers controlling the larger carrier flow. It also may be caused by material defects (Motchenbacher & Connelly 1993).

Almost any resistor through which current is flowing exhibits voltage fluctuations with a power spectral density inversely proportional to frequency. This $1/f$ noise is also called excess noise, because it is present in addition to the thermal noise of a resistance, which is always present. It is superimposed on the white noise.

Just as $1/f$ noise phenomena, in general, are not well understood, neither is $1/f$ electrical noise understood. Several mechanisms have been described, but none are universally accepted. Two features of $1/f$ noise are especially interesting. First, its near ubiquity suggests that at least some feature of the explanation should not depend on detailed models of particular materials. The form of the noise spectrum is about the same in metals, semiconductors, semimetals, and Josephson junctions (Weissman 1988). Second, the spectral form is nearly scale invariant.

One possible reason for the ubiquity of $1/f$ noise is its origin from parallel relaxation processes which abound in nature (Schroeder 1991). In a relaxation process, the trapped particle enters an excited state, where it remains for an exponentially distributed time interval with relaxation time τ. In many systems there exist a spectrum of relaxation times that depend on the energy barriers present in the system. The result of analyzing the superposition of these relaxation times is that the resultant interval is generally very wide, indicating a hyperbolic decay.

Overall, a detailed look at $1/f$ noise in a variety of materials fails to confirm the initial impression of universality. Even in semiconductors, there is some evidence of variety in the origins of the noise. In the case of metals, another class of $1/f$ noise-making materials, a unitary cause is even less likely. Whether the ubiquity of $1/f$ noise implies a universal cause clearly requires further investigation (Weissman 1988).

3.6 Low frequency noise in materials

In general, the term $1/f$ noise is applied to any fluctuating quantity whose spectral density, $S_v(f)$, varies as $\frac{1}{f^{\beta}}$ over many decades with $0.5 < \beta < 1.5$. In the case of high electron mobility transistors (HEMTs), the varying quantity is current or voltage.

Based on measurements on a number of materials, Hooge (Hooge 1969, 1976, 1981) postulated the following empirical relationship:

$$\frac{S_i(f)}{\bar{I}^2} = \frac{\alpha_H}{f\bar{N}},$$

where S_i is the spectral intensity of the 1/f noise current,

$\bar{I}$ is the average current,

$\bar{N}$ is the average number of charge carriers,

and α_H is the Hooge parameter.

Hooge found α_H to be a constant equal to 2×10^{-3}. Recent research has indicated that other values of α_H are required to describe different types and quality of materials. Smaller values of α_H generally apply to smaller devices (Yngvesson 1991). This may be important for HEMTs, since HEMTs have very short gate lengths. There is also evidence that there is a universal limit for how small α_H can be in a given material, based on the theory of quantum $1/f$ noise (Handel 1975, 1980).

First $1/f$ noise in a resistor or bulk piece of semiconductor will be considered. The resistance, R, is (Van de Ziel 1986)

$$R = \frac{L}{wt} \cdot \frac{1}{qn\mu},$$

where L is the length,

w is the width,

t is the thickness,

n is the number of electrons/cm^3,

q is the electronic charge,

and μ is the mobility.

Fluctuations in the resistance can come about via fluctuations in either μ or n, termed mobility fluctuation noise, $S_\mu(f)$, or number fluctuation noise, $S_n(f)$. The total spectral noise density may be expressed as the sum of these (Yngvesson 1991),

$$S_{total}(f) = S_\mu(f) + S_n(f).$$

It has been shown that mobility fluctuations may result in $1/f$ noise. The carrier mobility will show random variations due to the scattering processes which the carriers undergo. This phenomenon is central to the quantum $1/f$ noise theory (Handel 1975, 1980).

Number fluctuations noise may be due to electrons being randomly absorbed and reemitted by traps in the semiconductor, either at the surface or in the bulk. This is termed generation-recombination noise, or g-r noise. If a number of different traps exist with an appropriate distribution of time constants, a frequency dependence which is close to $1/f$ could be simulated.

Quantum $1/f$ noise and g-r noise will be discussed below.

3.6.1 Quantum $1/f$ noise

Quantum $1/f$ noise is generated whenever charged particles are accelerated or decelerated. Some of the particles emit very low frequency radiation, bremsstrahlung radiation, of frequency $F \approx 10^{-4} - 10^{4}\,Hz$ (Van der Ziel 1986). Since the energy per photon is hf, and the energy per unit Hz is a constant for bremsstrahlung radiation, N, the number of photons per unit Hz, will be proportional to $1/f$. This bremsstrahlung part of the beam modulates the rest of the electron beam producing a $1/f$ noise spectrum.

The Hooge parameter can be derived in terms of the average change in velocity, v, for the scattering event the electrons go through,

$$\alpha_H = \frac{4\alpha}{3\pi}\left(\frac{\overline{\Delta v^2}}{c^2}\right).$$

where α is the fine-structure constant (α =1/137). For an elastic scattering process, one can show that $\overline{\Delta v^2} = 2\overline{v^2}$. Since $\overline{v^2} = 3kT/m^*$,

$$\alpha_H = \frac{4\alpha}{3\pi}\left(\frac{6kT}{m^* c^2}\right)$$

where m^* is the effective mass

k is Boltzman's constant,

T is the absolute temperature,

c is the speed of light.

For a given material, the strength of the $1/f$ noise is inversely proportional to the effective mass. This result agrees with the observation that Si devices have much lower $1/f$ noise than GaAs devices, for the effective mass of GaAs is smaller than the effective mass of Si. Van der Ziel *et al.* (1985) compared experimentally measured and predicted Hooge parameters for several Si and GaAs devices (TABLE 3.1).

Device	Experimental α_H	Theoretical α_H
Silicon MOSFET *p*-channel	$3\times10^{-7}-9\times10^{-7}$	$8.8\times10^{-8}-8.3\times10^{-7}$
Silicon MOSFET *n*-channel	2.9×10^{-6}	2.2×10^{-8}
Silicon JFET *n*-channel	2.5×10^{-8}	2.2×10^{-8}
NEC GaAs MESFET	2×10^{-4}	7.1×10^{-6}
GaAs MESFET MBE	5.6×10^{-6}	7.1×10^{-6}

TABLE 3.1 Representative values of the Hooge-parameter (α_H) for several devices at T=300*K*

There is agreement for some and, when there is disagreement between experiment and theory, the experimental value is always the largest. This may imply that in the cases where the experimental Hooge parameter is larger than what the quantum model predicts, other processes are contributing to the $1/f$ noise. These other processes could be attributed to traps. In the cases where there is the least disagreement between experiment and theory, the material tested was high quality, therefore more likely to be freer of traps than the others. Quantum $1/f$ noise is often regarded as the lower limit for $1/f$ noise. Van

der Ziel suggests that the measured $1/f$ spectrum is the superposition of quantum $1/f$ noise, g-r noise, and thermal noise, as shown in FIG. 3.7.

Similarly, Liu *et al.* (1985) measured equivalent gate noise voltage spectra of 1um gate-length HEMTs for the frequency range of 0.01Hz-100MHz. They found that the noise consists of several high intensity trap-related g-r noise components superimposed on background $1/f$ noise. The g-r noise is reduced as the Al mole fraction was lowered. At 100K the g-r noise bulge moves towards subaudio frequencies clearly revealing the quantum $1/f$ noise (FIG. 3.8).

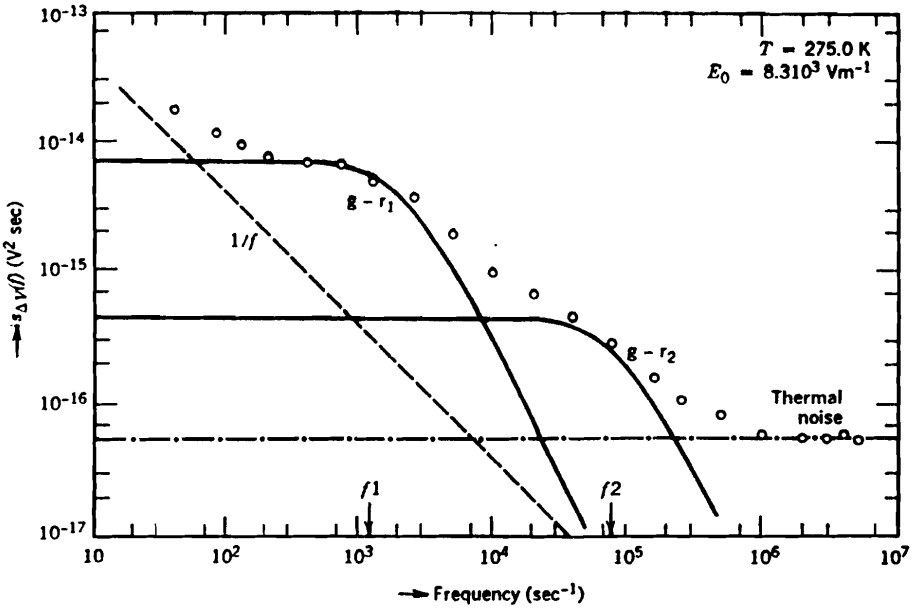

FIG. 3.7 Superposition of a $1/f$ noise spectra, two g-r spectra, and thermal noise spectra. The open circles represent experimental data. (Van der Ziel 1986)

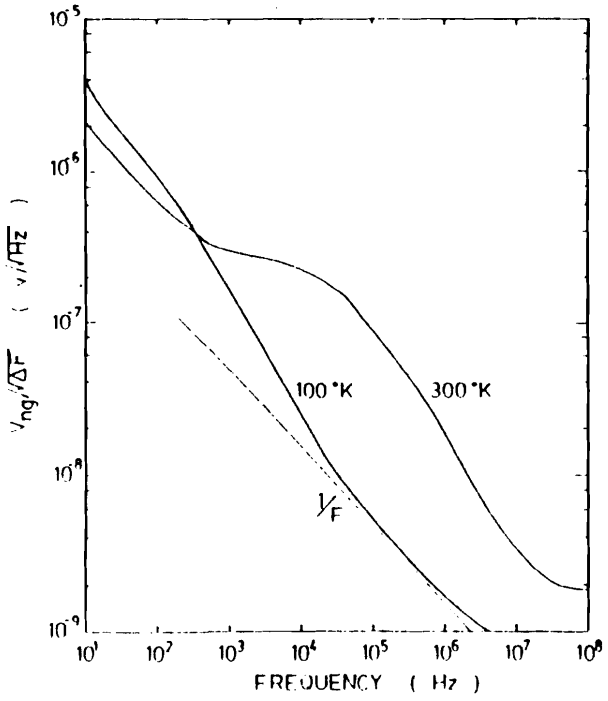

FIG. 3.8 Reduction of g-r noise bulges as temperature is reduced, revealing quantum 1/*f* noise for an AlGaAs/GaAs HEMT (Liu, *et al.* 1985)

3.6.2 g-r noise

All amplifying devices exhibit $1/f$ noise. Ali and Gupta (1991) describe how the origin and magnitude depend on the type of device. The continuum of surface states is believed to cause $1/f$ noise in Si MOSFETs. Multiple deep level traps cause $1/f$ noise in JFETs. Deep level traps within the emitter-base space charge region and the presence of surface states on the surface of the base near the emitter-base junction have been proposed as the cause of $1/f$ noise in BJTs. In addition to these traps and continuum of surface states, it has been suggested that current carried by a beam of electrons and scattered from an arbitrary potential barrier exhibits fluctuations with a $1/f$ spectrum. The scattering process has a $1/f$ noise coefficient, α_H. In n-type Si, $\alpha_H = 2.2E-8$. In n-type GaAs, $\alpha_H = 7.1E-6$. A nearly constant value of $\alpha_H = 3-4.5E-8$ has been determined from conventional HEMTs with effective gate lengths of 0.2 to 1.1um.

In semiconductors with nonideal crystalline structures and defects, the $1/f$ noise coefficient is expected to be higher than that in ideal materials. When traps with discrete energy levels are present in high concentrations, the background $1/f$ noise can become submerged in the trap-related g-r noise. Defects in heterointerfacial layers, in quantum wells, and superlattice structures, as used in the designs of many HEMT structures, can cause discrete or narrowband noise bulges in the device's low frequency noise spectrum. Unlike the background $1/f$ noise, these are temperature sensitive. When the temperature is lowered, the g-r bulges move along the frequency axis towards the lower frequencies and their magnitudes increase. When the temperature is raised, the bulge moves toward higher

frequencies and the magnitude decreases. This temperature dependence can be used to characterize the related deep level trap energy and its capture cross-section. This is an example of how the study of $1/f$ noise may give insight into the physics of devices (Ali & Gupta 1991).

There are three components of drain noise current in HEMTs (Ali & Gupta 1991). These three components are the thermal, the g-r, and the $1/f$ noise sources. There is also thermal noise associated with the series resistances. As will be done in the model developed, the frequency dependence of the noise sources in HEMTs can be studied by reflecting the noise to the gate terminal and measuring the composite noise voltage as a function of frequency.

Chapter 4

CAD for noise analysis

"If I had influence with the good fairy who is supposed to preside over the christening of all children I should ask that her gift to each child in the world be a sense of wonder so indestructible that it would last throughout life, as an unfailing antidote against boredom and disenchantment of later years, the sterile preoccupation with things that are artificial, the alienation from the sources of our strength."

Rachel Carson

4.1 Noise modeling

Although HEMTs continue to set records for noise performance, a noise model that can be helpful in understanding noise sources within a HEMT and at the same time be useful in circuit design has not really emerged (Pospieszalski 1989). The published studies of noise properties of FETs may be divided into two groups. The first group uses an analytical approach which considers fundamental equations of transport in semiconductors. The second group uses a more empirical approach, addressing the issue of what needs to be known about the device in addition to its equivalent circuit to predict the noise performance. Both approaches may yield parameters useful for CAD of circuits containing HEMTs.

4.1.1 Analytical models

The first group's models range from purely analytical to fully two-dimensional analysis. HEMT operating and noise models have been based on a self-consistent solution of Schrodinger and Poisson's equations (Ando & Itoh (1990); Anwar & Liu (1994); Ahn & Nokali (1994)). DasGupta & DasGupta (1993) formulated a new analytical expression for variation of sheet carrier concentration in the 2-DEG as a function of the applied gate voltage for HEMT modeling.

HEMTs are innately two-dimensional devices (Ladbrooke *et al.* 1993). With 1 or 2V applied to the drain, the electrons in the 2-DEG acquire energy in excess of the thermal lattice energy. Electron scattering into the higher-energy valleys in GaAs gives rise to a mean carrier velocity that is a highly non-linear function of the x and y components of the two-dimensional electric field. Tan *et al.* (1994) describe a two-dimensional simulation that solves Poisson's equations. Dollfus et al (1992) applied the particle ensemble Monte Carlo technique to take into account a two-dimensional potential distribution and real-space transfer. Ahmad-Shawki, *et al.* (1990) applied hydrodynamic equations to two-dimensional HEMT modeling. Fully two-dimensional approaches using Monte Carlo techniques or hydrodynamic equations require very long computation times.

Simulators which use a fine mesh, referred to as micro-mesh simulators, apply exactly the same equation throughout the entire device Only when the overall solutions

are obtained does the simulator recognize that some regions are depleted of electrons, others contain cool electrons, and yet others hot electrons.

In an effort to be more accurate than the purely analytic models yet avoid the long computation times required for the fully two-dimensional approaches, a quasi-two-dimensional (Q2D) approach was developed named HELENA, for HEMT ELEctrical properties and Noise Analysis (Happy *et al.* 1993). In the Q2D approach, the device is divided in slices. In each slice, the appropriate electron transport law is combined with a charge control law and Poisson's equation to give a quadratic equation for the longitudinal electrical field for each slice from source to drain. HELENA provides for inclusion of the effects of DX centers in the case of AlGaAs layers as well as strain effects in the case of pseudomorphic materials. The resultant small-signal and noise parameters may be applied to the CAD of HEMT circuits.

4.1.2 Empirical models

Several empirical models exist which include the noise figure with equivalent circuit parameters. The Fukui noise model (1979), an empirical model, relates minimum noise

figure and device equivalent circuit parameters, such as tranconductance, gate-to-source capacitance, source and gate resistances, finding the best fit values of associated coefficients. The Pucel-Haus-Statz (PHS) model requires three independent noise

coefficients to be known in addition to the small signal parameters of the device to predict the noise.

Pospieszalski (1989) models noise properties of HEMTs from direct measurements of the device's noise. From such data the four noise parameters, minimum noise temperature, $T_{\min}$, optimal source impedance, $R_{opt} + jX_{opt}$, and noise conductance, g_n, are determined. They are functions of the elements of the small-signal equivalent circuit and two frequency independent constants called the equivalent gate temperature and the equivalent drain temperature. The equivalent temperatures are demonstrated to be independent of frequency in the frequency range in which $1/f$ noise is negligible (Pospieszalski 1989).

4.1.3 Noise simulation with CAD

Before modeling noise parameters, the circuit simulators require device equivalent circuit parameters. The most common method for determination of the equivalent circuit of microwave FETs has been through minimization of the least squares difference between measured and computed *S*-parameters versus frequency (Eskandarian & Weinreb 1993). Dambrine *et al.* (1988) have presented methods that include *S*-parameters of the FET biased into a "passive" state, as pinch-off or forward-biased gate, to provide additional data on the equivalent circuit. These are referred to as "coldfet" measurements. With this additional data they could uniquely determine equivalent circuit values from measurements at a single frequency. White (1993) and Eskandarian & Weinreb (1993)

have developed improvements to the "hotfet/coldfet" method increasing the accuracy of parasitic capacitance determination including application to HEMTs. Mahon & Skellern (1992) determine device structure from AlGaAs/GaAs HEMT DC I-V characteristic curves. Angelov & Zirath (1992) extract HEMT parameters, including drain current and its derivatives, from inspection of experimental I-V and g_m characteristics.

Once the equivalent circuit has been determined, the noise characteristics of devices derived from either the analytical or empirical methods can be integrated in CAD circuit simulators as Touchstone (from EEsof), MMICAD (from Optotek), Libra (from Hewlett-Packard), and SPICE. For example, MMICAD includes a noise model that accepts Pospieszalski's equivalent noise temperatures as input parameters.

4.2 Noise analysis with Micro-Cap

While their provision for high frequency noise simulation can be applied to determine the white noise baseline, which will help determine the $1/f$ noise corner frequency, many of these circuit simulators do not model low frequency noise. Although SPICE provides for $1/f$ noise in its diode and transistor models, SPICE does not have a model for HEMTs. This inspired the development of the $1/f$ noise models for HEMTs described in Chapters 5 and 6. The discrete $1/f$ noise model takes the empirical approach, while the distributed $1/f$ noise model applies a more analytical approach. Both models were created using Micro-Cap, a member of the SPICE family of circuit simulators.

The discrete $1/f$ noise model lumps all the noise produced by the transistor into one noise source. Since SPICE provides for $1/f$ and shot noise in diodes, a diode was used as a noise source and its noise was reflected to the desired device nodes using dependent current and voltage sources. The method used by Meyer *et al.* (1973) to empirically determine the values of the two noise parameters for transistors was applied, with some modification, to extract the SPICE $1/f$ noise parameters, AF and KF, from low frequency noise data to apply to SPICE's $1/f$ noise calculations for the diode. A detailed description of this method is given in the chapter on the discrete $1/f$ noise model.

The distributed $1/f$ noise model uses SPICE to create noise sources via Micro-Cap's macro function. These sources reflect the physical processes responsible for the noise in the device. Superposition of traps is believed to be the cause of one component of $1/f$ noise measured in HEMTs. In the distributed $1/f$ noise model, each trap is simulated via a low pass filter that possesses the time constant and magnitude of the noise power of the trap. These traps will be superimposed when an AC circuit analysis is performed by SPICE. Quantum $1/f$ noise, the other component of the HEMT's $1/f$ noise, is simulated by a source that uses SPICE's diode model to generate the desired $1/f$ noise and corner frequency. Both the g-r noise and quantum $1/f$ noise sources can be positioned in the circuit where they are actually occurring in the device to accurately simulate their effect on the output and equivalent input noise.

The equivalent circuit was created with discrete resistors and capacitances whose values were derived empirically from HEMT I-V characteristics and verified analytically given the material properties and dimensions of the HEMT. The HEMT's channel current is modeled using a function source available in Micro-Cap. The source's value for the channel current is determined by an algebraic expression that is a function of the device's physical characteristics as well as the gate and source voltages. Details of the distributed $1/f$ noise model are given in Chapter 6.

4.2.1 Micro-Cap circuit analysis

Micro-Cap contains built-in models for passive elements, semiconductor devices, and independent current and voltage sources. By either sketching a schematic or by writing a SPICE text description of the circuit to be analyzed, Micro-Cap can perform many kinds of analysis. When using the "sketch and simulate" method, Micro-Cap works with a schematic editor which provides a netlist for the simulator to analyze. Results may be viewed graphically or in tabular form.

4.2.2 Micro-Cap noise analysis

Micro-Cap allows various types of analyses, such as AC, transient, DC, distortion, and spectral. Noise analysis directs Micro-Cap to perform noise calculations and specifies the input and output nodes. The output may be a single node, where the noise voltage is referenced to ground, or it may be a pair of nodes, in which case the noise voltage is taken across two nodes. The input node must be an independent voltage or current source to

which the total output noise will be referred when the equivalent input noise is calculated. This source is not a noise generator. It is a place at which the equivalent noise input is computed. For a voltage source, the equivalent input is in units of $V / \sqrt{Hz}$. For a current source, it is in units of $A / \sqrt{Hz}$.

The noise-generating devices in a circuit are the resistors and the semiconductor devices. During noise analysis, Micro-Cap calculates the thermal noise spectral density for every resistor in the circuit and shot and flicker noise spectral densities for every semiconductor device in the circuit. To model the noise generators, Micro-Cap generates an equivalent noise current in parallel with the noise generator (which is then noiseless). Alternatively, the equivalent thermal noise could be represented by a mean-square voltage source in series with the noise generator. The two methods are equivalent, however, the "series voltage" technique adds another node to the circuit. Thus Micro-Cap uses the "parallel current" technique (Tuinenga 1992).

Noise analysis is always done in conjunction with an AC, or small-signal, analysis. Each noise generator's contribution is calculated and propagated to the specified output node by the appropriate transfer function. At the output node, all of these contributions are rms-summed to obtain the total root mean square output noise voltage. However, it is generally convenient to refer the noise to the input of the device where it may be directly compared to the signal. The convention of reporting equivalent input noise also facilitates comparison of device noise performances without requiring specification of the impedance

at the output nodes. Equivalent input noise is determined by dividing the noise at the output node by the gain from the specified input source to the specified output node.

4.2.3 Micro-Cap AC analysis

AC analysis is small-signal or linear analysis. All circuit variables are assumed to be linearly related. Using a small-signal model of each device in the circuit, Micro-Cap constructs a set of linear network equations and solves for every voltage and current in the circuit over the specified frequency range. The program obtains the small-signal models for each device by performing a DC analysis to determine the quiescent point prior to the actual AC analysis and then linearizes each device in the circuit about the operating point. Linearizing means replacing a device's non-linear model with a simple constant that expresses a linear relationship between the terminal voltages and currents of the device. The linear model is assumed to hold for small signal changes about the DC operating point.

Micro-Cap requires that an AC source be present in the circuit to perform noise analysis. If a circuit does not contain a source that generates AC signals, all other circuit voltages and currents will be zero. Since AC analysis is linear, the noise output will be independent of the amplitude of the AC source.

4.2.4 Micro-Cap macros

Macros are schematic equivalents of subcircuits. They are circuit building blocks that have been created and saved to disk as part of the component library for use in other circuits. A unique symbol may be created and defined to represent the macro. The macro may define parameters to be specified by the user which will be passed to the macro by the calling circuit.

The virtue of macros is that the behavior of a complex circuit block can be incorporated into and represented by a single component. The complexity and detail of the macro is hidden from view in the calling circuit.

The noise sources in the distributed $1/f$ noise model are macros. A macro was also developed for a noiseless resistor.

4.2.5 Micro-Cap noiseless resistors

It is not possible to turn off the noise model for select devices during noise analysis. However there may be times it is desirable for an element to act like a resistor without generating noise. For example, to determine the noise due to the HEMT alone, it is necessary to exclude the noise of the load resistor. It is possible to substitute a noiseless resistor for the load resistor (Chapter 6).

A noise-free resistor can be simulated using a voltage-controlled current source or a current-controlled voltage source provided by Micro-Cap. These are ideal controlled sources, so they do not create noise. The method is to replace the resistor by a voltage-controlled current source, where the voltage across the device is proportional to the current through the device, or as a current-controlled voltage source, where the current through the device is proportional to the voltage across the device.

The voltage-controlled current source device form is simpler and does not create an additional node in the circuit, but it is still an ideal current source and will not provide a DC path. If this form is used in series with a capacitor, the node connecting the noise-free resistor and capacitor will be a floating node. However, using the current-controlled voltage source device in parallel with an inductor forms a voltage loop. Since a DC path was required and there would not be an inductor in parallel with the noise-free bias resistor, the current-controlled voltage source was used to create the noiseless resistor macro.

The macro shown in FIG. 4.1 was developed to represent a noiseless resistor.

NLR -NoiseLess Resistor - argument is desired resistance value

.parameters(resistance)

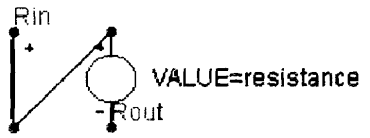

FIG. 4.1 Noiseless resistor macro

The nodes of the macro symbol shown in FIG. 4.2 are equivalent to the nodes Rin and Rout shown in the macro in FIG. 4.1.

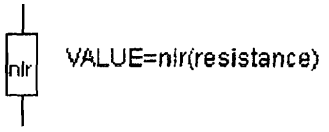

FIG. 4.2 Noiseless resistor macro symbol

4.3 Micro-Cap applications

The two $1/f$ noise models developed demonstrate many of Micro-Cap's features. The discrete $1/f$ noise model takes advantage of dependent sources and one of Micro-Cap's built-in devices, the diode, and AC and noise analysis.

In the distributed $1/f$ noise model, macros that simulate noise mechanisms were created and inserted in the equivalent HEMT circuit. One of Micro-Cap's built-in functions, the derivative, was used to determine g_m. AC and noise analysis were used to learn about the effect of varying the location and strength of internal noise sources.

The application of these features is described in the next two chapters which detail the development of two HEMT $1/f$ noise models.

Chapter 5

Discrete $1/f$ noise model

Prediction is difficult, especially of the future.
Niels Bohr

5.1 Presentation of the problem

It was desired to model published $1/f$ noise measured in a HEMT using Micro-Cap. The low-frequency noise spectra of a T8901 AlGaAs/GaAs HEMT was published in "Comparison of $1/f$ Noise of AlGaAs/GaAs HEMTs and GaAs MESFETs" by Munecazu Tacano and Yoshinobu Sugiyama (1991). The spectra are shown in FIG. 5.1.

There are two popular methods to model $1/f$ noise using Micro-Cap. One method is to use the semiconductor device noise models which include $1/f$ parameters provided by Micro-Cap. The other method is to use diodes as noise sources and to reflect their noise to the desired nodes using dependent voltage and/or current sources, as described by both Motchenbacher and Connelly (1993) and by Connelly and Choi (1992). These two methods are described below.

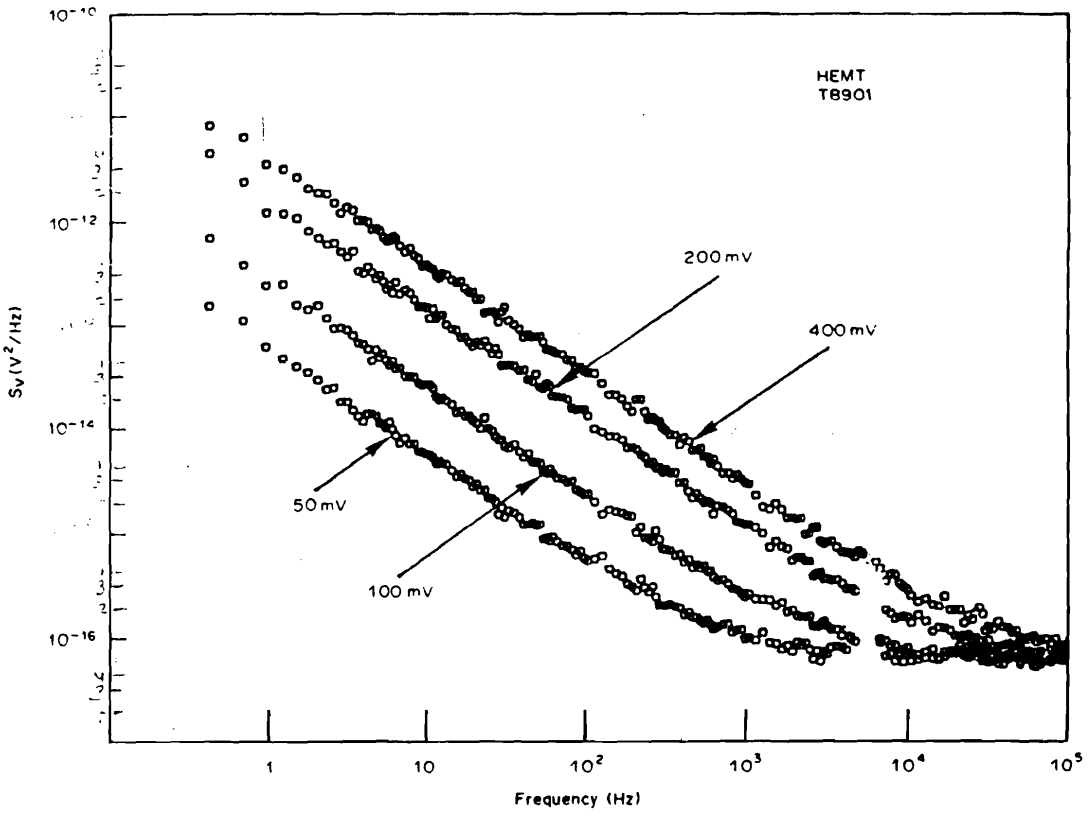

FIG. 5.1 Low frequency noise spectra of AlGaAs/GaAs HEMT T8901 at V_g=0V, with drain voltage as a parameter (Tacano & Sugiyama 1991)

Neither of these methods alone could be used to model $1/f$ noise in a HEMT. The first, using Micro-Cap device models, was not applicable, because Micro-Cap does not contain a model for a HEMT. The second method could not be used without modification to the authors' procedures. The modified model, however, yielded simulated $1/f$ noise levels that are all within a factor of 1.5 of the published data.

5.2 Two things Micro-Cap can do

Detailed descriptions of the two popular methods used to model $1/f$ noise with SPICE follow.

5.2.1 Model $1/f$ noise using Micro-Cap device models

Micro-Cap provides for inclusion of $1/f$ noise contributions for many devices including diodes, MOSFETs, BJTs, and GASFETs. The equations Micro-Cap uses to calculate the noise for several semiconductor devices are described below.

Micro-Cap models $1/f$ noise in BJTs with a current generator connected across the base-emitter junction. This can be combined with the base current shot noise generator to give the mean square noise current in a 1Hz bandwidth,

$$i_B^2 = 2qI_B + \frac{(KF)I_B^{AF}}{f},$$

where q is the electronic charge, I_B is the dc base current, f is the frequency, KF is the flicker noise coefficient, and AF is the flicker noise exponent.

$1/f$ noise in FETs can be represented by a current generator from drain to source. This is combined with the thermal noise generator from drain to source to give the mean square noise current, in a 1Hz bandwidth,

$$i_{D\square}^2 = 4kT\left(\tfrac{2}{3}g_m\right) + KF\frac{I_D^{AF}}{f},$$

where k is Boltzman's constant, T is the absolute temperature, g_m is the FET transconductance, I_D is the drain current, KF is the flicker noise coefficient, and AF is the flicker noise exponent.

Micro-Cap calculates the mean square noise current in a diode, in a 1Hz bandwidth, according to

$$i_D^2 = \frac{KF\left(I_{DC}\right)^{AF}}{f} + 2qI_{DC}, \qquad (5.1)$$

where KF is the flicker noise coefficient in amps, AF is the flicker noise exponent, q is the electronic charge, f is the frequency in hertz, and I_{DC} is the dc bias current through the diode.

The three relationships above are included in the noise analysis routines in Micro-Cap. For each device in the circuit the coefficient, KF, and the exponent, AF, can be specified. If KF or AF are not specified, they are assigned default values of 0 and 1, respectively, by Micro-Cap. Therefore, the default is inclusion of shot noise with no flicker noise. Micro-Cap then automatically couples bias point information to these

formulas, evaluates the noise generators, and computes the circuit noise performance.

In an early publication on the topic of simulating $1/f$ noise in transistors with SPICE by Meyer, *et al.* (1973), the success of simulation of the $1/f$ noise associated with 741 opamps is described. Initially, they describe preliminary measurements made on integrated test transistors, an npn and a pnp BJT. These measurements are used to determine the number of parameters required to model $1/f$ noise over a wide range of bias conditions and the method used to extract these parameters from the data. The equations they used were the same as the equations Micro-Cap uses which were presented above.

In their model, Meyer, *et al.* found the parameters AF and KF adequate to simulate $1/f$ noise. The exponent AF and coefficient KF to include in the Micro-Cap device model can be determined from a log-log plot of measured mean square noise current vs base current (for BJTs) or drain current (for FETs) at a single frequency. As reported in the paper by Meyer, *et al.* and as verified by the present study, the value of AF is independent of frequency.

The derivation of how the log-log plots were used to find AF and KF follows, where i_n^2 is the mean square noise current and I_B is the base current:

$$i_n^2 = (KF)\frac{I_B^{AF}}{f}$$

$$\log\left(i_n^2\right) = \log\left(\frac{(KF)I_B^{AF}}{f}\right)$$

$$\log(i_n^2) = \log\frac{KF}{f} + \log I_B^{AF}$$

$$\log(i_n^2) = \log\frac{KF}{f} + AF\log I_B \tag{5.2}$$

The last relation is of the form

$$y = b + mx$$

where the slope of the noise, i_n^2, vs I_B at a given frequency can be used directly to find AF and the intercept can be used to find KF via

$$\text{intercept} = \log\frac{KF}{f},$$

$$10^{\text{intercept}} = \frac{KF}{f},$$

$$KF = 10^{\text{intercept}} * f.$$

The data used for the determination of AF and KF were included in the paper by Meyer, *et al.* It is important to keep in mind that the data was presented in graphical form while the authors had access to numerical data points. To verify that the procedure for determining these parameters was understood, linear equations were derived from this data as shown in FIG. 5.2 below. Then, using Equation 5.2 derived above, values for AF and KF were determined for both the npn and pnp transistor. The resultant values of AF and KF were compared to those of the authors.

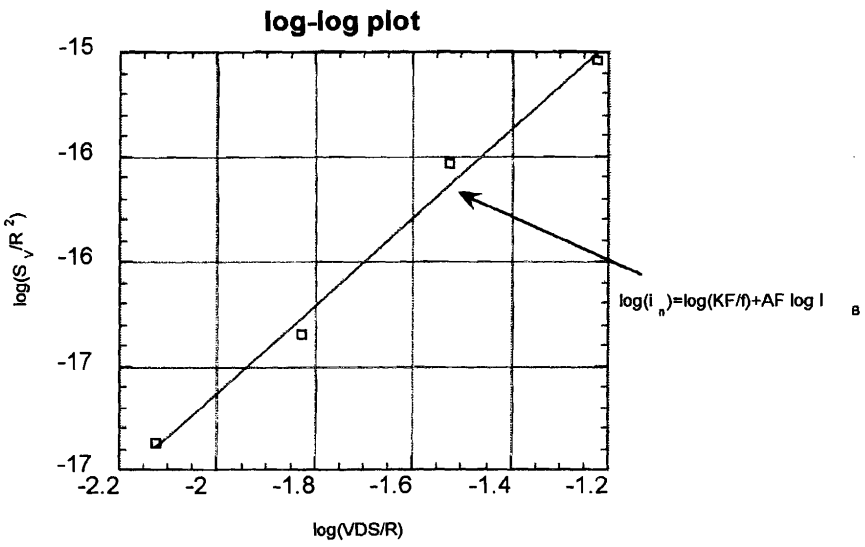

FIG. 5.2 Log-log plot of mean square noise current vs base current for a fixed frequency

AF and especially KF were sensitive to the care taken to read the data from the published graphs. Although it must be stressed that the values of AF and KF are sensitive to variations in the data, this method provides a valuable means to obtain the values of AF and KF, which are necessary for simulation of $1/f$ noise.

5.2.2 Micro-Cap can be used to model $1/f$ noise externally

There are several situations in which it would be advantageous to model noise externally instead of using the noise parameters in Micro-Cap device model. For example, it might be desirable to lump all the noise produced by a circuit into two noise sources, one noise current source and one noise voltage source, or, if the two sources are uncorrelated, only one source. This can be done by using resistors as thermal noise

sources and reflecting their noise to the desired nodes using dependent voltage or current sources. Similarly, diodes can be used as sources of shot and $1/f$ noise. This procedure, described by Motchenbacher & Connelly (1993), is outlined below.

Micro-Cap defines the mean square noise current in a diode as the sum of the flicker noise and the shot noise. The mean square noise current is calculated according Equation (5.1). At the corner frequency, f_{nce}, the flicker noise and shot noise terms are equal,

$$\frac{KF(I_{DC})^{AF}}{f_{nce}} = 2qI_{DC}, \qquad (5.3)$$

both white and $1/f$ noise are present and it is seen that the $1/f$ noise dominates at low frequencies and the white noise at high frequencies. The thermal noise component of a diode calculated by SPICE is generated by the user-specified parasitic resistance. It was assumed that the parasitic resistance of the diode was negligible, therefore the thermal noise component of the diode was zero. The shot noise component of the white noise was not zero, for it is a funciton of I_{DC}. The noise power is independent of frequency for the shot noise but is proportional to $1/f$ for the low frequency noise. The frequency at the transition between $1/f$ noise dominance and white noise dominance is called the corner frequency.

In the Motchenbacher & Connelly method, independent current sources are used to set a dc diode current, I_{DC}, which will produce an arbitrary reference noise current

level, I_{ref}, in the diode. The noise current produced by this reference bias current through the diode is sensed by an independent voltage source, V_{sense}, in parallel with the diode. (In Micro-Cap an independent voltage source of zero value can be used as an ammeter. That is, in order to measure a current, a zero-valued voltage source can be inserted in series with the element where the current is desired. The zero-valued voltage source will not disturb the circuit since it is equivalent to a short circuit. These zero-valued voltage sources are necessary because the only current Micro-Cap is designed to output is the current in sources.) The resultant noise is then reflected to a dependent voltage source at the desired node, H_{noise}, via the independent voltage source, V_{sense}, as shown in FIG. 5.3. A gain factor, specified by the SPICE program, scales the noise sensed by V_{sense} to the amplitude required at the desired node. The 1GF capacitor blocks the dc bias current and permits the ac short-circuit noise current to be sensed by V_{sense}.

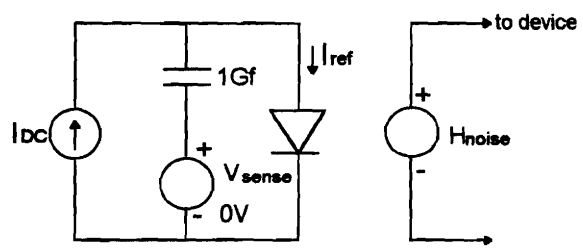

FIG. 5.3 Circuit to produce noise with $1/f$ component

The reference dc bias current can be found via

$$I_{dc} = \frac{I_{ref}^2}{2q}.$$

Knowing the corner frequency, f_{nce}, and assuming AF=1, as prescribed by Motchenbacher and Connelly (1993), KF can be calculated by equating the shot and $1/f$ noise components of the noise at the corner frequency as in Equation 5.3, yielding

$$KF = 2qf_{nce}.$$

It is important to realize that the Motchenbacher-Connelly method relies upon the assumption that AF=1. This is only true if the noise power scales directly with the applied voltage. If the noise power does not vary directly with the applied voltage, another method must be found to determine AF, and, subsequently, KF.

5.3 What Micro-Cap cannot do

The goal is to model $1/f$ noise in a HEMT. Neither the Motchenbacher-Connelly method nor the Meyer, *et al.* method for modelling $1/f$ noise described above can be directly applied to modeling $1/f$ noise in a HEMT. Micro-Cap does not have a model for HEMTs, so the $1/f$ noise parameters included in other Micro-Cap semiconductor models are not available. The Micro-Cap GaAs MESFET model is often used to approximate the HEMT. While it is true that the HEMT is similar to the GaAs MESFET, there are important differences that affect the noise properties of each.

Due to the discontinuity between the conduction bands of the high-band-gap AlGaAs and the undoped GaAs, electrons are localized to a thin two-dimensional electron

gas layer on the GaAs side of the AlGaAs/GaAs heterojunction interface. Because there are no donor atoms intentionally present in the undoped GaAs layer, electrons in the 2-DEG channel do not undergo impurity scattering and hence exhibit high mobility and velocity. This structure gives the HEMT superior electron transport properties in the channel and a higher sheet charge density for high frequency operation. The need to modify the Micro-Cap equations of the GaAs MESFET model to simulate the HEMT was reported by T. Zimmer, *et al.* (1992) in their article titled "Kink Effect in HEMT Structures: A Trap-related Semiqualitative Model and an Empirical Approach for SPICE Simulation". They report that, in order to simulate the kink effect, which is an abnormal increase of the drain current in the saturation region, in HEMTs, they needed to extend the dc equations of the GaAs MESFET SPICE model by modifying the code in TECAP/SPICE.

Since Micro-Cap does not have a HEMT model, we are modelling the device with discrete components available in Micro-Cap. It was initially thought that the noise in the HEMT could be modelled using the diode as a source of $1/f$ noise, as described above, and reflecting this noise to the source-drain node of the HEMT. There are several problems with this method.

The first problem is that we cannot assume AF to be one, as Motchenbacher, et al did. AF and KF are properties of the device. Note that Meyer, *et al.*, found AF=1.0 for the npn transistor, but they found AF=1.5 for the pnp transistor. AF is a function of how

the noise current varies with bias current,

$$i_n = \left(\frac{KF}{f}\right) I_{\square D}^{AF},$$

where $\frac{KF}{f}$ is constant. AF ranges between 1 and 2 (Mochtenbacher & Connelly 1993).

Another problem is that the Motchenbacher-Connelly method assumes a known corner frequency and shot noise level. We do not necessarily know both of these parameters for the HEMT. Often, in modern low-noise devices, the shot noise level is well below the sensitivity of the measurement system.

The experimentally determined coefficient, KF, can be replaced by $2qf_L$, where q is the electronic charge and f_L is a constant having values from 3.7KHz to 7Mhz (Mochtenbacher & Connelly 1993). The value of f_L is a representation of the corner frequency. Its value does not match the corner frequency, but there is gross correlation.

5.4 The discrete 1/*f* noise model

The two procedures above were combined to simulate the low-frequency noise spectra of the AlGaAs/GaAs HEMT published by Tacano. et al. We used a diode to generate 1/*f* noise, as Motchenbacher & Connelly did. However, we could not find AF and KF via their method, because we could not assume AF to be equal to one and we did not know the corner frequency. Rather AF and KF for the diode were determined using the method described by Meyer, *et al.*, which is used for finding AF and KF for insertion

directly into SPICE models of devices. The I_{DC} used in the diode model was found by dividing the drain voltage of the HEMT by the source-drain resistance, NOT by using the shot noise level.

5.5 Results

The HEMT noise data published by Tacano, *et al.* was used to extract values of AF and KF. The data was given in terms of voltage spectral density. To be consistent with Micro-Cap's specification of noise in terms of *current* spectral power densities, these voltages were changed to current using the HEMT's source-drain resistance of 6.7 ohms published in the article. Noise current was obtained by dividing the spectral density by the square of the resistance. The drain current was obtained by dividing the applied drain voltage by the channel resistance. The noise voltages and drain voltages were used to plot $\log\left(\frac{\square_V}{R^2}\right) vs \log\left(\frac{V_{DS}}{R}\right)$, shown in FIG. 5.4. This was done for four frequencies. Linear regression output from each of these four plots was used to find AF and KF. These plots and the resultant values of AF and KF are shown in TABLE 5.1.

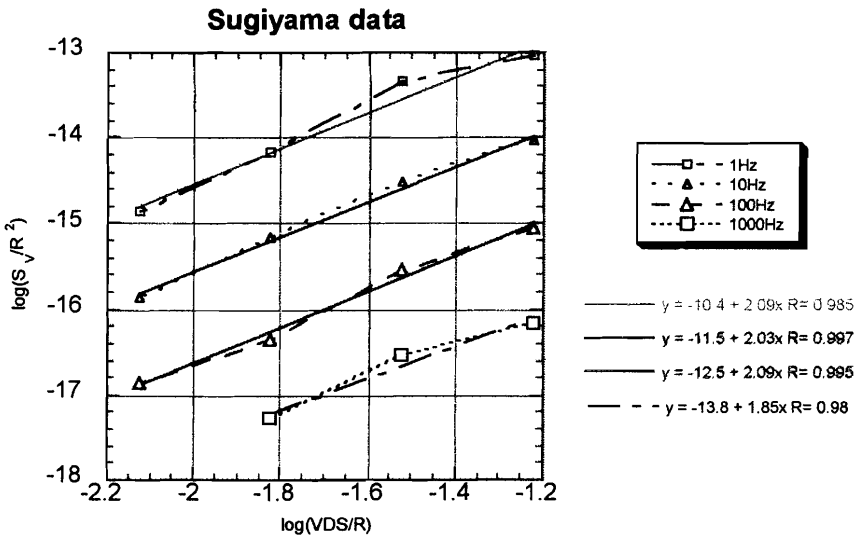

FIG. 5.4 $\log\left(\frac{S_V}{R^2}\right) vs \log\left(\frac{V_{DS}}{R}\right)$ for four frequencies

frequency	AF	KF
1	2.09	4.38E-11
10	2.02	3.095E-11
100	2.08	3.5075E-11
1000	1.85	1.438E-11
average	2.01	3.105E-11

TABLE 5.1 Resultant values of AF and KF

The average values of AF and KF were then applied to the diode model and used as parameters in the Micro-Cap simulation of the published data. The following Micro-Cap program was used to simulate the data.

```
1/F NOISE
IEN 0 100 7.462E-3A
CEN 100 101 1GF
VESEN 101 0 DC 0
DENOISE 100 0 DENOISE
.MODEL DENOISE D (KF=3.105E-11, AF=2.01)
V1 1 0 DC 0V
HEN 1 2 VESEN 6.7
R1 2 0 1OHM
.AC DEC 4 1HZ 1E7HZ
.NOISE V(2) V1 1
.PROBE
.END
```

The programs used to simulate the HEMT for each of the four values of drain voltage, $V_{D\square}$, were identical except for the value of IEN, which was calculated from data and biasing conditions via

$$IEN = \frac{V_{D\square}}{6.7\Omega}.$$

Each of the $1/f$ noise curves in FIG. 5.1 was measured under unique biasing conditions, requiring the above parameter to define the small-signal operating conditions for the simulation of each curve. The channel resistance, 6.7Ω, is unique to the particular HEMT being modeled, and must be adjusted for the simulation of a different device.

The following circuit shown in FIG. 5.5 was used.

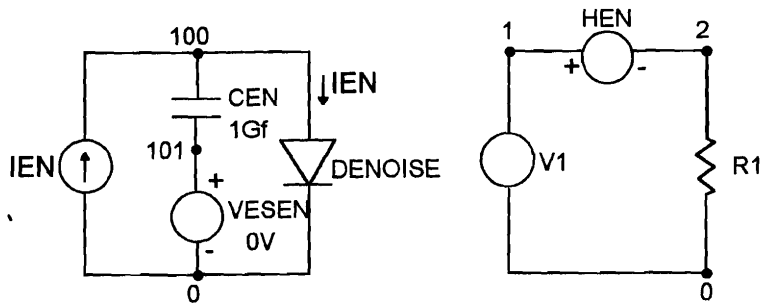

Figure 5.5 Circuit to produce noise with 1/*f* component

FIG. 5.6 shows the schematic generated with Micro-Cap that represents the circuit in FIG. 5.5 above.

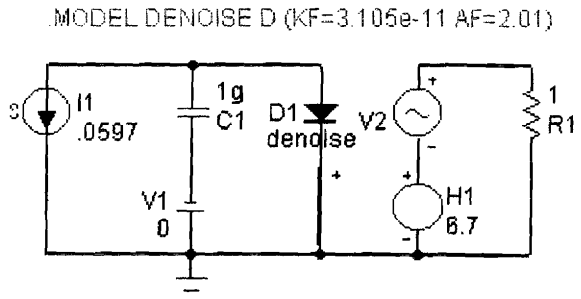

FIG. 5.6 Micro-Cap schematic of 1/*f* noise generator

Micro-Cap calculates the flicker noise via Equation 5.1. The input noise, as specified by the program, is

$$i_n^2 = \frac{(KF)(I_D^{AF})}{f}(gain),$$

where *gain* is the gain of the current dependent voltage source. Notice that the voltage gain of the current dependent voltage source, HEN, is 6.7, which is the channel resistance. This was used to convert noise current to voltage.

The output noise is converted to current via

$$V(INOISE) = \sqrt{i_n^2} = R_D\sqrt{(KF)(I_D^{AF})},$$

where R_D is the channel resistance.

The results to the simulation for each of four frequencies, labeled "Simulation" are presented in TABLE 5.2. The values of the published noise are labeled "Data". The "% diff" is the difference between the published and simulated noise power.

	1Hz	10Hz	100Hz	1000Hz
400mV				
Data	4E-12	4E-13	4E-14	3E-15
Simulation	4.807E-12	4.830E-13	4.830E-14	4.830E-15
% diff	-20.17%	-20.75%	20.75%	20.75%
200mV				
Data	2E-12	1.3E-13	1.3E-14	1.3E-15
Simulation	1.199E-12	1.199E-13	1.199E-14	1.199E-15
% diff	40.05%	7.77%	7.77%	7.77%
100mV				
Data	3E-13	3E-14	2E-15	2.3E-16
Simulation	3.001E-13	2.975E-14	2.975E-15	2.977RE-16
% diff	-0.033%	0.833%	-48.75%	-29.43%
50mV				
Data	6E-14	6E-15	6E-16	------
Simulation	7.305E-14	7.390E-15	7.391E-16	------
% diff	-21.75%	-23.17%	-23.18%	------

TABLE 5.2 Comparison of the noise from the discrete $1/f$ noise model and the published $1/f$ noise evaluted at four frequencies with drain current as a parameter

Chapter 6

Distributed 1/*f* noise model

According to an Old Norse folktale the sea is salt because somewhere at the bottom a magic salt mill is grinding away. The tale is perfectly true. Only the details need to be worked out.

-Oceanographer Ferren MacIntyre

6.1 Introduction

Unlike the discrete noise model described in the previous chapter in which all the noise was represented by one source, the distributed noise model allows variation of the physical location and type of noise in the equivalent circuit of a HEMT, providing insight into the mechanisms of the sources of the noise. The model was tested by simulating the equivalent gate 1/*f* noise voltage measurement of a GaInP/GaInAs/GaAs HEMT shown in FIG. 6.1 and published in the thesis, "GaInP/GaInAs/GaAs MODFETs for High Power and High Frequency Applications" (Pereiaslavets 1997). The development of this HEMT was described in Section 2.5.

Two types of noise voltage sources were created using MicroCap's macro function. The "1/*f* noise macro" simulates 1/*f* noise of a given magnitude and corner

frequency. This noise may be due to quantum $1/f$ noise or it may be due to the presence a number of different traps with a uniform distribution of time constants that produces a noise spectrum which is close to $1/f$. The "g-r noise macro" simulates g-r noise bulges. The two noise macros are represented by discrete noise voltage sources which can be inserted at the desired locations in the equivalent circuit of the HEMT. The amplitude and number of these sources are specified by the user. The sensitivity of the equivalent noise to the location, characteristics, and number or these noise sources in the HEMT equivalent circuit can be tested by comparing simulation results. However, for the distributed noise sources to have the correct transfer function to the output nodes of the HEMT, it is critical that the HEMT first be accurately characterized. The decision to test the distributed $1/f$ noise model by trying to simulate the measured $1/f$ noise of the GaInP/GaInAs/GaAs HEMT (FIG. 6.1) was driven by the availability of device parameters, material properties, and layer structure (TABLE 6.1) required to create an equivalent network that would reproduce the measured I-V characteristics (FIG. 6.2) and transconductance, g_m, all provided in Pereiaslavets' thesis (1997).

The basic structure of the GaInP/GaInAs/GaAs HEMT as shown in TABLE 6.1 is similar to the structures of the three more common HEMTs shown in FIG. 2.5. The thicknesses of several layers were required to determine some of the parameters required for the equivalent circuit. A brief description each layer follows.

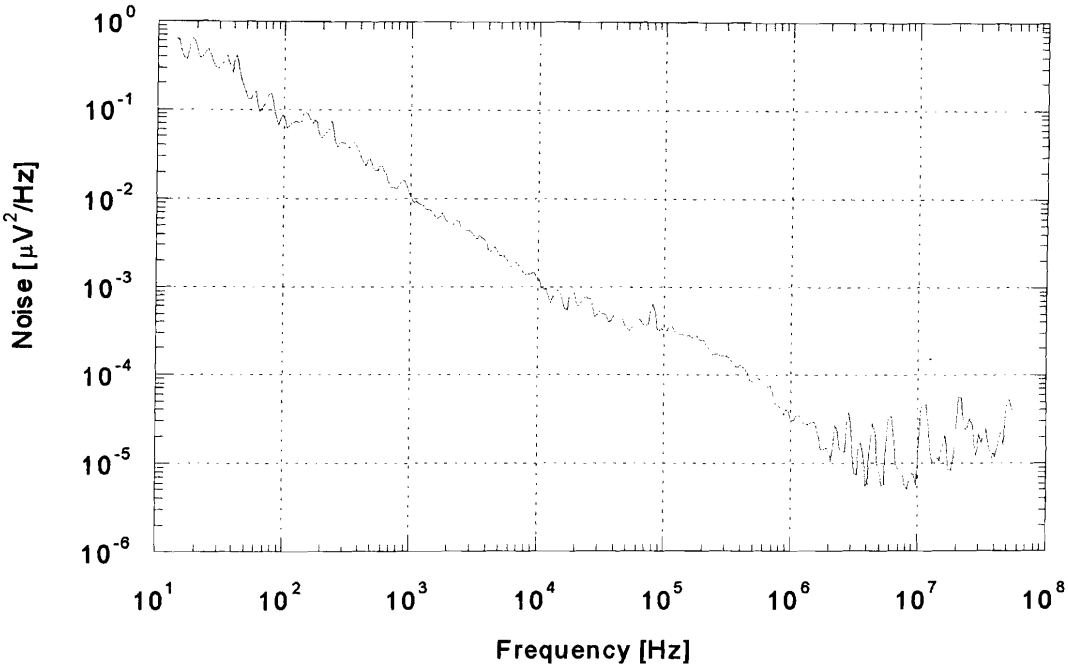

FIG. 6.1 Equivalent gate noise spectra of a GaInP/GaInAs/GaAs HEMT (Pereiaslavets 1997)

	In Composition	Description	Thickness (Å)	Doping
GaAs	0	Cap layer	250	Si $5 \cdot 10^{18} cm^{-3}$
GaInP	0.33	Barrier	160	n.i.d.
GaInP	0.33	Planar Doping	—	Si $6 \cdot 10^{12} cm^{-2}$
GaInP	0.33	Spacer	28	n.i.d.
GaAs	0	Smoothing Layer	10	n.i.d.
GaInAs	0.33	Channel	72	n.i.d.
GaAs	0	Buffer	2000	n.i.d.

TABLE 6.1 GaInP/GaInAs/GaAs HEMT layer structure
In Composition = indium fraction
n.i.d. = not intentionally doped (Pereiaslavets 1997)

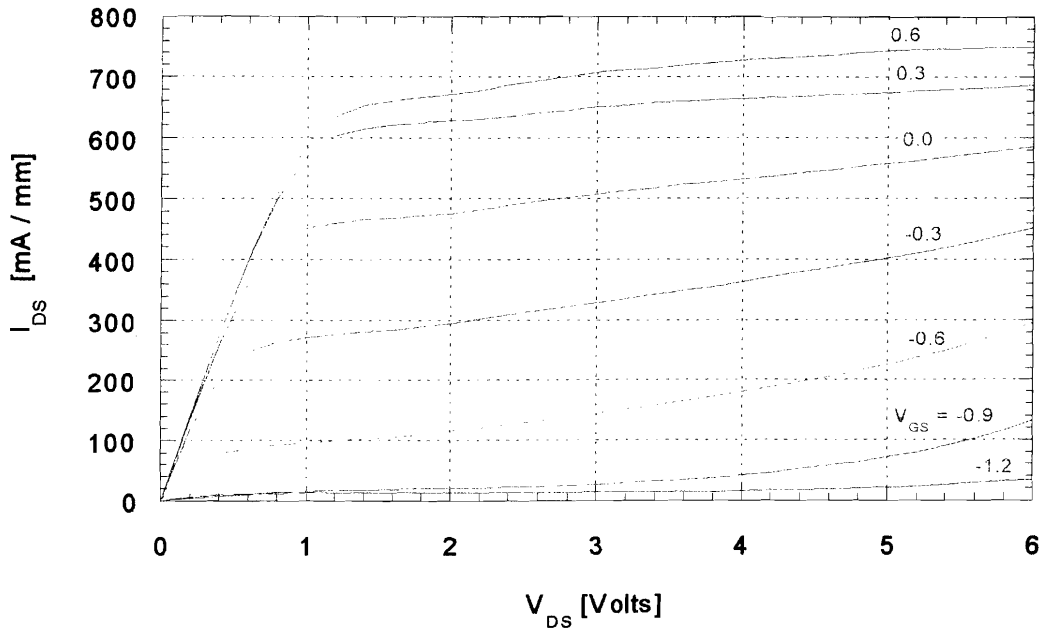

FIG. 6.2 I-V characteristics of a GaInP/GaInAs/GaAs HEMT (Pereiaslavets 1997)

The heavily doped cap layer is necessary to form low resistance ohmic contacts. It also reduces the parasitic source and drain resistance.

The GaInP barrier is a wide bandgap material between the gate and channel. The minimum thickness is 160 Angstroms, because there is danger of a high gate leakage current if it is thinner (Pereiaslavets 1997).

The supply layer (labeled Planar Doping in TABLE 6.1) is the source of electrons for the 2-DEG in the channel. To improve the breakdown voltage and the gate leakage, the donors were introduced in a very thin layer via a process called atomic planar doping (Pereiaslavets 1997).

The spacer layer reduces remote ion scattering. Even though the electrons and donors are separated spatially, their close proximity permits an electrostatic interaction resulting in Coulomb scattering. This scattering can be attenuated by placing a thin spacer layer of undoped GaInP between the planar doped region and the GaInAs channel to separate the negatively charged 2-DEG from the ionized dopant atoms.

The purpose of the smoothing layer is to improve the interface roughness between GaInP and GaInAs. Buffer-channel interface roughness reduces the mobility in the channel (Ali & Gupta 1991).

The channel is the undoped component of the heterojunction in which the 2-DEG will form.

There are two purposes for growing a buffer layer. The first is to prevent impurities in the substrate from propagating into the channel during growth. The second purpose is to reduce the penetration of the electric field from the source and drain into the substrate thus improving the breakdown voltage.

The distributed $1/f$ noise model is presented as a tool to model $1/f$ noise in HEMTs. This chapter presents an example of application of this model by simulating the $1/f$ noise in the GaInP/GaInAs/GaAs HEMT published in Pereiaslavets' thesis (1997).

The determination of the values of the internal and parasitic resistances and capacitances of the GaInP/GaInAs/GaAs HEMT is described in the next two sections. The device parameters and their values required to simulate the channel current in the published I-V characteristics (FIG. 6.2) of the device are described in the section on DC characteristics. Next, the small-signal model is presented. Biasing and resultant transconductance are determined. The $1/f$ noise (both g-r noise and quantum $1/f$ noise) models and SPICE's model for thermal noise are explained. The chapter is concluded with possible implementations of the distributed $1/f$ noise model which reproduce the measured noise (the $1/f$ noise, two g-r noise bulges at 100Hz and 30,500Hz, and the thermal noise) of the GaInP/InGaAs/GaAs HEMT shown in FIG. 6.1.

6.2 Resistances

The equivalent network model of the specific GaInP/GaInAs/GaAs MODFET being modeled, based on a low-frequency equivalent network model for HEMTs including intrinsic and extrinsic parameters derived by Ali & Gupta (1991), is shown in FIG. 6.3.

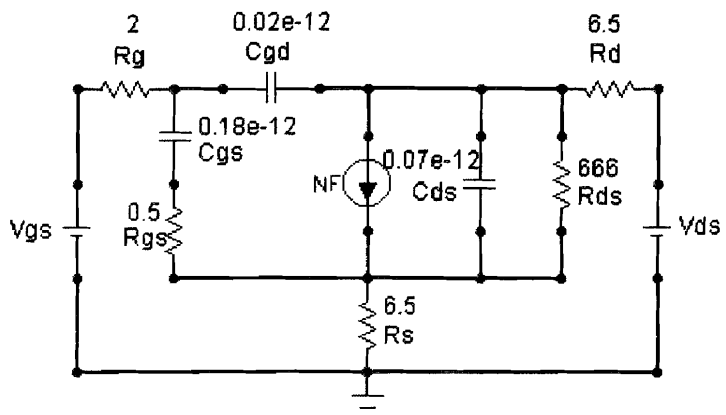

FIG. 6.3 Equivalent network model of GaInP/InGaAs/GaAs HEMT including intrinsic and extrinsic parameters (units are ohms and farads)

The definition and values of the resistances and capacitances that comprise the equivalent network model are described below.

6.2.1 Source and drain resistance

Good ohmic contacts are required to produce near-ideal device performance. Heavy doping of the cap layer is required to produce low resistance ohmic contacts and to

reduce parasitic source and drain resistance. Tunnelling determines the contact resistivity for metal-semiconductor contacts involving high doping concentrations.

Since the resistances in a HEMT are a function of the gate width, it has become standard practice to report resistances in units of $\Omega \cdot mm$ (Eastman 1998). Therefore, to determine the value of the resistance to be used in the equivalent network, a resistance, given in $\Omega \cdot mm$, must be divided by the gate width. Similarly, currents are presented in units of A / mm. In this case, the current can be calculated by multiplying this value by the gate width. These conversions will be applied in many of the calculations that follow.

A source resistance, Rs (FIG. 6.3), of $6.5\,\Omega$ was derived by combining the $0.65\,\Omega \cdot mm$ source resistance and gate width, w_g, of $100um$ given in Pereiaslavets' thesis (1997).

Two approaches were applied to cross-check this value. The first used the definition of the source-to-drain conductance, g_{sd}, which is the slope of the I-V curves in the linear region. This slope is the ratio of the source-drain current, I_{ds}, scaled by the given gate width, and drain-source voltage, V_{ds}. Using the curve for $V_g = 0.3V$ in FIG.6.2 and noting that, since the ordinate is given in mA / mm, it must be multiplied by the gate width of $0.1mm$ to find I_{ds}, the slope in the linear region of the I-V curves was

$$\frac{\Delta I_{ds}}{\Delta V_{ds}} \cong \frac{(400mA/mm)(0.1mm)}{0.55V} = 0.0727 = g_{sd},$$

$$\frac{1}{g_{sd}} = r_{sd} = 13.5\Omega$$

where r_{sd}, is the combined resistance of the source and drain. From the known device geometry this combined resistance can be assumed to be split evenly between the source and drain (Eastman, 1998), yielding Rs=Rd=6.75 Ω (FIG. 6.3). This is consistent with the source resistance of 6.5 Ω given in Pereiaslavets' thesis (1997).

The other check was to use the $200\frac{\Omega \cdot mm}{square}$ sheet resistance, R_{sheet}, of the GaInAs channel layer measured on a test pattern and the $0.2\Omega \cdot mm$ transfer resistance, R_T, which is the resistance between the source metal and the 2-DEG (Eastman 1998). The source resistance is,

$$Rs = R_T + R_{sheet}\frac{l_g}{w_g},$$

$$Rs = 0.2\Omega \cdot mm + \left(100\frac{\Omega \cdot mm}{square}\right)\left(\frac{0.25um}{100um}\right),$$

$$Rs = 0.7\Omega \cdot mm,$$

where w_g and l_g are the gate width and length. Scaling for the $100um$ gate width,

$$Rs = 7\Omega,$$

also consistent with the source resistance given in Pereiaslavets' thesis (1997)..

6.2.2 Gate Resistance

The gate series resistance, Rg (FIG. 6.3), is due to the gate metalization resistance. The gate is in the form of a stripe of width, length, and height. The electrical contact is made from three gate pads. To determine the actual value, the actual number of gate pads and the end-to-end resistance of the equivalent linear gate normally provides a good estimate (Ali and Gupta 1991).

The gate resistance was calculated from the relation (Eastman 1998)

$$Rg = \frac{(R_{sheet})\frac{l_g}{w_g}}{(L_f)(N_{fingers})},$$

where L_f is the length of each finger,

R_{sheet} is the sheet resistance of the gate,

$N_{fingers}$ is the number of gate structures (fingers),

and w_g and l_g are the gate width and length.

This yields

$$Rg = \frac{(80\Omega \cdot mm)\left(\frac{0.25um}{100um}\right)}{(50 \times 10^{-3} mm)(2\,fingers)}.$$

$$Rg = 2\Omega.$$

6.2.3 Gate-to-source Leakage Resistance

The gate-to-source leakage resistance, Rgs (FIG. 6.3), is a function of bias. The channel conduction region is distributively coupled to the gate by the distributed gate-to-channel capacitance, Cgs. It can be estimated by (Eastman 1998)

$$Rgs = Rg\left(\frac{l_g}{l_{channel}}\right),$$

where Rg is the gate resistance,

l_g is the length of the gate,

and $l_{channel}$ is the length of the channel.

The resultant gate-to-source leakage resistance is

$$Rgs = (2\Omega)\frac{0.25um}{1mm},$$

$$Rgs = 0.5\Omega.$$

6.2.4 Output conductance

The measured output conductance, g_o, for the GaInP/InGaAs/GaAs HEMT was $15\frac{mS}{mm}$ (Pereiaslavets 1997). With a $100um$ gate width, this translates to $1.5mS$, which is equivalent to a source-to-drain resistance, Rds (FIG. 6.3), of 667Ω.

The output conductance can also be derived from the slope of the published I-V curves (FIG. 6.2) in the saturation region,

$$g_o = \frac{\Delta I_{ds}}{\Delta V_{ds}},$$

$$g_o = \frac{\left(20\frac{mA}{mm}\right)\left(\frac{0.100mm}{gatewidth}\right)}{1V} = 0.002\frac{A}{V}.$$

$$Rds = \frac{1}{g_o} = 500\Omega.$$

6.2.5 Summary of resistances

Circuit resistance	Schematic symbol	Resistance Ω
Source	Rs	6.5
Drain	Rd	6.5
Gate	Rg	2.0
Channel	Rgs	0.5
Output conductance	Rds	667

TABLE 6.2 Equivalent network resistances of GaInP/GaInAs/GaAs HEMT

6.3 Capacitances

6.3.1 Gate-to-drain capacitance

Cgd (FIG. 6.3) is the parasitic feedback capacitance between the gate and drain. Cgd will decrease as the drain voltage increases until the lateral depletion reaches the edge of the n+ AlGaAs cap layer. Thus, the component of Cgd involving the depleted semiconductor material can be approximated by (Ali and Gupta 1991),

$$Cgd \approx \varepsilon w_g \frac{d + d_i + \Delta d}{l_g},$$

where ε is the permittivity of GaInP,

w_g is the gate width,

l_g is the gate length,

d is the nGaInP thickness,

d_i is the spacer thickness,

and Δd is the mean distance of the 2-DEG from the GaInP/GaAs interface.

Additional contribution to Cgd arises from the fringing capacitance between the gate and drain metalizations. The behavior of this capacitance under saturation drain current operation can best be determined by S-parameter measurements at microwave frequencies.

The value of Cgd was not presented in Pereiaslavets' thesis, so a value of 0.02pF was chosen as typical from a survey of the value of Cgd in other HEMTs (Ali and Gupta 1991). This value is consistent with that calculated from the above relation using the device parameters in TABLE 6.4 below.

6.3.2 Drain-to-source capacitance

The drain-to-source capacitance, Cds (FIG. 6.3), is due to the fringing electric field between the two coplanar conducting regions of the 2-DEG. One of these regions is under the drain ohmic contact, and the other is under that part of the gate which lies towards the source, and where carrier velocity saturation does not occur. The high field carrier saturation region separates these regions that are coupled by the fringing capacitance Cds This capacitance is also distributed, but can be approximated by a single element in the equivalent network (Ali and Gupta 1991).

The value of Cds was not presented in Pereiaslavets' thesis, so a value of 0.07pF was chosen as typical from a survey of the value of Cdg in other HEMTs (Ali and Gupta 1991).

6.3.3 Gate-to source capacitance

Cgs (FIG. 6.3) represents the intrinsic gate charging capacitance.

The value of Cgs was not presented in Pereiaslavets' thesis, so a value of 0.18pF was chosen as typical from a survey of the value of Cdg in other HEMTs (Ali and Gupta 1991).

6.3.4 Summary of capacitances

Circuit capacitance	Schematic symbol	Capacitance (pF)
Gate-to-drain	Cgd	0.02
Drain-to-source	Cds	0.07
Gate-to-source	Cgs	0.18

TABLE 6.3 Equivalent network capacitances of GaInP/GaInAs/GaAs HEMT

6.4 DC characteristics

The DC network model incorporating the resistances and capacitances explained above is shown in FIG. 6.4.

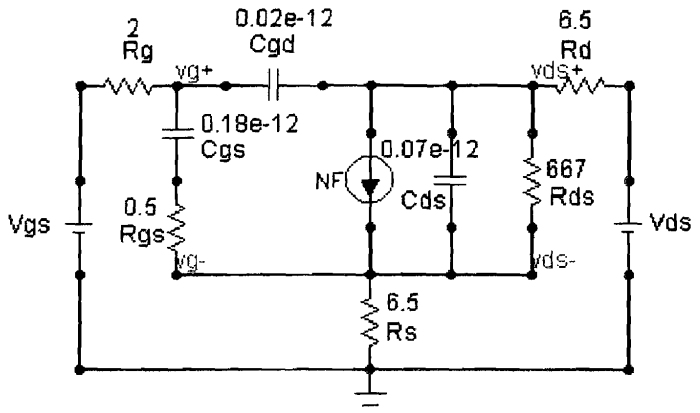

FIG. 6.4 DC equivalent network for GaInP/InGaAs/GaAs HEMT

The channel current was simulated in Micro-Cap by a voltage-controlled current source labeled NF in the schematic shown in FIG. 6.4. NF is Micro-Cap's label for a function source, in which an algebraic formula or expression is used to compute the value of the output variable as a function of any set of time-domain functions. The channel current relations were derived from the charge control model (Ali & Gupta 1991). The charge control model investigates how the mobile current carrier charge in the conductive channel between the source and drain can be altered by the controlling gate potential, thus determining the channel conduction current. The controlling voltages were the gate voltage, measured from nodes vg+ to vg-, and the source-to-drain voltage, measured from nodes vds+ to vds-. These gate, vg+ and vg-, and source-to-drain, vds+ and vds-, nodes are shown in FIG. 6.4. Micro-Cap provides a function source that allows the current to

be evaluated as a function of the result of an inequality. Since the expression that describes the channel current in the linear region is different from the expression that describes the channel current in the saturation region, a function source was convenient to use to simulate the channel current. The appropriate channel current expression would be chosen after comparing the relation of V_{ds} to $V_{d,sat}$, thus differentiating between the linear and saturation regions. These expressions, as derived by Ali and Gupta (1991), are presented in Equations 6.1 to Equation 6.7, with all parameters defined in TABLE 6.4, follow:

When

$$V_{ds} < V_{d,sat},$$

where

$$V_{d,sat} = \sqrt{V_c^2 + 2V_cV_g} - V_c,$$

the expression for the drain current in the linear operating region was applied,

$$I_{ds} = \beta_0 \frac{\left(V_gV_{ds} - \frac{V_{ds}^2}{2}\right)}{\left(1 + \frac{V_{ds}}{V_c}\right)}, \qquad (6.1)$$

and when

$$V_{ds} \geq V_{d,sat},$$

the saturation drain current relation was applied,

$$I_{d,sat} = \frac{\beta_0 V_c^2}{2}\left(\sqrt{1 + \frac{2V_g}{V_c}} - 1\right)^2, \qquad (6.2)$$

where

$$\beta_0 = \left(\frac{w_g}{l_g}\right)\mu_0 c_0, \tag{6.3}$$

$$V_g = V_{gs} - V_{TH}, \tag{6.4}$$

$$V_c = l_g \mathbf{E}_c, \tag{6.5}$$

and

$$\mathbf{E}_c = \frac{v_{sat}}{\mu_0}, \tag{6.6}$$

$$\mathrm{c}_0 = \frac{\varepsilon}{d + d_i + \Delta d}. \tag{6.7}$$

Parameter	Description	Value
w_g	Gate width	100um
l_g	Gate length	0.25um
u_0	Hall mobility	$6000\frac{cm^2}{Vs} \pm 10-20\%$
d	n-GaInP thickness	160A
d_i	Spacer thickness	28A
Δd	Mean distance of 2-DEG from GaInP/GaAs interface	30A
$\varepsilon_{r\,GaP}$	Relative permittivity of GaP	11.1
$\varepsilon_{r\,InP}$	Relative permittivity of InP	12.4
$\varepsilon_{r\,GaIn_{0.33}P_{0.67}}$	Relative permittivity of $GaIn_{0.33}P_{0.67}$	11.97
ε_0	Permittivity of free space	$8.85\times10^{-14}\frac{F}{cm}$
$\varepsilon_{GaIn_{0.33}P_{0.67}}$	Permittivity of $GaIn_{0.33}P_{0.67}$	$1.059\times10^{-12}\frac{F}{cm}$
c_0	gate-to-2-DEG channel capacitance/area	$4.858\times10^{-7}\frac{F}{cm^2}$
β_o	$\left(\frac{w_g}{l_g}\right)\mu_0 c_0$	1.1659
v_{sat}	Saturation velocity	$(2\pm0.2)\times10^7\frac{cm}{s}$
E_c	Critical field	$3.33\frac{kV}{cm}$
V_c	Critical voltage	$0.0833V$
V_{TH}	Threshold voltage	1.05V

TABLE 6.4
GaInP/InGaAs/GaAs HEMT Parameters

Since the model does not predict the second order effects as the crowding of the I-V curves for both high gate voltages and low gate voltages, due to decreased mobility resulting from electrons entering the barrier where the doping causes lower carrier velocity and due to pinchoff, respectively, the quality of the fit of model curves to published data was determined by striving for a the best match for $-0.9V \le Vgs \le 0.3V$. The upturn in the I-V curves is space-charge-limited current caused by both short channel effects and high

voltage operation. Various simulations are shown in FIGS. 6.5-6.7. The simulated I-V curves shown in FIG. 6.7 compare favorably with the measured I-V curves shown in FIG. 6.2, requiring only slight adjustment of the ideal threshold voltage of 0.7V-0.8V given by Pereiaslavets (1997) and are used as a basis for the small-signal model and noise analysis.

Although the second order effects mentioned above were not included in the simulation, the effect of the parasitic source and drain resistances and the effect of the output source-to-drain resistance were included, as shown in FIG. 6.7. With these effects excluded, shown in FIG. 6.5, the resultant I-V curves do not resemble the desired characteristics shown in FIG. 6.2.

By comparing the resultant I-V characteristics with (FIG. 6.7) and without (FIG. 6.5) inclusion of the voltage drops across the parasitic resistances, it is clear that inclusion of the parasitic losses is required to accurately simulate the measured I-V curves shown in FIG. 6.2. The effect is to lower the channel current for a given gate voltage, which is seen by comparing the I-V curves in Fig. 6.5 and FIG. 6.7, which are plotted on the same scale. Instead of including this drop in the analytic expressions for the channel current (Equations 2.1 and 2.2), the location of the source to drain (nodes vds+ and vds-) and gate (nodes vgs+ and vgs-) nodes were redefined in the schematic. The effect of the excluding ohmic drops across the parasitic drain and source resistances was simulated by moving the gate and drain voltage nodes outside of the resistances.

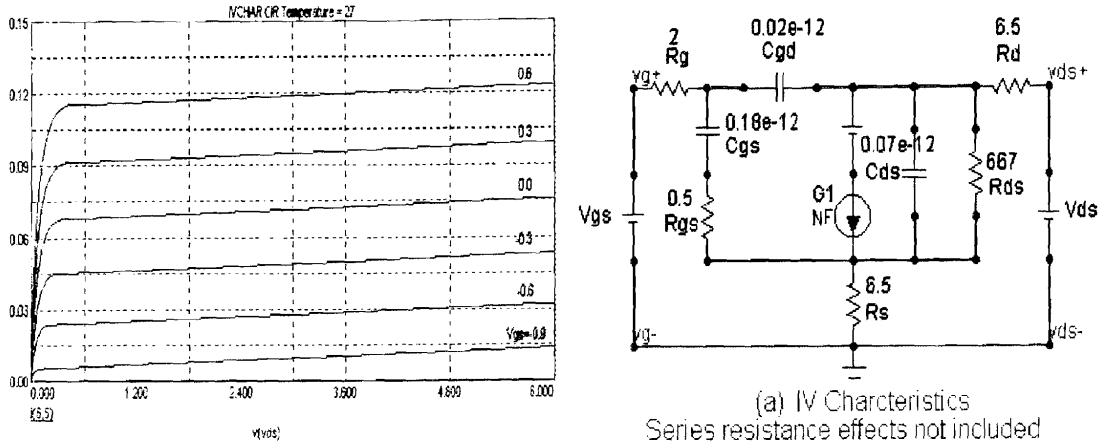

(a) IV Charcteristics
Series resistance effects not included

FIG. 6.5 DC I-V characteristic curves excluding ohmic voltage drops across the source and drain parasitic resistances, Rs and Rd.

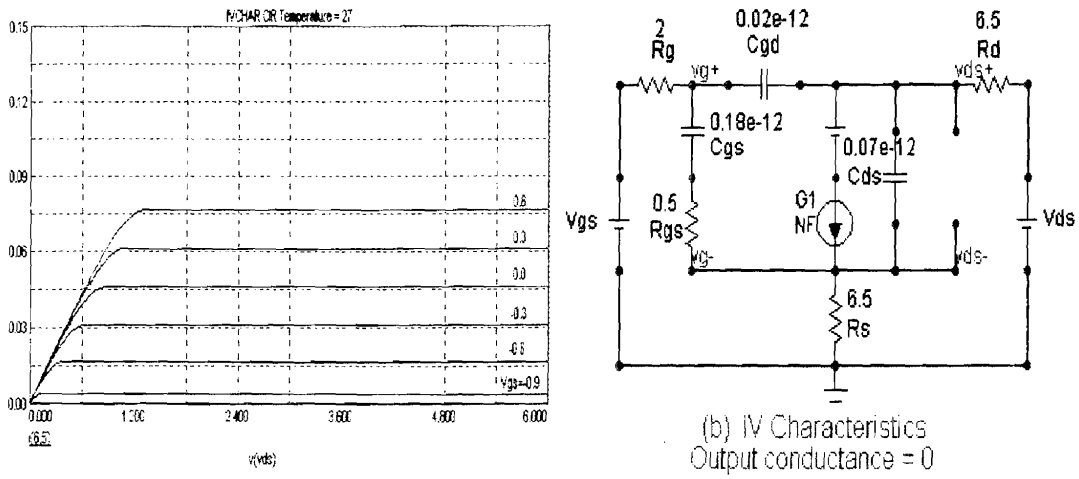

(b) IV Characteristics
Output conductance = 0

FIG. 6.6 DC I-V characteristic curves with output resistance, Rds, excluded displays no upturn of the curves at higher values of Vds

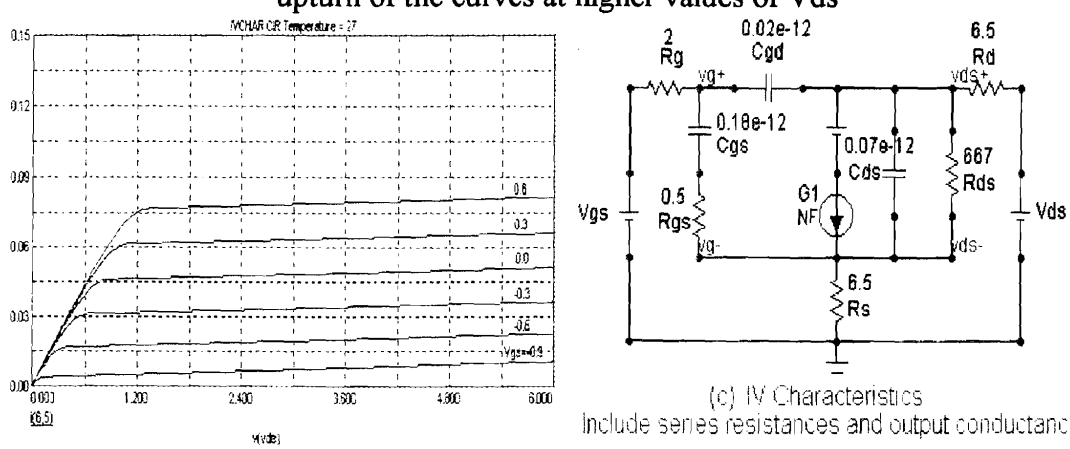

(c) IV Characteristics
Include series resistances and output conductance

FIG. 6.7 DC I-V characteristic curves including ohmic voltage drops across the source and drain parasitic resistances, Rs and Rd, and including the output resistance, Rds.

It is also interesting to compare the I-V characteristics with (FIG. 6.7) and without (FIG. 6.6) the presence of the output resistance, represented by Rds in the schematic. Rds simulates the upturn in the I-V curves caused by both short channel effect and high voltage operation. The curves in FIG. 6.6 do not show any upturn in the saturation region because of the exclusion of the output resistance.

6.5 Small-signal characteristics

Noise analysis is performed in AC analysis in SPICE. To insure linear operation during the noise analysis, it is necessary to create a small signal model for the HEMT. The small signal transconductance, g_m, can be obtained by differentiating $I_{d,sat}$, Equation 6.2, with respect to V_g,

$$g_m = \frac{dI_{d,sat}}{dV_g} = \frac{d\left[\frac{\beta_0 V_c^2}{2}\left(\sqrt{1+\frac{2V_g}{V_c}}-1\right)^2\right]}{dV_g}, \tag{6.8}$$

$$g_m = \beta_o V_c\left[1-\left(1+\frac{2V_g}{V_c}\right)^{-1/2}\right], \tag{6.9}$$

where

$$V_g = V_{gs} - V_{TH}. \tag{6.10}$$

This relation for g_m applies to the HEMT model shown in FIG. 6.8, but for the final equivalent circuit, the nodes vg+ and vg- were moved inside Rg to include the parasitic loss (as shown in the circuit in FIG. 6.7).

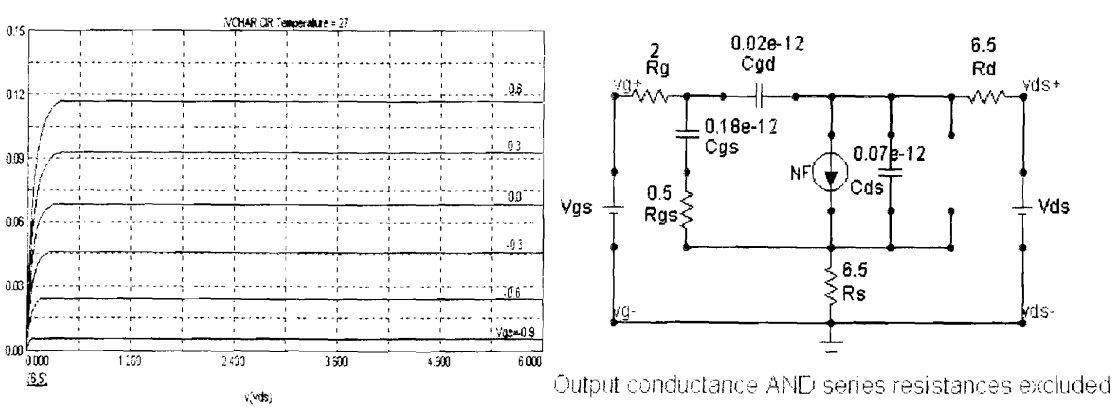

FIG. 6.8 DC I-V characteristic curves with output conductance AND series resistances excluded

Its application results in a g_m that is in agreement with the measured g_m calculated using

$$g_m \cong \frac{\Delta I_{ds}}{\Delta V_{gs}}$$

on I-V curves generated by that model. This model presents an additional scenario to those in FIGS. 6.5, 6.6, and 6.7. Neither ohmic voltage drops across the drain and source series parasitic resistances nor the output conductance have been included in the analytic expression. As shown above, these effects must be included for the model to accurately simulate the measured I-V characteristics of FIG. 6.2. Fig. 6.7 accurately simulated the I-V characteristics by moving the gate and source-to-drain nodes to include the effects of the parasitic losses. It would be interesting to derive how the inclusion of these effects alters the g_m analytically.

It is important to realize that these effects did not need to be included in the channel current expressions used to define the voltage-controlled current source in the final model because the effects were accounted for, not analytically, but by physically including these effects in the equivalent network by addition of Rds in parallel with the channel current, placing the gate and source-to-drain voltages used by the analytic relation for the drain current inboard of the parasitic resistances, and measuring the channel current through Rd, thereby including the current through Rds in the total channel current.

The following derivation of the relation for g_m', the transconductance that includes these effects, will reveal that the parasitic resistances have a greater effect than output conductance on the tranconductance, and that inclusion of both effects results in a calculated tranconductance that agrees with the measured transcondcutance.

The derivation refers to the parameters shown in FIG. 6.9.

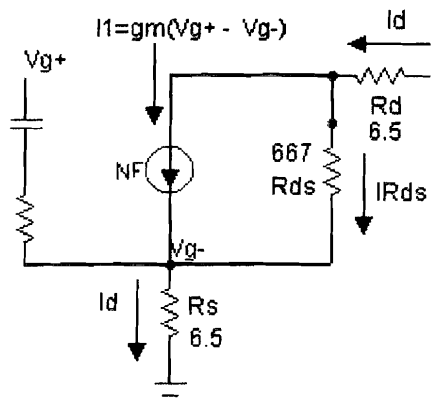

FIG. 6.9 Schematic used for g_m' derivation

Writing I_d in terms of the currents, I_1 and I_{Rds}, yields:

$$I_d = I_1 + I_{Rds}. \qquad (6.11)$$

The expression for I_{Rds} is

$$I_{Rds} = \frac{(V_d - I_d R_d) - V_g^-}{R_{ds}}.$$

Substituting this expression for I_{Rds} into Equation 6.11 yields

$$I_d = I_1 + \frac{(V_d - I_d R_d) - V_g^-}{R_{ds}},$$

Substituting $g_m(V_g^+ - V_g^-)$ for I_1 (as shown in FIG. 6.9),

$$I_d = g_m(V_g^+ - V_g^-) + \frac{(V_d - I_d R_d) - V_g^-}{R_{ds}}$$

Collecting terms,

$$I_d = g_m V_g^+ - V_g^-(g_m + \frac{1}{R_{ds}}) + \frac{V_d - I_d R_d}{R_{ds}}.$$

Substituting $I_d R_s = V_g^-$,

$$I_d = g_m V_g^+ - (I_d R_s)(g_m + \frac{1}{R_{ds}}) + \frac{V_d}{R_{ds}} - I_d \frac{R_d}{R_{ds}}$$

Rearranging terms

$$I_d\left[1 + g_m R_s + \frac{R_s}{R_{ds}} + \frac{R_d}{R_{ds}}\right] = g_m V_g^+ + \frac{V_d}{R_{ds}}$$

Solving for I_d

$$I_d = \frac{g_m V_g^+ + \frac{V_d}{R_{ds}}}{1 + g_m R_s + \frac{R_s}{R_{ds}} + \frac{R_d}{R_{ds}}}$$

Taking the partial derivativewith respect to V_g^+ to get $g_m^{'}$ (it is a partial derivative because $g_m^{'} = f(V_g^+, V_d)$),

$$g_m^{'} = \frac{\partial I_d}{\partial V_g^+} = \frac{g_m}{1 + g_m R_s + \frac{R_s R_d}{R_{ds}}}. \qquad (6.12)$$

Substituting values into Equation 6.12,

$$g_m' = \frac{g_m}{1 + \frac{6.6\Omega}{667\Omega} + 6.5\Omega \cdot 780mS/mm + \frac{6.5\Omega}{667\Omega}}$$

$$g_m' = 0.655 g_m .$$

The relation of g_m vs g_m' to the I-V characteristics generated by exclusion (FIG. 6.9) vs inclusion (FIG. 6.8) of the output conductance and series resistances is shown in TABLE 6.4 for a chosen $V_{gs} = 0V$ and $V_{ds} = 3.6V$. g_m is the tranconductance based on the model without including the parasitic voltage drops while g_m' is the transconductance based on the model including the parasitics. The resultant transconductance is in agreement with that measured on the GaInP/InGaAs/GaAs HEMT (Pereiaslavets 1997).

Measured using the circuit in FIG. 6.10, including Rds $g_m \cong \frac{\Delta I_{ds}}{\Delta V_{gs}}$	Measured using the circuit in FIG. 6.6, excluding Rds $g_m' \cong \frac{\Delta I_{ds}}{\Delta V_{gs}}$	Calculated g_m using Equation 6.9 $g_m = \beta_o V_c \left[1 - \left(1 + \frac{2V_g}{V_c}\right)^{-1/2}\right]$	Calculated g_m' using Equation 6.12 $g_m' = \frac{\partial I_d}{\partial V_g^+} = \frac{g_m}{1 + g_m R_s + \frac{R_s R_d}{R_{ds}}}$
750mS/mm	500mS/mm	780mS/mm	510mS/mm

TABLE 6.4 Comparison of measured and calculated transconductances

Micro-Cap was also used to determine g_m by plotting the derivative of $I_{d,sat}$ with respect to V_g. The plot of g_m vs V_{gs} is shown in FIG. 6.10. The cursor function was

used to determine g_m for the chosen operating point and load line,

$V_{gs} = 0$ and $V_{ds} = 3.6V$.

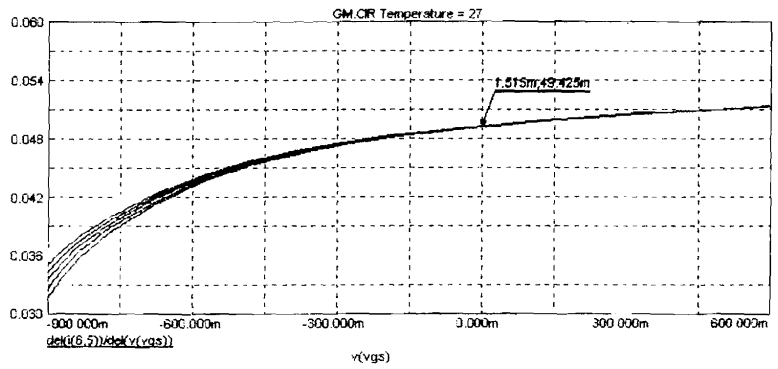

FIG. 6.10 g_m vs V_{gs} for $V_{ds} = 2V, 3V, 4V, 5V, 6V$

$g_m' = 0.494 mS / mm$ for $V_{gs} = 0V$

Using the relation derived above, this corresponds to

$$g_m = \frac{g_m'}{0.655},$$

$$\text{where } g_m' = 0.494 \frac{S}{mm},$$

$$g_m = 0.754 \frac{S}{mm},$$

and, for $100um$ gate,

$$g_m = 0.0754 S.$$

This value was used for the transconductance for all of the following noise simulations $V_{gs} = 0V$ as shown in FIG 6.11.

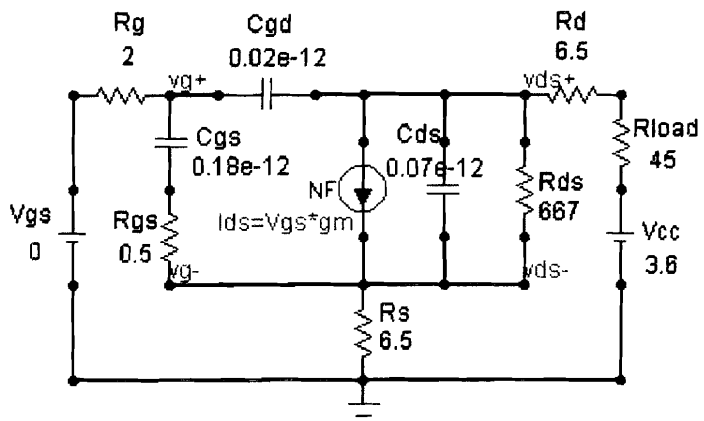

FIG. 6.11 Equivalent small signal network model of GaInP/InGaAs/GaAs HEMT

6.6 Noise sources

During the last decade, AlGaAs was generally used as the barrier material for HEMTs grown on a GaAs substrate. This material has several limitations. The Al mole fraction has to be kept below 23% to reduce the effect of DX centers which can deteriorate device low frequency noise figure. This has the undesirable consequence of limiting the conduction band offset (the difference in the energy levels of the conduction bands of the materials crating the heterojunction) to 180meV (Pereiaslavets 1997). This has led to development of HEMTs with other materials, as GaInP.

The resultant discrete model described in Chapter 5 succeeds in predicting the total $1/f$ noise measured at the output of a HEMT. That model effectively places all of the $1/f$ noise in the channel. A different approach is now presented. Inspired by the notion that the low frequency noise seen in HEMTs is due to a superposition of $1/f$ noise and g-r noise bulges (Section 3.6), two macros were developed in Micro-Cap that would simulate each of these noises. These macros could be distributed throughout the HEMT model to gain insight into the distribution and mechanism of $1/f$ noise in various layers and interfaces of the HEMT. The $1/f$ noise from these macros would be superimposed on the thermal noise from the resistances in the model, thus completing the simulated noise spectrum,

$$S_{total}(f) = \sum S_{1/f}(f) + \sum S_{g\text{-}r\ bulges}(f) + \sum S_{thermal}(f).$$

Each macro is described below, followed by the equivalent noise spectra produced by the macro. The transfer functions from possible noise generation locations in the HEMT are presented. Simulations of the low frequency noise by inserting the noise sources at two different locations in the HEMT equivalent circuit are presented.

6.6.1 1/*f* noise macro

The macro developed to simulate 1/*f* noise is shown in FIG. 6.12.

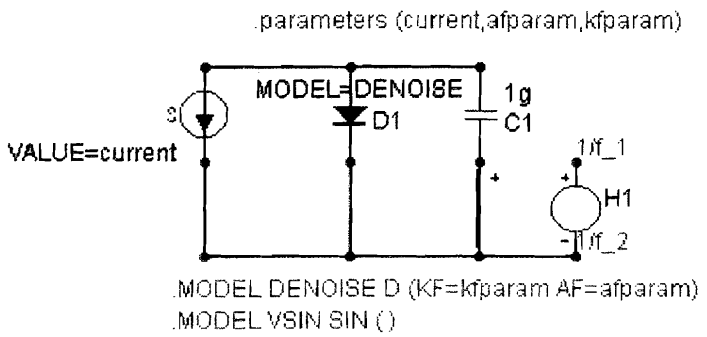

FIG. 6.12 1/*f* noise macro

The 1/*f* noise power falls off at 10dB/decade. The 1/*f* noise macro simulates this spectrum using a diode as a source of 1/*f* noise. Micro-Cap calculates the noise current in a diode as the sum of the 1/*f* noise and the shot noise according to Equation 5.1.

The 1GF capacitor blocks the dc bias current and permits the ac short-circuit noise current to be sensed through the current nodes of the current controlled voltage source. In this way the diode noise current is transferred to a noise voltage at the nodes 1/f_1 and 1/f_2.

The nodes of the macro symbol for the 1/*f* noise shown in FIG. 6.13 are equivalent to the nodes 1/f_1 and 1/f_2 in the macro.

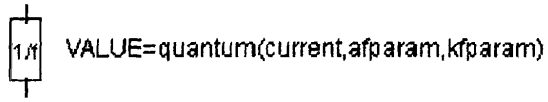

FIG. 6.13 1/*f* noise circuit element

When using the macro, the user only needs to input the three macro parameters, *current, AFparam, and Kfparam*. The parameter *current* is the dc diode current, I_{dc}, *Afparam* is the 1/*f* noise exponent, *AF*, and *Kfparam* is the 1/*f* noise coefficient, *KF*, in the diode noise current equation above. In FIG. 6.14, for example, the user specified 0.035A for I_{dc}, 2.01 for *AF*, and 3.105e-11A for *KF*.

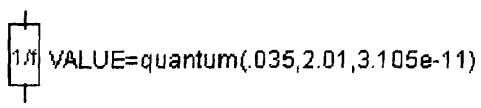

FIG. 6.14 1/*f* noise circuit element

Letting AF=1, KF is calculated by equating the 1/*f* noise term and the shot noise term in the above expression for the diode noise current,

$$KF = 2qf_{corner}.$$

Knowing *KF*, I_{dc} can be calculated by solving the diode noise current expression for the dc bias current,

$$I_{dc} = \frac{I_d^2}{KF + 2q}.$$

It is intended for the $1/f$ noise macro to simulate a $1/f$ spectrum exclusive of shot noise, but Micro-Cap automatically includes shot noise in its model for diode noise current. Choosing a very high value for f_{corner} will result in a negligible shot noise amplitude compared to the thermal noise of the resistances in the equivalent network of the HEMT.

6.6.2 g-r bulge noise macro

As described in Chapter 3, $1/f$ noise spectra can be attributed to the superposition of many traps whose spectral intensity shows a frequency dependence which is constant up to a corner frequency and then falls off as $1/f^2$. The macro shown in FIG. 6.15 was developed to simulate a trap.

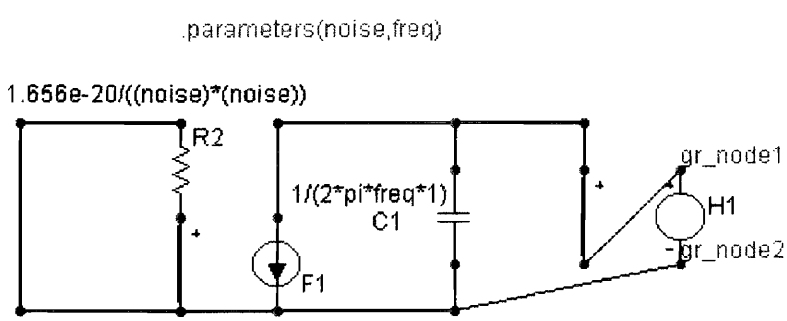

FIG. 6.15 g-r noise macro

The noise generated by a resistor is passed through a low pass filter whose output is detected across the current-controlled voltage source at the nodes labeled gr_node1 and

gr_node2. The nodes of the macro symbol shown in FIG. 6.16 are equivalent to the nodes gr_node1 and gr_node2.

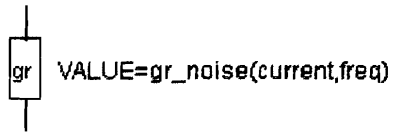

FIG. 6.16 g-r noise circuit element

When using the macro, the user only needs to input the macro's parameters which are *current* and *freq*. *Freq* determines the corner frequency of the trap. In FIG. 6.17, for example, the user specified $1e-6\frac{V}{\sqrt{Hz}}$ noise voltage and a corner frequency at *1000Hz*. *Current* refers to the constant noise amplitude before the corner frequency of the trap is reached

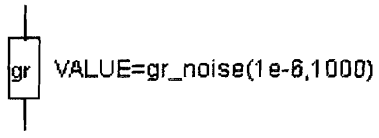

FIG. 6.17 g-r noise circuit element

The macro is designed to calculate the resistor value required to produce the requested noise level and corner frequency via the relation

$$\text{resistance} = \frac{4kT}{(current * current)},$$

where k is Boltzman's constant

T the absolute temperature,

current is the noise current in $\frac{A}{\sqrt{Hz}}$.

The low-pass filter is formed by the noise current in parallel with a capacitor and a fixed 1Ω noiseless resistor. The macro also calculates the capacitance required to produce the specified corner frequency via

$$C = \frac{1}{2\pi freq(1\Omega)}.$$

Micro-Cap's noise output is in $\frac{V}{\sqrt{Hz}}$, so to plot the noise power, which is the unit in which the noise data being modeled was presented (FIG. 6.1), it is necessary to plot the square of the Micro-Cap's noise output. This explains why a low pass filter, which falls off at 20dB/decade, produces noise power that falls off at the desired 20dB/decade, simulating the $1/f^2$ dependence of bulge noise.

6.6.3 Thermal noise

Micro-Cap calculates the spectral density of the thermal noise current in a resistor, $I^2_{thermal}$, according to

$$I^2_{thermal} = \frac{4kT}{R},$$

where k is Boltzman's constant,

T is the temperature in Kelvin,

and R is the resistance in ohms.

The measured noise shown in FIG. 6.1 includes the thermal noise from all the resistances in the HEMT but does not include the noise of the load resistor. Therefore, to simulate the noise only due to the HEMT, the 45Ω load resistor is represented by a 45Ω noiseless resistor.

6.6.4 Noise transfer functions

Micro-Cap calculates the noise at the output, ONOISE, and then calculates the equivalent noise at the input, INOISE. To determine the expected noise from a noise source placed at selected points in the HEMT model, a test noise source of $1 \times 10^{-6}\ \mathrm{V}/\sqrt{\mathrm{Hz}}$ was placed, *one at a time*, at the location of interest. It was desired to detect noise only from the inserted noise source. Since SPICE does not permit turning on/off selected noise generators, all the resistors in the model were replaced by noiseless resistors, described in Chapter 4. For example, the circuit in FIG. 6.18 was used to determine the transfer function for a noise source located in series with Rg.

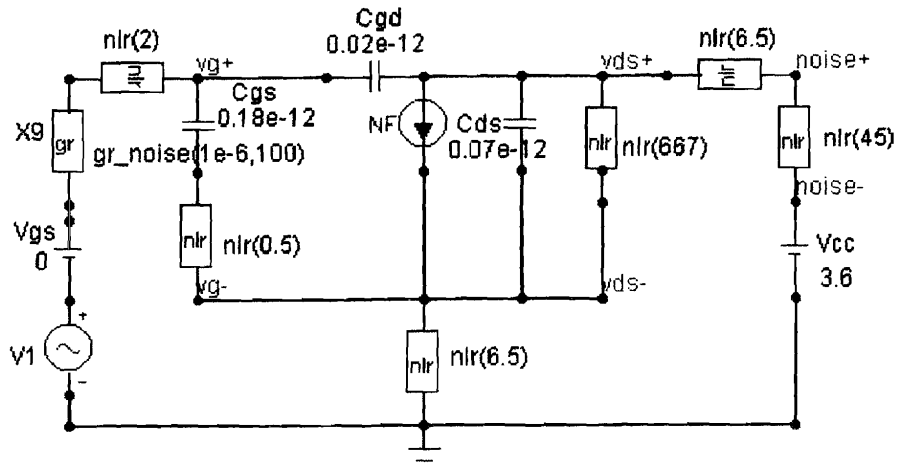

FIG. 6.18 Schematic used to measure noise transfer function for noise at Rg

The amount of noise seen at the output nodes, noise+ and noise-, and the input, vgs, for test sources in series with each resistor in the model is tabulated in TABLE 6.5. The electric field characteristic is also listed. The electric field strength is important in evaluating the likelihood of $1/f$ noise in that region. The higher the field, the shorter the time constant of a trap (Eastman 1998).

Noise location (in series with indicated resistor)	*INOISE*^{2}	*ONOISE*^{2}	Electric field characteristics
Rg	1.00085e-12	4.58123e-12	
Rd	4.02178e-16	1.84090e-15	low E
Rds	4.02178e-16	1.84090e-15	high E
Rs	1.04138e-12	4.76674e-12	low E
Rgs	9.53733e-35	4.3655e-34	high E
Rgd	7.65074e-36	3.50200e-35	substrate/deep levels/ surface

TABLE 6.5 Noise transfer functions

6.6.5 Noise simulation

To demonstrate the superposition of the two noise sources, each noise source is inserted, one-by-one, in series with Rg, in order to see the effect of that source. For example, in FIG. 6.19, the noise source to produce $1/f$ noise is inserted in series with Rg. All resistors are replaced by noiseless resistors (labeled "nlr") to simulate the noise from the $1/f$ noise source only. The resultant noise power spectrum, in V^2 / Hz, is shown in the plot below the circuit. The same process was used for FIG. 6.20-6.22 with g-r bulge noise sources replacing the $1/f$ noise source. The noise sources are labeled "1/f" or "gr" as shown in FIG. 6.14 and FIG. 6.17. All resistors are replaced by noiseless resistors (labeled "nlr" in the schematic) so they will not contribute to the noise. In FIG. 6.23, there are no $1/f$ or g-r bulge noise sources present; only the thermal noise from the discrete resistors in the circuit produce noise. FIG. 6.24 shows the results to a simulation that includes a $1/f$ noise source, two g-r bulge noise sources, and the thermal resistor noise superimposed. FIG. 6.25 presents the same information as FIG. 6.19-6.24 on one page to facilitate comparison of the noise spectra.

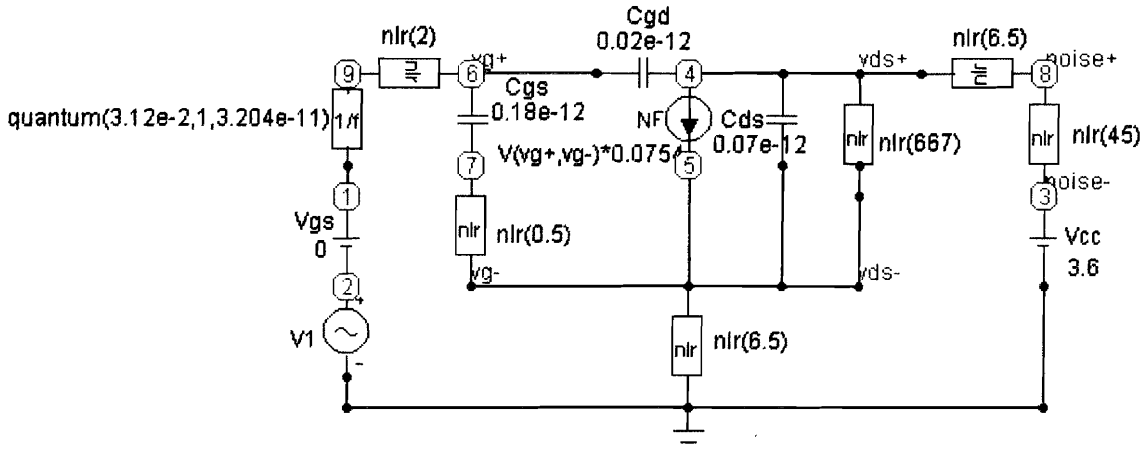

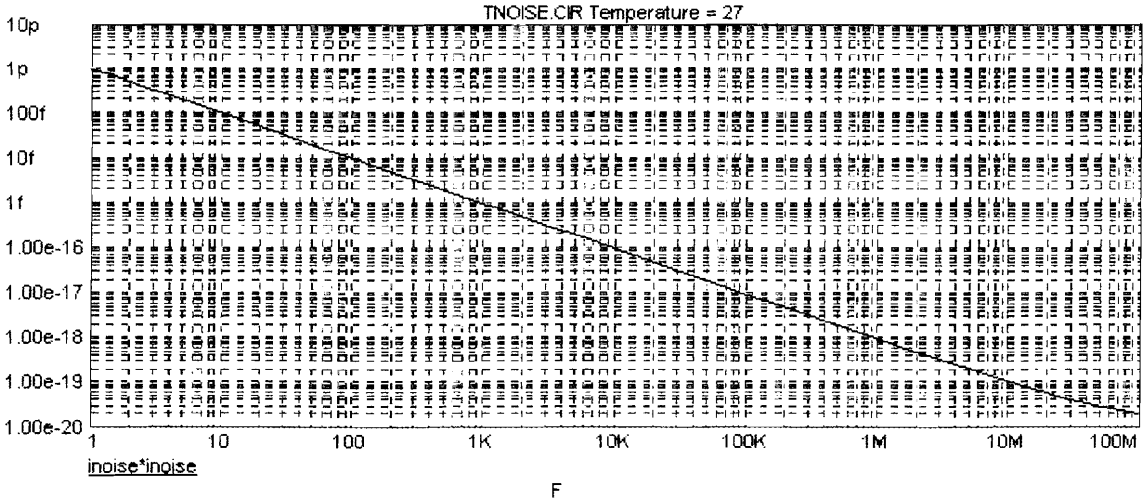

FIG. 6.19 1/*f* noise only

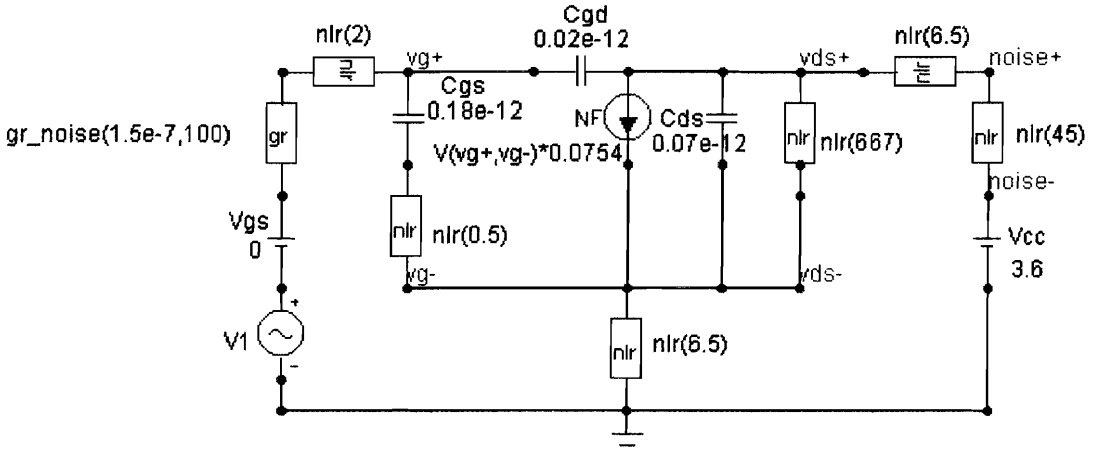

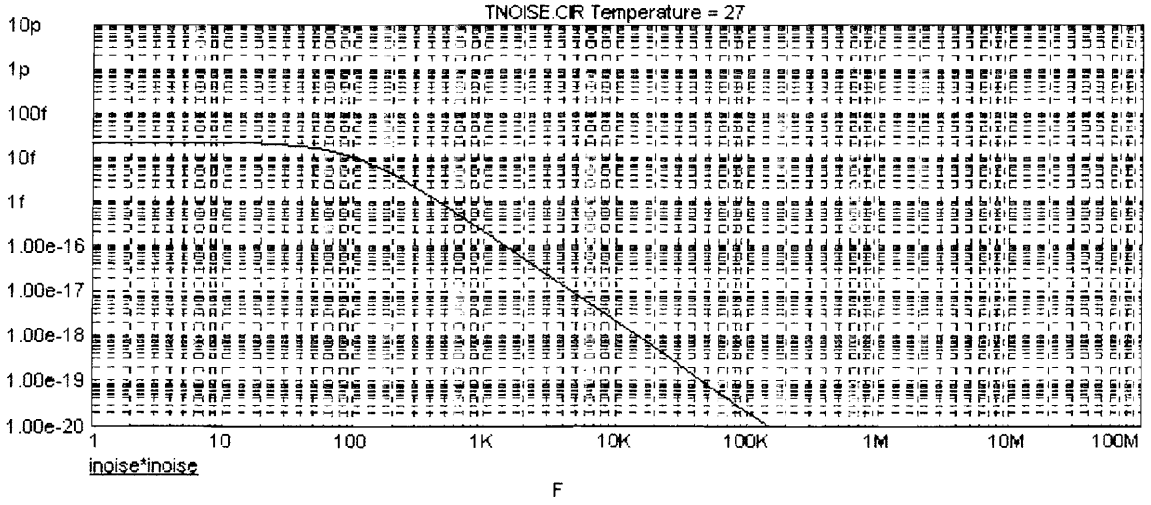

FIG. 6.20 g-r bulge noise only

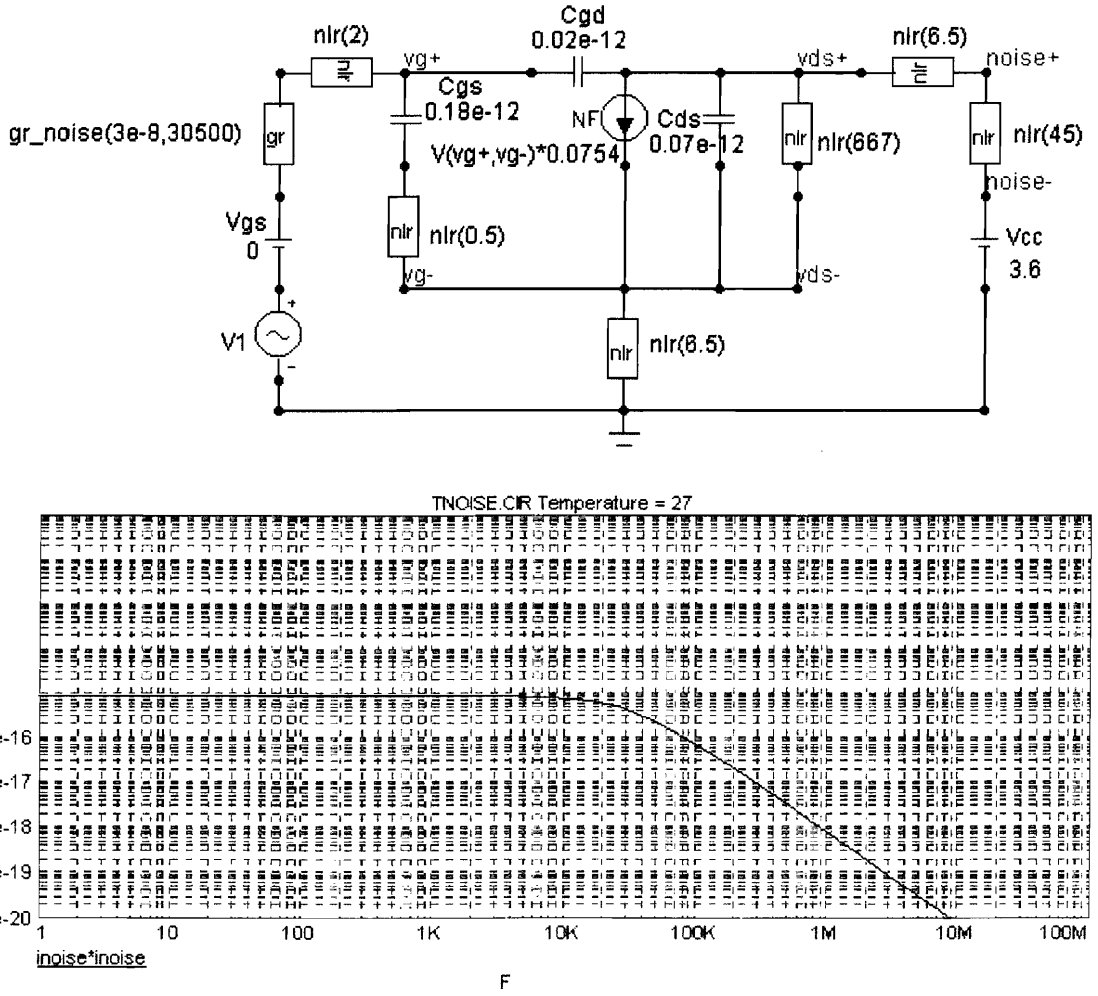

FIG. 6.21 g-r bulge noise only

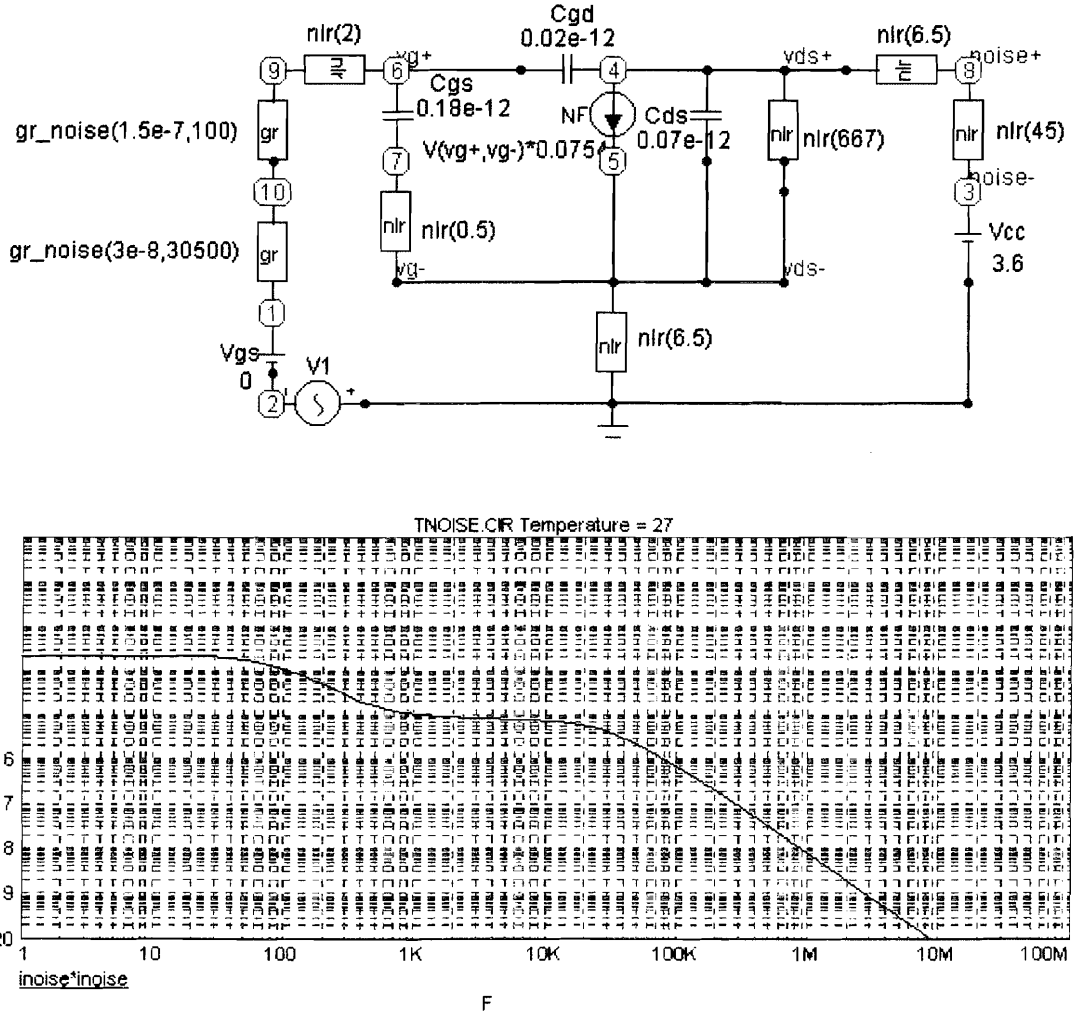

FIG. 6.22 Two g-r bulge noise sources

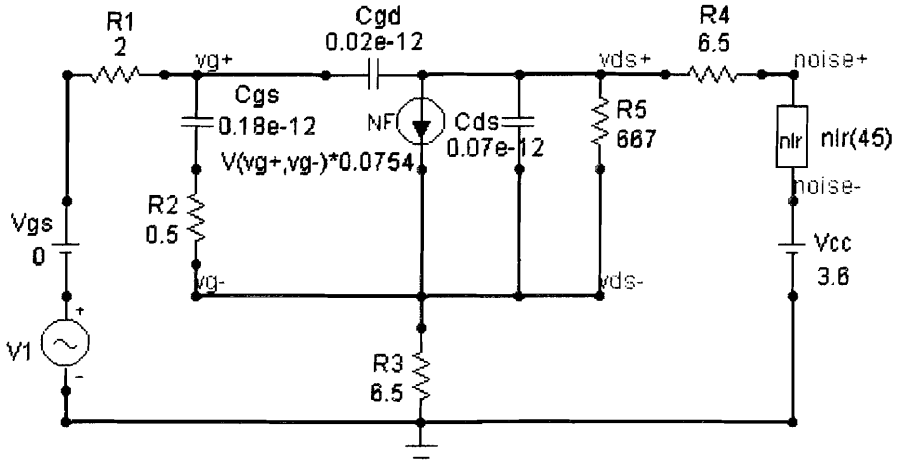

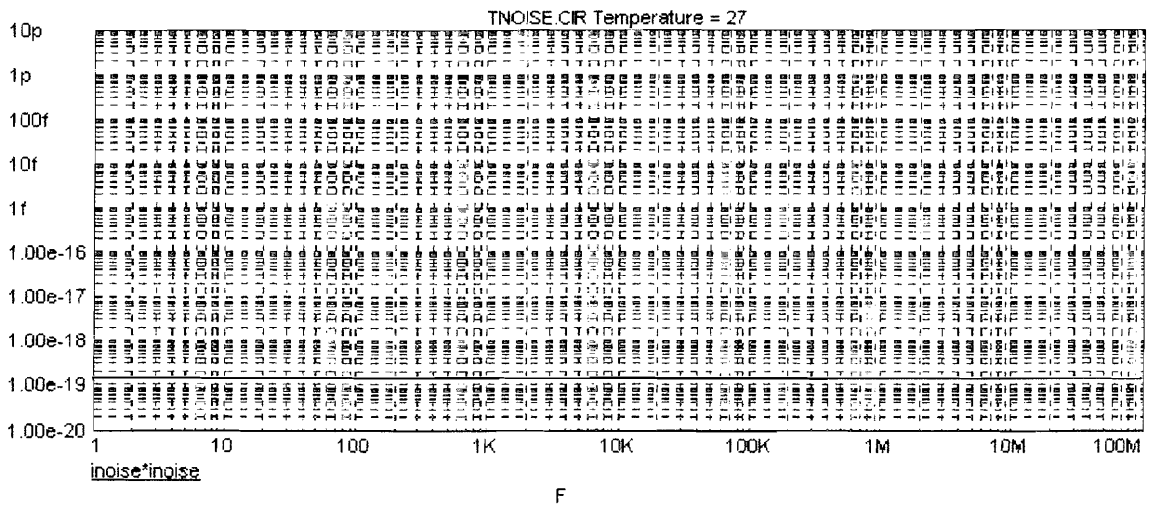

FIG. 6.23 Thermal noise from resistances only

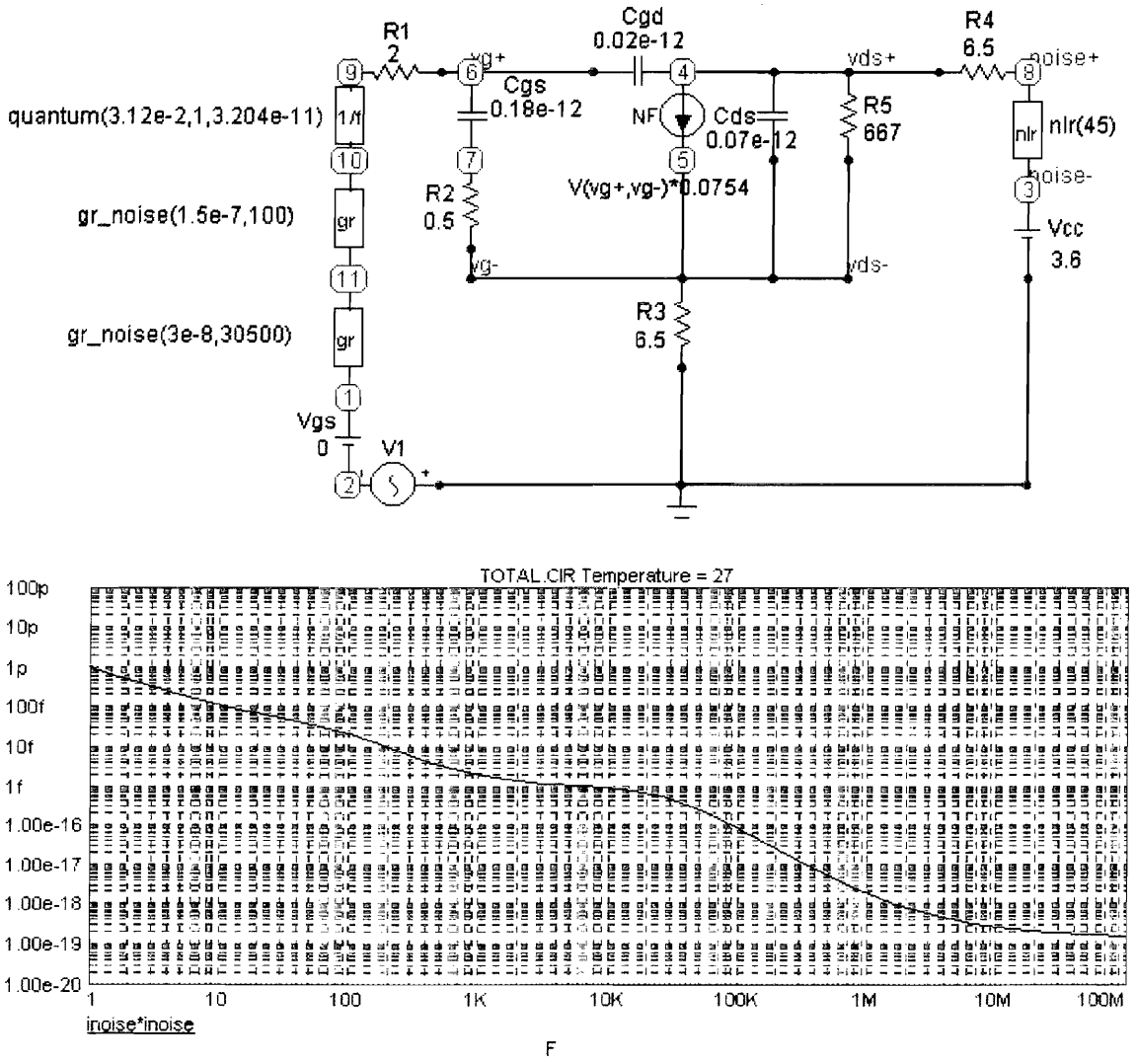

FIG. 6.24 Total noise power

$$S_{total}(f) = \sum S_{1/f}(f) + \sum S_{g\text{-}r\ bulge\ noise}(f) + \sum S_{thermal}(f)$$

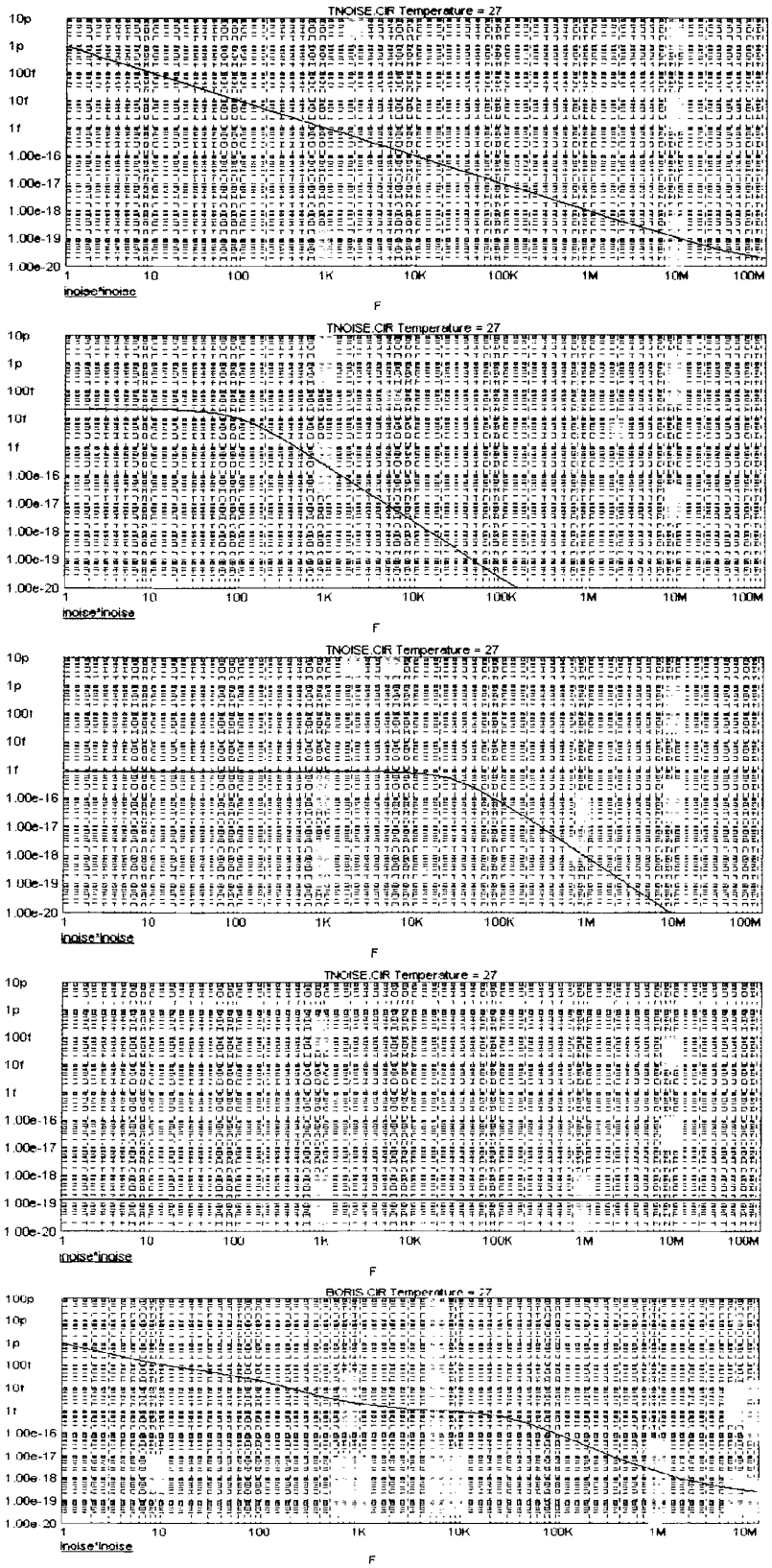

FIG. 6.25 Composite view of individual noise sources and their superposition

Next another scenario is investigated in which the noise is located in a different part of the HEMT. If instead of locating all the noise sources in series with Rg, they were all located in series with Rd, *which has a different transfer function to the output nodes* (TABLE 6.5), the resultant equivalent input noise power, shown in FIG. 6.26, is several orders of magnitude too low. When the amplitude of the noise sources are appropriately scaled by the ratio of the transfer functions, the simulation yields the desired noise amplitudes (FIG. 6.27), consistent with the published, measured noise (compare FIG. 6.24 and FIG. 6.27). Due to the difference in the transfer function from the different locations, the noise sources at Rd do not result in the same noise power at the output as they do when located at Rg in FIG. 6.25. For a given amount of measured noise at the output, the noise amplitude would have to be much greater if the sources of the noise were at Rd. There would have to be more traps and more $1/f$ noise in that part of the HEMT.

FIG. 6.28 shows the simulated equivalent gate noise after fine-tuning the noise parameters in the model with the equivalent gate noise spectra of the GaInP/GaInAs/GaAs HEMT below for comparison. The $1/f$ noise and the noise bulges compare favorably with the measured noise. However, if the measured noise level of $\sim 2 \times 10^{-17}\ \mathrm{V}^2 / \mathrm{Hz}$ shown between 1MHz and 100MHz represents the white noise level, the simulated thermal noise from the resistances in the equivalent network of the HEMT is about two orders of magnitude too low.

These simulations are examples of how insight into the physical source of $1/f$ noise in HEMTs may be gained by examining the effect of varying the location, number, and properties of the noise sources.

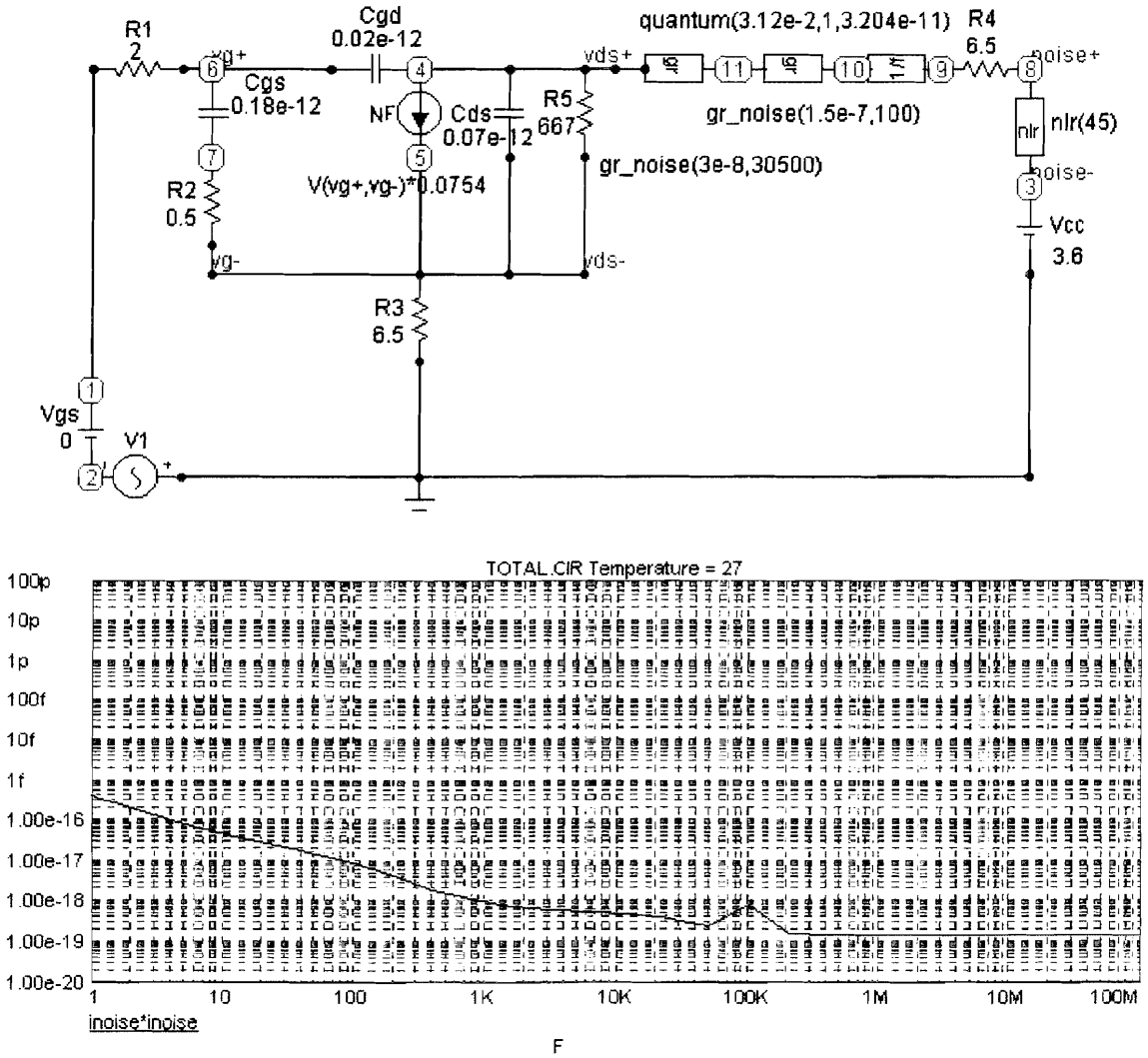

FIG. 6.26 Total noise power with all sources located at Rd. The magnitude of each noise source is the same as in FIG. 6.25, where the noise sources were located at Rg. Due to the difference in the transfer function from the different locations, the noise sources at Rd do not result in the same noise power as in FIG. 6.25.

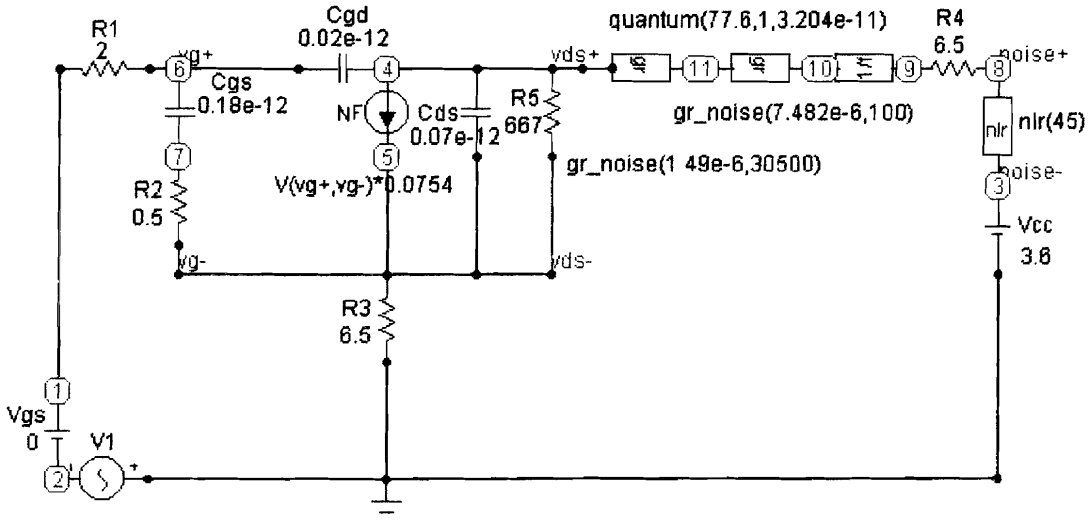

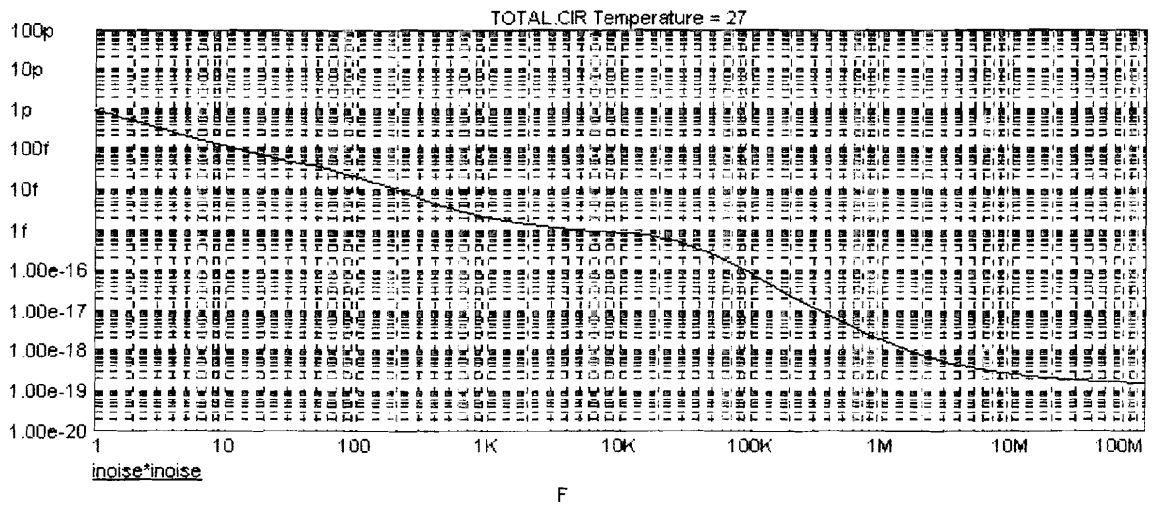

FIG. 6.27 Amplitude of the noise sources is adjusted to yield the desired noise amplitudes when located in series with Rd.

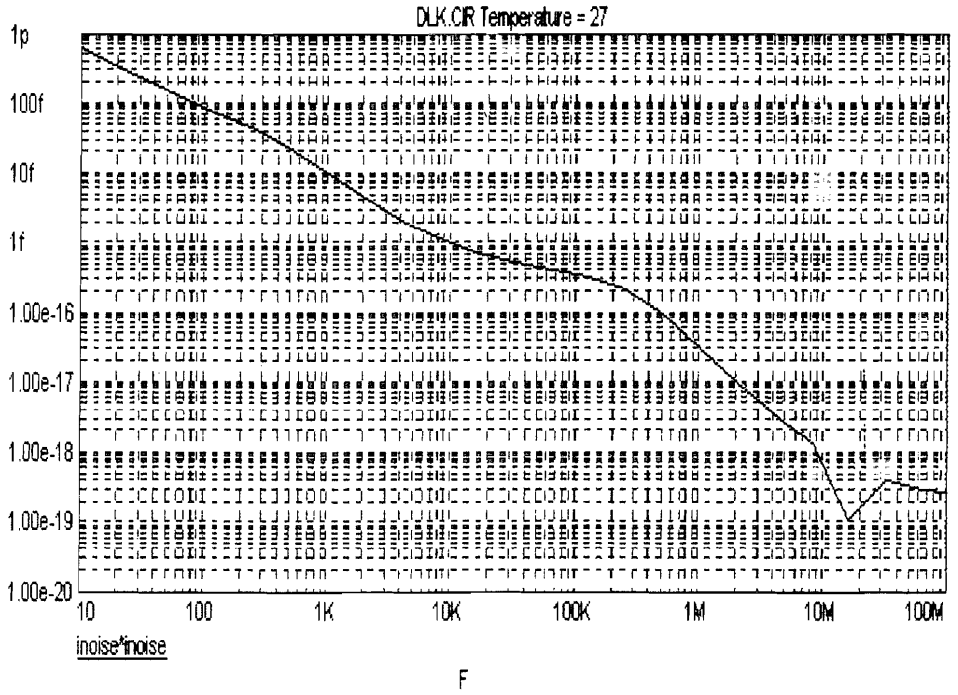

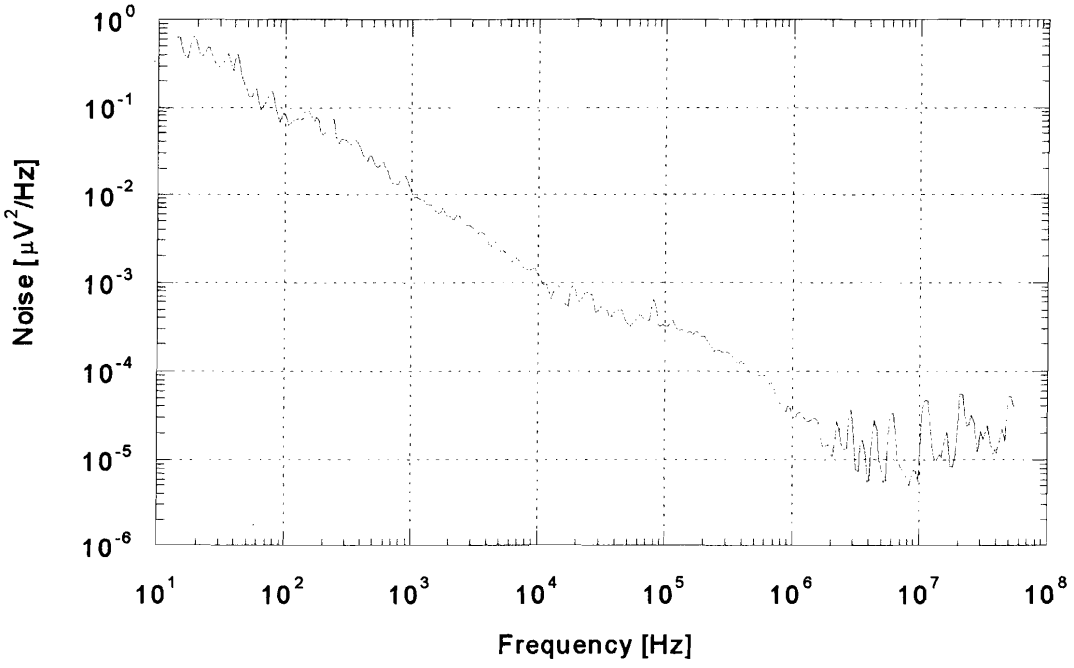

FIG. 6.28 Micro-Cap noise simulation of equivalent gate noise spectra (above) and equivalent gate noise spectra of GaInP/GaInAs/GaAs HEMT (below, repeated from FIG. 6.1) with slight adjustment of the noise parameters shown in the circuit in FIG. 6.27.

Conclusion

> To myself I seem to have been only a boy playing on the seashore, and diverting myself in now and then finding a smoother pebble or a smoother shell than ordinary, whilst the great ocean of truth lay all undiscovered before me.
>
> Sir Isaac Newton

Both the discrete $1/f$ noise model and distributed $1/f$ noise model demonstrated their ability to simulate measured $1/f$ noise in HEMTs. Although the resultant noise spectra output by both models appear similar, the intended application for each model differ significantly. The discrete $1/f$ noise model is useful in circuit design while the distributed $1/f$ noise model is intended as a tool to understand noise sources within a HEMT.

The application of both models requires information about the equivalent circuit of the HEMT. The discrete $1/f$ noise model requires noise data from at least two known biasing conditions. The distributed $1/f$ noise model requires an accurate equivalent network for the HEMT in order to accurately simulate the transmission of noise from internal noise sources to the output nodes.

Martin Gardner (1978) writes that scientists tend to overlook $1/f$ noise because there are no good theories to account for them, but there is scarcely an aspect of nature in which they cannot be found.

Noting whether the phenomena of interest is scale invariant or not may provide additional insight into the processes involved.

Philosophically, it has been suggested that $1/f$ phenomena are indicators of the characteristic way our world changes in time. $1/f$ noise is intermediate between randomness and predictability. There is something interesting on all (in this case, time) scales. Hopefully this study of low frequency noise in HEMTs will provide additional insight into interesting $1/f$ phenomena.

REFERENCES

Ahn, H., & Nokali, M. E. 1994, "An Analytical Model for High Electron Mobility Transistors", *IEEE Transactions on Electron Devices*, Vol. 41, No. 41, pp. 874-878.

Ali, A. and Gupta, A. 1991, *HEMTs and HBTs: Devices, Fabrication, and Circuits*, (Boston:Artech House).

Ando, Y. & Itoh, T. 1990, "DC, Small-Signal, and Noise Modeling for Two-Dimensional Electron Gas Field-Effect Transistors Based on Accurate Charge-Control Characteristics", *IEEE Transactions on Electron Devices*, Vol. 37, No. 1, pp. 67-78.

Angelov, I. & Zirath, H. 1992, "New Empirical Nonlinear Model for HEMT Devices", *Electronics Letters*, Vol. 28, No. 2, pp.140-142.

Anwar, A. F. & Liu, K. W. 1994, "Noise Temperature Modeling of AlGaAs/GaAs and AlGaAs/InGaAs/GaAs HEMTs, *Solid State Electronics*, Vol. 37, No. 9, pp. 1585-1588.

Connelly, J. A., & Choi, P. 1992, *Macromodelling with SPICE*, (Prentice Hall, New Jersey).

Conti, P. C., Marchisio, L., & Titinet, G. C. 1992, "Performances and Reliability of HEMTs: State of the Art and Experimental Analysis", *Microelectronic Reliability*, Vol. 32, No. 11, pp. 1577-1583.

Dambrine, G., Cappy, A., Heliodore, F., & Playez, E. 1988, "A New Method for Determining the FET Small-Signal Equivalent Circuit", *IEEE Trans. Microwave Theory Tech.*, Vol. MTT-36, pp. 1151-1159.

DasGupta, N. & DasGupta, A. 1993, "An Analytical Expression for Sheet Carrier Concentration vs Gate Voltage for HEMT Modeling", *Solid-State Electronics*, Vol. 36, No. 2, pp. 201-203.

Dingle, R., Stormer, H. L., Gossard, A. C., & Wiegmann, W. 1978, "Electron Mobilities in Modulation Doped Semiconductor Heterojunction Superlattices", *Applied Physics Letters*, Vol. 33, pp. 665-667.

Dollfus, P., Galdin, S., & Hesto, P. 1992, "Microwave Analysis of AlGaAs/InGaAs HEMT using Monte Carlo Simulation", *Electronics Letters*, Vol. 28, No. 5, pp. 458-460.

Esaki, L.& Tsu, R. 1969, IBM Research Report No. RC-2418.

Eskandarian, A. & Weinreb, S. 1993, "A Note on Experimental Determination of Small-Signal Equivalent Circuit of Millimeter Wave FETs", *IEEE Transactions on Microwave Theory and Techniques*, Vol. 41, No. 1, pp. 159-162.

Fano, R. M. 1950, "Theoretical Limitations on the Broadband Matching of Arbitrary Impedances", *Journal of the Franklin Institute*, Vol. 249, No. 1, pp. 57-154.

Fukui, H. 1979, "Optimal Noise Figure of Microwave GaAs MESFETs", *IEEE Trans. Electron Devices*, Vol. ED-26, pp.1032.

Gardner, M. 1978, "White and Brown Music, Fractal Curves, and $1/f$ Fluctuations", *Scientific American*, Vol. 238.

Gonzalez, Guillermo 1984, *Microwave Transistor Amplifiers*, (Prentice-Hall, Inc, New Jersey).

Happy, H., Dambrine, G., Alamkan, J., Danneville, F., Kaptche-Tagne, F., & Cappy, A. 1993, "HELENA: A Friendly Software for Calculating the DC, AC, and Noise Performance of HEMTs", *International Journal of Microwave and Millimeter-Wave Computer-Aided Engineering*, Vol. 3, No. 1, pp. 14-28.

Horowitz, P. & Hill, W. 1994, *The Art of Electronics*, (Cambridge University Press, New York).

Kitchin, C. R. 1991, *Astrophysical Techniques*, (Adam Hilger, Bristol).

Ladbrooke, P. H., Hill, A. J., & Bridge, J. P. 1993, "Fast FET and HEMT Solvers for Microwave CAD", *International Journal of Microwave and Millimeter-Wave Computer-Aided Engineering*, Vol. 3, No. 1, pp. 37-60.

Liu, S. M., Das, M. B., Kopp, W. & Morkoc, H. 1985, "Noise Behavior of 1um Gate-Length Modulation-Doped FETs from 10^{-2} to 10^{8} Hz", *IEEE Electron Device Letters*, Vol. EDL-6, No. 9, pp. 453-455.

Mahon, S. J. & Skellern, D. J. *1992*, Determination of Device Structure from GaAs/AlGaAs HEMT DC *I-V* Characteristic Curves", *IEEE Transactions on Electron Devices*, Vol. 39, No. 5, pp. 1041-1049.

Meyer, R. G., Nagel, L. & Lui, S. K. 1973, "Computer Simulation of 1/*f* Noise Performance of Electronic Circuits", *IEEE Journal of Solid State Circuits*, June, pp. 237-240.

Mladentsev, A. L. & Yakimov, A. V. 1993, "Wandering Defects: A Source of 1/*f* noise?", *Radiophysics and Quantum Electronics*, Vol. 36, No. 8, pp. 579-581.

Morgan, D. V. & Williams, R. H. 1991, *Physics and Technology of Heterojunction Devices* (Peter Peregrinus Ltd, London, UK)

Morkoc, H. & Solomon, P. M. 1984, "The HEMT: A Superfast Transistor", *IEEE Spectrum*, Vol. 21, February, pp. 28-35.

Motchenbacher, C. D. & Connelly, J. A. 1993, *Low Noise Electronic System Design*, (John Wiley & Sons, New York).

Peitgan, H. & Saupe, D 1988, *The Science of Fractal Images* (Springer-Verlag, New York)

Pereiaslavets, Boris 1997, *GaInP/GaInAs/GaAs MODFETs for High Power and High Frequency Applications*, PhD thesis, Cornell University

Pierret, R. F. 1990, *Field Effect Devices* (Addison-Wesley Publishing Company, Reading, Massachusetts)

Pospieszalski, M. W. and Wollack, E. J. 1997, *1997 Topical Symposium on Millimeter Waves*, (Japan)

Pospieszalski, M. W. 1989, "Modeling of Noise Parameters of MESFETs and MODFETs and Their Frequency and Temperature Dependence", *IEEE Transactions on Microwave Theory and Techniques*, Vol. 37, No. 9, September, pp. 1340-1350.

Pucel, R. A., Haus, H. A., & Statz, H. 1975, "Signal and Noise Properties of GaAs Microwave FET", *Advances in Electronics and Electron Physics*, Vol. 38, pp. 195.

Rothke, H, & Dahlke, W. 1956, "Theory of Noisy Fourpoles", *Proc. IRE*, Vol. 44, pp. 811-818.

Schroeder, M. 1991, *Fractals, Chaos, and Power Laws* (W. H. Freeman & Co., New York)

Smith, P. M. & Swanson, A. W. 1989, "HEMTs - Low Noise and Power Transistors for 1 to 100GHz", *Applied Microwave*, May, pp.63-70.

Streetman, Ben 1990, *Solid State Electronic Devices*, (Prentice Hall, New Jersey)

Tacano, M & Sugiyama, Y. 1991, "Comparision of 1/*f* noise of AlGaAs/GaAs HEMTs and GaAs MESFETs", *Solid-State Electronics*, Vol. 34, No. 10, pp.1049-1053.

Tan, L. S., Lau, W. S., Samudra, G. S., Lee, K. M., & Ang, B. Y. 1994, "Numerical Simulation of Backgating Suppression in High Electron Mobility Transistors and Low Temperature Beam Epitaxy (MBE)-Grown Gallium Arsenide Buffer Layer Between the Substrate and Active Layers", *Japanese Journal of Applied Physics*, Vol. 33, pp. 826-829.

Tiwari, Sandip 1992, *Compound Semiconductor Device Physics* (Academic Press, Boston)

Van der Ziel, A., Handel, P. H., Zhu, X., & Duh, K. H. 1985, "A Theory of the Hooge Parameters of Solid-State Devices", *IEEE Transactions on Electronic Devices*, ED-32, pp. 667.

Van der Ziel, A. 1986, *Noise in Solid State Devices and Circuits* (John Wiley & Sons, New York)

Voss, R.F. & Clark, J., "1/*f* Noise in Music: Music from 1/*f* Noise', *Journal of the Acoustical Society of America*, Vol. 63, No. 1, January, pp. 258-263.

Weissman, M. B. 1988, "1/*f* Noise and Other Slow, Nonexponential Kinetics in Condensed Matter", *Review of Modern Physics*, Vol. 60, No. 2, pp. 537-571.

West, B. J. & Shlesinger, M. 1990, "The Noise in Natural Phenomena", *American Scientist*, Vol. 78, pp. 40-45.

White, P. M. & Healy, R. M. 1993, "Improved Equivalent Circuit for Determination of MESFET and HEMT Parasitic Capacitances from "Coldfet" Measurements", *IEEE Microwave and Guided Wave Letters*, Vol. 3, No. 12, pp. 453-454.

Yngvesson, S. 1991, *Microwave Semiconductor Devices* (Kluwer Academic Publishers, Boston).

Zimmer, T., Ouro Bodi, D., Dumas, J. M., Labat, N., Touboul, A., & Danto, Y. 1992, "Kink Effect in HEMT Structures: A Trap-related Semi-quantitative Model and Empirical Approach for SPICE Simulation", *Solid-State Electronics*, Vol. 35, No. 10, pp. 1543-1548.